ISAC CYTOMETRY Journal of Quantitative Cell Science PART A

MIFlowCyt

OMIP-069: Forty-Color Full Spectrum Flow Cytometry Panel for Deep Immunophenotyping of Major Cell Subsets in Human Peripheral Blood

Lily M. Park,[1] Joanne Lannigan,[2] Maria C. Jaimes[3*]

[1]Research and Development, Cytek Biosciences, Inc., Fremont, California, 94538-6407,

[2]Flow Cytometry Support Services, LLC, Alexandria, Virginia, 22314,

[3]Research and Development, Cytek Biosciences, Inc., Fremont, California, 94538-6407,

Received 3 June 2020; Revised 27 July 2020; Accepted 17 August 2020

Additional Supporting Information may be found in the online version of this article.

*Correspondence to: Maria C. Jaimes, Research and Development, Cytek Biosciences, Inc., 46107 Landing Parkway, Fremont, CA 94538-6407.
Email: mjaimes@cytekbio.com

Published online in Wiley Online Library (wileyonlinelibrary.com)

DOI: 10.1002/cyto.a.24213

• PURPOSE AND APPROPRIATE SAMPLE TYPES

This 40-color flow cytometry-based panel was developed for in-depth immunophenotyping of the major cell subsets present in human peripheral blood. Sample availability can often be limited, especially in cases of clinical trial material, when multiple types of testing are required from a single sample or timepoint. Maximizing the amount of information that can be obtained from a single sample not only provides more in-depth characterization of the immune system but also serves to address the issue of limited sample availability. The panel presented here identifies CD4 T cells, CD8 T cells, regulatory T cells, γδ T cells, NKT-like cells, B cells, NK cells, monocytes and dendritic cells. For each specific cell type, the panel includes markers for further characterization by including a selection of activation and differentiation markers, as well as chemokine receptors. Moreover, the combination of multiple markers in one tube might lead to the discovery of new immune phenotypes and their relevance in certain diseases. Of note, this panel was designed to include only surface markers to avoid the need for fixation and permeabilization steps. The panel can be used for studies aimed at characterizing the immune response in the context of infectious or autoimmune diseases, monitoring cancer patients on immuno- or chemotherapy, and discovery of unique and targetable biomarkers. Different from all previously published OMIPs, this panel was developed using a full spectrum flow cytometer, a technology that has allowed the effective use of 40 fluorescent markers in a single panel. The panel was developed using cryopreserved human peripheral blood mononuclear cells (PBMC) from healthy adults (Table 1). Although we have not tested the panel on fresh PBMCs or whole blood, it is anticipated that the panel could be used in those sample preparations without further optimization. @ 2020 Cytek Biosciences, Inc. *Cytometry Part A* published by Wiley Periodicals LLC on behalf of International Society for Advancement of Cytometry.

• Key terms

Aurora; broad immunophenotyping; full spectrum; high-dimensional flow cytometry; OMIP; spectral; PBMCs

Background

The need to understand the mechanisms and pathways of immune evasion seen either post immunotherapy or during natural immune responses to cancer, autoimmunity, and infectious diseases, requires methods and protocols which will enable a deeper profiling of the immune system. Greater characterization of immune subpopulations allows for more informed decisions regarding the identification of targetable biomarkers and the development of new therapeutic approaches. (1-4)

Unraveling the complexity of the human immune response requires the ability to perform high-throughput, in-depth analysis, at the single cell and population levels. Flow cytometry has sought to address this need by allowing the characterization of single-cell protein expression, through the binding of fluorochrome-labeled antibodies

to specific markers of interest. Over the years, manufacturers have increased the capabilities of flow cytometers through the incorporation of additional lasers and detectors, allowing detection of greater numbers of markers per cell. Concurrently, reagent manufacturers have worked to provide additional fluorophores to meet the demands of this rapidly expanding field. This has led to panel expansion over the last two decades, with a 17-color assay reported in 2004 (5) and up to 28 colors in more recent years (6-11). With the arrival of mass cytometry in 2009 (12), the number of markers assessed was expanded to 32, using metal-conjugated antibodies (13), and most recently a panel using 43 markers has been published (14).

In contrast to conventional flow cytometry, which primarily measures the peak emission of each fluorochrome, full spectrum flow cytometry measures the entire emission spectra for every fluorochrome, across all laser lines. As a result of collecting substantially more information about each cell, full spectrum flow cytometry is well suited to the development of highly multiparametric panels. Reports of applying the concepts of measuring fluorescence spectra by flow cytometry can be found as early as the 1970s (15), which was followed by a number of subsequent publications in later years (16-20). In order to expand the number of fluorochromes beyond the 28-color mark, a very high level of detail is needed to distinguish fluorochromes whose spectral signatures, particularly their peak emissions, are similar. This level of detail requires high-quality signals, low noise, and excitation specific full-emission profiles. It also requires extremely careful panel design and optimization. Here, we define full spectrum flow cytometry as measuring the entire fluorochrome emission, from ultraviolet to near-infrared, across multiple lasers using many more detectors, when compared to a conventional flow cytometer. This produces very specific spectral fingerprints that are used to mathematically distinguish one fluorophore from another, even when their maximum emissions are very similar. Leveraging this full spectrum technology in a five-laser system, the ability to combine 30–40 fluorescently labeled antibodies becomes possible using a fluorescence-based flow cytometer.

As mentioned previously, mass cytometry is also capable of assessing similarly high numbers of parameters. Currently, this technology has the advantage of additional detection channels to accommodate bar coding schemes for sample pooling, and as a more mature technology, high complexity panels using mass cytometry have been previously published and are widely available, including the publication of multiple OMIPs (21-24). However, limitations such as sample throughput, cell transmission efficiency, and overall cost of ownership have impacted the practicality, and broader adoption, of this technology in some laboratory environments (25-27). Spectral flow cytometers share a very common workflow with conventional flow cytometers and are therefore not hindered by these limitations. However, there are no previously published reports of panels beyond 28 fluorescent parameters, a fact which further supports the need for a fluorescent OMIP panel of this complexity.

The panel presented in this OMIP examines the frequency of CD4 and CD8 T cells, regulatory T cells (T_{regs}), γδ T cells, NKT-like cells, B cells, NK cells, monocytes, basophils, innate lymphoid cells (ILCs), and dendritic cells. Additional markers allow for the characterization of the main B and T cell subsets—naïve, memory, and effector—as well as putative T helper subsets. Dead cells were excluded using a viability dye (LIVE/Dead Fixable Blue). The following markers were used to characterize the indicated cell types: CD45 for all leukocytes; pan-γδ TCR for γδ T cells; CD3, CD4, and CD8 for the main T cell populations; CD19 and CD20 for B cells; CD16 and CD56 for NK cells; CD123 and HLA-DR for basophils; lineage markers and CD127 for total ILCs; and CD14 and CD16 for monocytes.

NK cells were identified by expression of CD56 (neural cell adhesion molecule [NCAM]) and CD16 (FcγRIII) (28), while CD2 was used to identify NK cells most likely to be involved in cytotoxicity (29). We included two natural cytotoxicity receptors (NCRs), NKG2D (natural killer group 2, member D [CD314]) and NKp30 (CD337); as well as the inhibitory receptor NKG2A (CD159a), identified as a possible target for immunotherapy (30), and the activation receptor NKG2C (CD159c) known to be relevant for NK cells in infectious diseases and vaccine effector response (31). CD57 was included as a maturation marker for NK cells, identifying cells with potent cytotoxic and reduced replicative potential (32). CD56 was further used for the identification of NKT-like cells, defined as $CD56^{+}CD3^{+}$, as cells with this phenotype might play a role in infectious diseases (33).

γδ T cells are regarded as an important bridge between the innate and adaptive immune systems because their response precedes adaptive immunity, making γδ T cells a unique component of the immune system (34-36). They are also associated with major autoimmune rheumatic diseases, such as rheumatoid arthritis, juvenile idiopathic arthritis, ankylosing spondylitis, systemic lupus erythematosus, and scleroderma (37). Although we included CD16 and CD56 to define NK cell subsets, CD16 and CD56 are also associated with an activated phenotype in γδ T cells (6,38). γδ T cells have also been shown to have effector/memory subsets based on expression of CD45RA, CD27, and CCR7 (39).

To characterize T cells, the memory and differentiation markers CD45RA, CCR7, CD27, and CD28 were used. Using CD45RA and CCR7, T cells can be classified into naïve ($CD45RA^{+}CCR7^{+}$), central memory ($CD45RA^{-}CCR7^{+}$), effector memory ($CD45RA^{-}CCR7^{-}$), and terminal effector memory ($CD45RA^{+}CCR7^{-}$) subsets (40,41). The addition of CD27 and CD28 allows further refinement of those subsets, identifying early effector ($CD45RA^{-}CCR7^{-}CD28^{+}CD27^{+}$), early-like effector ($CD45RA^{-}CCR7^{-}CD28^{+}CD27^{-}$), intermediate effector ($CD45RA^{-}CCR7^{-}CD28^{-}CD27^{+}$), terminal effector ($CD45RA^{-}CCR7^{-}CD28^{-}CD27^{-}$), and RA-terminal effector ($CD45RA^{+}CCR7^{-}CD28^{-}CD27^{-}$) (42,43).

Other surface markers, including CD127, CD95, PD-1, CD57, CD38, and HLA-DR, were included to further characterize T cell subsets (1,44,45). The IL-7 receptor (CD127) is involved in homeostatic proliferation and survival of memory T cell precursors (46), while CD57 is indicative of cell senescence, failure to proliferate, and susceptibility to activation-induced cell death (47,48). CD38 and HLA-DR were included

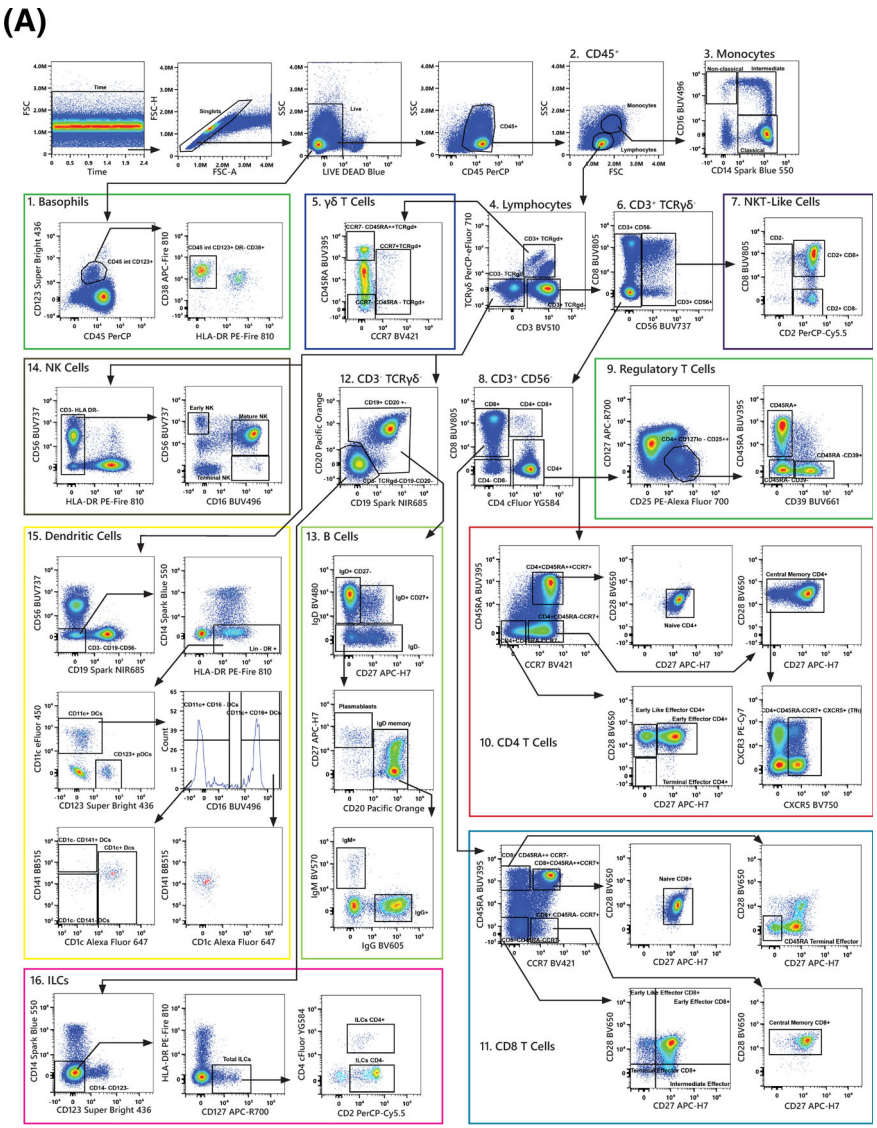
(A)
1. Basophils
2. CD45+
3. Monocytes
4. Lymphocytes
5. γδ T Cells
6. CD3+ TCRγδ-
7. NKT-Like Cells
8. CD3+ CD56-
9. Regulatory T Cells
10. CD4 T Cells
11. CD8 T Cells
12. CD3- TCRγδ-
13. B Cells
14. NK Cells
15. Dendritic Cells
16. ILCs

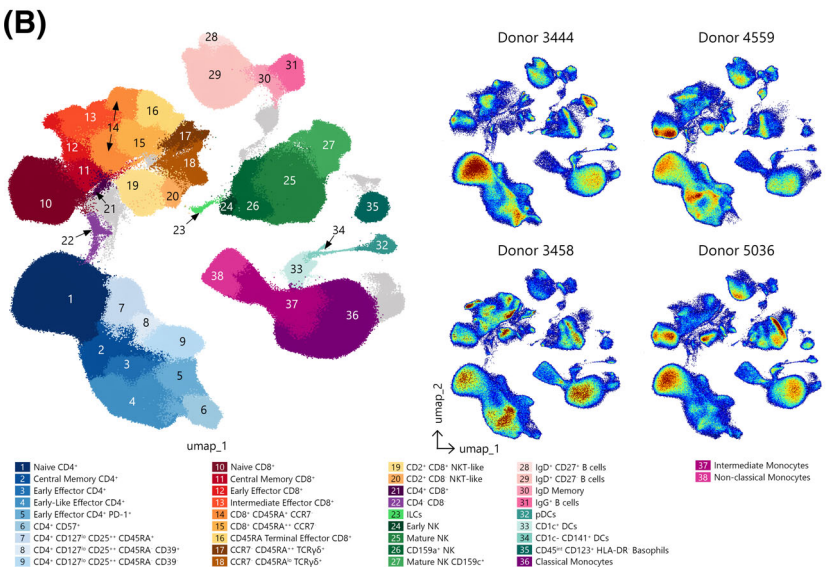
(B)
Donor 3444
Donor 4559
Donor 3458
Donor 5036
umap_1
umap_2
1 Naive CD4+
2 Central Memory CD4+
3 Early Effector CD4+
4 Early-Like Effector CD4+
5 Early Effector CD4+ PD-1+
6 CD4+ CD57+
7 CD4+ CD127hi CD25++ CD45RA+
8 CD4+ CD127hi CD25++ CD45RA CD39+
9 CD4+ CD127hi CD25++ CD45RA CD39-
10 Naive CD8+
11 Central Memory CD8+
12 Early Effector CD8+
13 Intermediate Effector CD8+
14 CD8+ CD45RA+ CCR7-
15 CD8+ CD45RA++ CCR7-
16 CD45RA Terminal Effector CD8+
17 CCR7- CD45RA++ TCRγδ-
18 CCR7- CD45RA++ TCRγδ+
19 CD2+ CD8+ NKT-like
20 CD2+ CD8- NKT-like
21 CD4+ CD8+
22 CD4- CD8-
23 ILCs
24 Early NK
25 Mature NK
26 CD159a+ NK
27 Mature NK CD159c+
28 IgD+ CD27+ B cells
29 IgD+ CD27- B cells
30 IgD Memory
31 IgG+ B cells
32 pDCs
33 CD1c+ DCs
34 CD1c- CD141+ DCs
35 CD45hi CD123+ HLA-DR- Basophils
36 Classical Monocytes
37 Intermediate Monocytes
38 Non-classical Monocytes

as T cell activation markers (49). Viral infections such as HIV-1, dengue virus, or influenza lead to increased frequencies of $CD38^+HLA\text{-}DR^+$ activated T cells (50,51). PD-1 and CD95 are both upregulated in activated T cells (52). The inhibitory receptor PD-1 is crucial for the regulation of immune responses and to avoid excessive immune activation (53).

In order to identify T_{regs}, we used CD25 (IL-2Rα) and CD127 (IL-7Rα) markers without the inclusion of FoxP3, which requires intracellular staining. Previous studies have shown that $CD25^{hi}CD127^{lo/-}CD4^+$ T cells are a good correlate of T_{regs} (54,55), although this strategy may over- or underestimate their frequency. It has been reported that T_{regs} can be further subsetted based on CD39 expression (7,56,57) and that $CD39^+$ T_{regs} might play a role in certain autoimmune diseases like multiple sclerosis (58).

CD27 and IgD were chosen for identification of naïve (IgD^+CD27^-), marginal zone-like (IgD^+CD27^+), and memory (IgD^-CD27^+) B cells as previously described (59). Marginal zone-like B cells can be further divided into IgM^+ marginal zone and IgD only memory B cells (8). When used in combination, CD24 and CD38 distinguish memory ($CD24^+CD38^{lo/neg}$), naïve ($CD24^{int}CD38^{int}$), and transitional ($CD24^{hi}CD38^{hi}$) B cells, and have been used for regulatory B cell identification (60,61). Plasmablasts can be identified based on expression of CD19, CD20, CD27, and CD38 (62). Memory B cells express different B cell receptor isotypes as a result of class switch recombination. This panel includes IgG and IgM, which are the most prevalent subsets of memory B cells found in blood. IgA was not included as this subpopulation of memory B cells is predominantly expressed in mucosa-associated lymphatic tissues, such as the intestine and mesenteric lymph nodes. IgE was excluded from this panel, since this subset of memory B cells is hardly detectable in human blood (63).

Chemokine receptors are important for the migration and positioning of immune cells (64). This panel includes CCR5, CCR6, CXCR3, and CXCR5. CCR5 is expressed by activated and memory T cells (65), γδ T cells (66), and T_{regs} (67). On human T cells, CCR6 is attributed to a Th17 (RORγt) phenotype (68). On B cells, CCR6 expression is restricted to functionally mature cells capable of responding to antigen challenge (69). CXCR3 has been reported to be necessary for T cell clustering around antigen presenting cells and T cell bystander activation (70) and also to be expressed on subsets of γδ T cells (66). CXCR5 interacts with CXCL13, which promotes T cell trafficking to B cell follicles and germinal centers. These are crucial sites for the generation of high-affinity antibody responses (71). Moreover, it has been shown that chronic inflammation leads to modulation of chemokine receptor expression on peripheral blood B cells. In patients with rheumatoid arthritis, B cells show decreased expression of CXCR5 and CCR6 and increased levels of CXCR3 (72).

Monocyte subsets were identified using CD14 (lipopolysaccharide binding protein) and CD16 (FcγRIII). These two markers allow the identification of classical monocytes

Table 1. Summary table for application of OMIP-069

PURPOSE	DEEP SUBSET PROFILING OF IMMUNE CELLS TO INCLUDE SUBSETS OF T, B, NK, NKT, MONOCYTE, AND DENDRITIC CELLS
Species	Human
Cell type	PBMCs
Cross references	OMIP-003, OMIP-004, OMIP-006, OMIP-013, OMIP-015, OMIP-017, OMIP-021, OMIP-023, OMIP-024, OMIP-029, OMIP-030, OMIP-033, OMIP-034, OMIP-039, OMIP-042, OMIP-044, OMIP-050, OMIP-051, OMIP-058, OMIP-060, OMIP-063

Figure 1. A. Manual gating strategy. The gating strategy used to identify the main cellular subsets is presented. Arrows are used to visualize the relationships across plots, and numbers are used to call attention to populations described here. After doublets and dead cells were excluded, basophils (1) were delineated as $CD45^+CD123^+HLA\text{-}DR^-$. Lymphocytes and monocytes (2) were gated based on FSC-A/SSC-A properties. Monocytes (3) were then classified by CD14 and CD16 expression as non-classical ($CD14^-CD16^+$), intermediate ($CD14^+CD16^{+/low}$), and classical ($CD14^+CD16^-$). From the lymphocyte gate (2), the following populations were identified: $CD3^-TCR\gamma\delta^-$, $CD3^+TCR\gamma\delta^+$, and $CD3^+TCR\gamma\delta^-$ (4). The $CD3^+TCR\gamma\delta^+$ population (5) was characterized based on CD45RA and CCR7 expression. The $CD3^+TCR\gamma\delta^-$ population was divided in $CD3^+CD56^+$ (NKT-like) and $CD3^+CD56^-$ subsets (6). The inclusion of CD2 and CD8 enables further classification of the NKT-like cells (7). $CD4^+$, $CD8^+$, $CD4^+CD8^+$ and $CD4^-CD8^-$ T cells were identified from the $CD3^+CD56^-$ gate (8). T_{regs} were identified from the $CD4^+$ population using CD127 and CD25 expression ($CD127^{lo/-}CD25^{hi}$) and CD39 and CD45RA were used to further classify these cells (9). CCR7, CD45RA, CD27, and CD28 allowed for further classification of memory/effector CD4 and CD8 T cell subsets (10, 11). $CD19^+$ and/or $CD20^+$ cells (B cells) were gated out of the $CD3^-TCR\gamma\delta^-$ population (12). $CD19^+CD20^{+/-}$ cells were further gated as IgD^+CD27^-, IgD^+CD27^+, or $IgD^-CD27^{+/-}$; the $IgD^-CD27^{+/-}$ subset was divided into plasmablasts or IgD^- memory B cells based on CD20 expression and IgG and IgM expression were assessed within the IgD^- memory B cells (13). NK cells were defined as $CD3^-TCR\gamma\delta^-HLA\text{-}DR^-$ and classified as early NK ($CD56^+CD16^-$), mature NK ($CD56^+CD16^+$), and terminal NK ($CD56^-CD16^+$) cells (14). Dendritic cells (DCs, 15) were identified first by gating on $CD3^-CD19^-CD56^-CD14^-HLA\text{-}DR^+$ and from there $CD123^+$ (pDCs) and $CD11c^+$ DCs were identified. $CD11c^+$ DCs were further divided into $CD16^-$ and $CD16^+$. CD1c and CD141 were then used to further classify the $CD11c^+CD16^-$ and $CD11c^+CD16^+$ DCs. Finally, innate lymphoid cells (ILCs, 16) were identified as $CD3^-CD19^-CD20^-CD14^-CD123^-CD127^+$ and subsetted based on CD2 and CD4 expression. All data presented is derived from frozen PBMCs of one healthy donor (donor ID 4559). **B.** High-dimensional data analysis on PBMCs from four donors displaying FlowSOM clusters projected on to two UMAP dimensions to show concordance between manual and automated analysis techniques. the overlay plot shows concatenated events from all four samples, while the density plots show differences in population distribution between the individual samples. As expected with a combination of high-resolution and high-dimensional data, several clusters contain events that evade a canonical definition. These populations are displayed in gray.

($CD14^{++}CD16^{-}$), non-classical monocytes ($CD14^{+}CD16^{++}$), and an intermediate monocyte population ($CD14^{+}CD16^{+}$) (73). Intermediate monocytes expand in the presence of cytokines and inflammation. Non-classical monocytes have also been shown to expand in inflammatory diseases. It has been demonstrated that, over the course of infection, there is first an increase in intermediate monocytes followed by an increase in non-classical monocytes (74).

Table 2. Reagents used for OMIP-069

SPECIFICITY	FLUOROCHROME	CLONE	PURPOSE
Viability	Live Dead UV Blue	—	Viability
CD45	PerCP	HI30	Leukocytes
CD3	BV510	SK7	Pan T cell, NKT-Like cells
CD4	cFluor YG584	SK3	CD4 T and NKT-Like cells
CD8	BUV805	SK1	CD8 T, NK, and NKT-Like cells
CD25	PE-Alexa Fluor700	CD25-3G10	Regulatory T cells
TCRγδ	PerCP-eFluor 710	B1.1	Pan γδ T cell
CD14	Spark Blue 550	63D3	Monocyte differentiation
CD16	BUV496	3G8	Monocyte, NK cell, and dendritic cell differentiation
CD11c	eFluor 450	3.9	Dendritic Cell differentiation
CD19	Spark NIR 685	HIB19	B cells
CD20	Pacific Orange	HI47	B cells
CD24	PE-Alexa Fluor 610	SN3	B cell differentiation
CD39	BUV661	TU66	B cell, T_{regs}, and monocyte differentiation
IgD	BV480	IA6-2	B cell differentiation
IgG	BV605	G18-145	B cell differentiation
IgM	BV570	MHM-88	B cell differentiation
CD141	BB515	1A4	Dendritic cell differentiation
CD1c	Alexa Fluor 647	L161	Dendritic cells, NKT-Like cells
CD123	Super Bright 436	6H6	Plasmacytoid dendritic cells
CD2	PerCP-Cy5.5	TS1/8	NK cell differentiation
CD56	BUV737	NCAM16.2	Pan NK cell, γδ T cell activation
CCR7	BV421	G043H7	T cell differentiation
CD27	APC-H7	M-T271	T and B cell differentiation
CD28	BV650	CD28.2	T cell and NK cell differentiation
CD45RA	BUV395	5H9	T cell and dendritic cell differentiation
CD95	PE-Cy5	DX2	T cell and B cell differentiation
CD127	APC-R700	HIL-7R-M21	Cytokine receptor; T cell differentiation
CD337	PE-Dazzle594	P30-15	NK cell differentiation
CCR6	BV711	G034E3	Chemokine receptor; T cell and B cell differentiation
CCR5	BUV563	2D7/CCR5	Chemokine receptor; Monocyte, dendritic cell, T cell, and B cell differentiation
CXCR5	BV750	RF8B2	Chemokine receptor; T cell differentiation
CXCR3	PE-Cy7	G025H7	Chemokine receptor; Dendritic cell, T cell, and B cell differentiation
HLA-DR	PE-Fire810	L243	T cell and monocyte activation, NK cell lineage discrimination, dendritic cell lineage marker
CD38	APC-Fire810	HIT2	Monocyte, dendritic cell, T cell, and B cell activation/differentiation
CD57	FITC	HNK-1	NK and $CD8^{+}$ T cell immune senescence
PD-1	BV785	EH12.2H7	T cell inhibitory receptor
CD159a	APC	REA110	NK, NKT-Like, and γδ T cell activation/differentiation
CD159c	PE	REA205	NK cell differentiation
CD314	BUV615	1D11	NK cell differentiation

With the markers present in this panel, basophils were identified as $CD45^{dim}CD123^{+}HLA\text{-}DR^{-}$ (75). The phenotype of these cells can then be further characterized by evaluating expression of CD38, CD95, and CD25.

Total ILCs were identified using a similar strategy as presented in OMIP-055 (76). This subset was identified as $CD45^{+}CD127^{+}Lin^{-}$. For lineage markers, we used CD14, CD19, CD20, and CD3. However, to fully identify these cells other markers should be excluded like CD1a, CD34, CD303, and FCεR1a. Despite lacking these markers, the cells identified as ILCs could be further classified based on expression of CD2, CD4, CCR6, CXCR3, CD27, CD28, CXCR5, and CCR7 as previously reported (77).

Finally, to identify the main dendritic cell subsets, CD11c, HLA-DR, CD141 (BDCA-3), CD1c (BDCA-1), and CD123 were used as previously described (9). pDCs were identified as lineage negative ($CD3^{-}CD19^{-}CD56^{-}CD14^{-}$) $HLA\text{-}DR^{+}CD123^{+}$ cells; conventional DCs were identified as $CD123^{-}CD11c^{+}HLA\text{-}DR^{+}$, and they were further subset based on CD141 (78) and CD1c expression (79).

The manual gating strategy used to identify the main cell subsets, based on the descriptions provided above, is shown in Figure 1A. As it is more likely that a complex data set such as this would be analyzed using a pipeline containing both dimensionality reduction and clustering algorithms, we present in Figure 1B the computationally derived analogs of manually gated canonical subsets using such an unsupervised approach. When preparing for any kind of automated analysis, it is imperative that the data be of the highest quality, as any undesirable events or processing artifacts will negatively affect the downstream results. In this case, the scaling of the data was first checked to ensure the arcsinh transformation was unimodal around 0 and then the data were cleaned by manual gating to remove doublets, debris, and dead cells. The data were then run through flowCut (80) to check for aberrant signal patterns or events, and with none found. UMAP (81) was run to group phenotypically similar events into "islands" to illustrate differences both between and inside each population. FlowSOM (82) was subsequently used to cluster the events based on UMAP parameters and selected surface markers in order to emphasize differences between hard to resolve populations and then the resulting clusters were overlaid on the initial UMAP parameters. A traditional clustered heatmap analysis then followed to aid in the identification and labeling of the FlowSOM clusters (See Supporting Information Fig. S11A).

This 40-color panel (Table 2) presents a powerful tool for in-depth characterization of lymphocytes, monocytes, and dendritic cells present in human peripheral blood. It covers almost the entire cellular composition of the human peripheral immune system and will be particularly useful for studies in which sample availability is limited or unique biomarker signatures are sought. Taking advantage of full spectrum cytometry, we present a panel that highlights the first published OMIP to go beyond 28-color fluorescence flow cytometry with excellent population resolution.

Similarity to published OMIPs

This panel is similar to OMIPs -015, -023, -024, -030, -033, -034, -042, -50, -058, -063, which are all aimed at identifying the main leukocyte subsets in human blood. It partially overlaps with OMIPs -013, -017, -021, -030, and -060 for characterization of T cells; OMIPs -004, -006, and -015 for T_{reg} immunophenotyping; OMIP -044 for dendritic cells; OMIPs -003, -033, and -051 for B cells; and OMIPs −029, and -039 for NK cells (6-11,22,29,44,45,55,83-96).

Statement of ethical use of human samples

All human PBMCs used in this study were obtained from AllCells Alameda. Ethical review and regulatory compliance were conducted by Alpha Independent Review Board under Protocol number: 7000-SOP-045 (effective through April 26, 2021).

Acknowledgments

The authors would like to thank BioLegend® for kindly providing the custom HLA-DR PE-Fire810 and CD38 APC-Fire810 (now commercially available). In addition, the authors would like to thank Janelle Shook and James Wei for their assistance with the manuscript and figure preparation, Geoff Kraker for doing the unsupervised analysis of the data, Patrick Duncker for critical reading of the manuscript, and Huimin Gu for her extensive work at testing different fluorochrome combinations in preparation for this panel development.

Author contributions

Lily M. Park: Conceptualization; data curation; formal analysis; methodology; validation; visualization. **Joanne Lannigan:** Data curation; formal analysis; project administration; resources; visualization; writing - original draft; writing - review and editing. **Maria C. Jaimes:** Conceptualization; data curation; formal analysis; methodology; project administration; resources; software; supervision; validation; visualization; writing - original draft; writing - review and editing.

Conflict of Interest

Lily Park and Maria C. Jaimes are employees of Cytek Biosciences, Inc., the manufacturer of the Aurora full spectrum flow cytometer used in these studies. Joanne Lannigan is a paid consultant for Cytek Biosciences, Inc.

Literature Cited

1. Maecker HT, McCoy JP, Nussenblatt R. Standardizing immunophenotyping for the human immunology project. Nat Rev Immunol 2012;12:191–200.
2. Aghaeepour N, Chattopadhyay PK, Ganesan A, O'Neill K, Zare H, Jalali A, Hoos HH, Roederer M, Brinkman RR. Early immunologic correlates of HIV protection can be identified from computational analysis of complex multivariate T-cell flow cytometry assays. Bioinformatics 2012;28:1009–1016.
3. Lin L, Finak G, Ushey K, Seshadri C, Hawn TR, Frahm N, Scriba TJ, Mahomed H, Hanekom W, Bart PA, et al. COMPASS identifies T-cell subsets correlated with clinical outcomes. Nat Biotechnol 2015;33:610–616.
4. Chattopadhyay PK, Roederer M. A mine is a terrible thing to waste: High content, single cell technologies for comprehensive immune analysis. Am J Transplant 2015; 15:1155–1161.

5. Perfetto SP, Chattopadhyay PK, Roederer M. Seventeen-colour flow cytometry: Unravelling the immune system. Nat Rev Immunol 2004;4:648–655.
6. Liechti T, Roederer M. OMIP-058: 30-parameter flow cytometry panel to characterize iNKT, NK, unconventional and conventional T cells. Cytom Part A 2019;95A: 946–951.
7. Liechti T, Roederer M. OMIP-060: 30-parameter flow cytometry panel to assess T cell effector functions and regulatory T cells. Cytom Part A 2019;95A:1129–1134.
8. Liechti T, Roederer M. OMIP-051 - 28-color flow cytometry panel to characterize B cells and myeloid cells. Cytom Part A 2019;95A:150–155.
9. Mair F, Prlic M. OMIP-044: 28-color immunophenotyping of the human dendritic cell compartment. Cytometry Part A 2018;93A:402–405.
10. Nettey L, Giles AJ, Chattopadhyay PK. OMIP-050: A 28-color/30-parameter fluorescence flow cytometry panel to enumerate and characterize cells expressing a wide Array of immune checkpoint molecules. Cytom Part A 2018;93A:1094–1096.
11. Payne K, Li W, Salomon R, Ma CS. OMIP-063: 28-color flow cytometry panel for broad human Immunophenotyping. Cytom Part A 2020;97A:777–781.
12. Bandura DR, Baranov VI, Ornatsky OI, Antonov A, Kinach R, Lou X, Pavlov S, Vorobiev S, Dick JE, Tanner SD. Mass cytometry: Technique for real time single cell multitarget immunoassay based on inductively coupled plasma time-of-flight mass spectrometry. Anal Chem 2009;81:6813–6822.
13. Bendall SC, Simonds EF, Qiu P, Amir el AD, Krutzik PO, Finck R, Bruggner RV, Melamed R, Trejo A, Ornatsky OI, et al. Single-cell mass cytometry of differential immune and drug responses across a human hematopoietic continuum. Science 2011;332:687–696.
14. Tsai AG, Glass DR, Juntilla M, Hartmann FJ, Oak JS, Fernandez-Pol S, Ohgami RS, Bendall SC. Multiplexed single-cell morphometry for hematopathology diagnostics. Nat Med 2020;26:408–417.
15. Wade CG, Rhyne RH Jr, Woodruff WH, Bloch DP, Bartholomew JC. Spectra of cells in flow cytometry using a vidicon detector. J Histochem Cytochem 1979;27: 1049–1052.
16. Futamura K, Sekino M, Hata A, Ikebuchi R, Nakanishi Y, Egawa G, Kabashima K, Watanabe T, Furuki M, Tomura M. Novel full-spectral flow cytometry with multiple spectrally-adjacent fluorescent proteins and fluorochromes and visualization of in vivo cellular movement. Cytom Part A 2015;87A:830–842.
17. Gauci MR, Vesey G, Narai J, Veal D, Williams KL, Piper JA. Observation of single-cell fluorescence spectra in laser flow cytometry. Cytometry 1996;25:388–393.
18. Nolan JP, Condello D. Spectral flow cytometry. Curr Protoc Cytom 2013;63(1): 1.27.1–1.27.13.
19. Sanders CK, Mourant JR. Advantages of full spectrum flow cytometry. J Biomed Opt 2013;18:037004.
20. Gregori G, Patsekin V, Rajwa B, Jones J, Ragheb K, Holdman C, Robinson JP. Hyperspectral cytometry at the single-cell level using a 32-channel photodetector. Cytom Part A 2012;81A:35–44.
21. Brodie TM, Tosevski V, Medova M. OMIP-045: Characterizing human head and neck tumors and cancer cell lines with mass cytometry. Cytom Part A 2018;93A: 406–410.
22. Baumgart S, Peddinghaus A, Schulte-Wrede U, Mei HE, Grutzkau A. OMIP-034: Comprehensive immune phenotyping of human peripheral leukocytes by mass cytometry for monitoring immunomodulatory therapies. Cytom Part A 2017;91A: 34–38.
23. Dusoswa SA, Verhoeff J, Garcia-Vallejo JJ. OMIP-054: Broad immune phenotyping of innate and adaptive leukocytes in the brain, spleen, and bone marrow of an Orthotopic murine glioblastoma model by mass cytometry. Cytom Part A 2019; 95A:422–426.
24. Jaracz-Ros A, Hemon P, Krzysiek R, Bachelerie F, Schlecht-Louf G, Gary-Gouy H. OMIP-048 MC: Quantification of calcium sensors and channels expression in lymphocyte subsets by mass cytometry. Cytom Part A 2018;93A:681–684.
25. Maecker HT, Harari A. Immune monitoring technology primer: Flow and mass cytometry. J Immunother Cancer 2015;3:44.
26. Nassar AF, Wisnewski AV, Raddassi K. Automation of sample preparation for mass cytometry barcoding in support of clinical research: Protocol optimization. Anal Bioanal Chem 2017;409:2363–2372.
27. Olsen LR, Leipold MD, Pedersen CB, Maecker HT. The anatomy of single cell mass cytometry data. Cytom Part A 2019;95A:156–172.
28. Montaldo E, Del Zotto G, Della Chiesa M, Mingari MC, Moretta A, De Maria A, Moretta L. Human NK cell receptors/markers: A tool to analyze NK cell development, subsets and function. Cytom Part A 2013;83A:702–713.
29. Mahnke YD, Beddall MH, Roederer M. OMIP-029: Human NK-cell phenotypization. Cytom Part A 2015;87A:986–988.
30. Creelan BC, Antonia SJ. The NKG2A immune checkpoint - a new direction in cancer immunotherapy. Nat Rev Clin Oncol 2019;16:277–278.
31. Ma M, Wang Z, Chen X, Tao A, He L, Fu S, Zhang Z, Fu Y, Guo C, Liu J, et al. NKG2C(+)NKG2A(−) natural killer cells are associated with a lower viral set point and may predict disease progression in individuals with primary HIV infection. Front Immunol 2017;8:1176.
32. Nielsen CM, White MJ, Goodier MR, Riley EM. Functional significance of CD57 expression on human NK cells and relevance to disease. Front Immunol 2013;4:422.
33. Jiang Y, Cui X, Cui C, Zhang J, Zhou F, Zhang Z, Fu Y, Xu J, Chu Z, Liu J, et al. The function of CD3+CD56+ NKT-like cells in HIV-infected individuals. Biomed Res Int 2014;2014:863625.
34. Wan F, Hu CB, Ma JX, Gao K, Xiang LX, Shao JZ. Characterization of γδ T cells from zebrafish provides insights into their important role in adaptive humoral immunity. Front Immunol 2016;7:675.
35. Davey MS, Willcox CR, Joyce SP, Ladell K, Kasatskaya SA, McLaren JE, Hunter S, Salim M, Mohammed F, Price DA, et al. Clonal selection in the human Vδ1 T cell repertoire indicates γδ TCR-dependent adaptive immune surveillance. Nat Commun 2017;8:14760.
36. Holtmeier W, Kabelitz D. Gammadelta T cells link innate and adaptive immune responses. Chem Immunol Allergy 2005;86:151–183.
37. Bank I. The role of Gamma Delta T cells in autoimmune rheumatic diseases. Cell 2020;9(2):462
38. Ryan PL, Sumaria N, Holland CJ, Bradford CM, Izotova N, Grandjean CL, Jawad AS, Bergmeier LA, Pennington DJ. Heterogeneous yet stable Vdelta2(+) T-cell profiles define distinct cytotoxic effector potentials in healthy human individuals. Proc Natl Acad Sci U S A 2016;113:14378–14383.
39. Dieli F, Poccia F, Lipp M, Sireci G, Caccamo N, Di Sano C, Salerno A. Differentiation of effector/memory Vdelta2 T cells and migratory routes in lymph nodes or inflammatory sites. J Exp Med 2003;198:391–397.
40. Mahnke YD, Brodie TM, Sallusto F, Roederer M, Lugli E. The who's who of T-cell differentiation: Human memory T-cell subsets. Eur J Immunol 2013;43:2797–2809.
41. Sallusto F, Lenig D, Forster R, Lipp M, Lanzavecchia A. Two subsets of memory T lymphocytes with distinct homing potentials and effector functions. Nature 1999; 401:708–712.
42. Appay V, van Lier RA, Sallusto F, Roederer M. Phenotype and function of human T lymphocyte subsets: Consensus and issues. Cytom Part A 2008;73A:975–983.
43. Oja AE, Piet B, van der Zwan D, Blaauwgeers H, Mensink M, de Kivit S, Borst J, Nolte MA, van Lier RAW, Stark R, et al. Functional heterogeneity of CD4(+) tumor-infiltrating lymphocytes with a resident memory phenotype in NSCLC. Front Immunol 2018;9:2654.
44. Staser KW, Eades W, Choi J, Karpova D, DiPersio JF. OMIP-042: 21-color flow cytometry to comprehensively immunophenotype major lymphocyte and myeloid subsets in human peripheral blood. Cytom Part A 2018;93A:186–189.
45. Wingender G, Kronenberg M. OMIP-030: Characterization of human T cell subsets via surface markers. Cytom Part A 2015;87A:1067–1069.
46. Kaech SM, Tan JT, Wherry EJ, Konieczny BT, Surh CD, Ahmed R. Selective expression of the interleukin 7 receptor identifies effector CD8 T cells that give rise to long-lived memory cells. Nat Immunol 2003;4:1191–1198.
47. Brenchley JM, Karandikar NJ, Betts MR, Ambrozak DR, Hill BJ, Crotty LE, Casazza JP, Kuruppu J, Migueles SA, Connors M, et al. Expression of CD57 defines replicative senescence and antigen-induced apoptotic death of CD8+ T cells. Blood 2003;101:2711–2720.
48. Focosi D, Bestagno M, Burrone O, Petrini M. CD57+ T lymphocytes and functional immune deficiency. J Leukoc Biol 2010;87:107–116.
49. Meditz AL, Haas MK, Folkvord JM, Melander K, Young R, McCarter M, Mawhinney S, Campbell TB, Lie Y, Coakley E, et al. HLA-DR+ CD38+ CD4+ T lymphocytes have elevated CCR5 expression and produce the majority of R5-tropic HIV-1 RNA in vivo. J Virol 2011;85:10189–10200.
50. Ndhlovu ZM, Kamya P, Mewalal N, Kloverpris HN, Nkosi T, Pretorius K, Laher F, Ogunshola F, Chopera D, Shekhar K, et al. Magnitude and kinetics of CD8+ T cell activation during Hyperacute HIV infection impact viral set point. Immunity 2015; 43:591–604.
51. Wang Z, Zhu L, Nguyen THO, Wan Y, Sant S, Quinones-Parra SM, Crawford JC, Eltahla AA, Rizzetto S, Bull RA, et al. Clonally diverse CD38(+)HLA-DR(+)CD8(+) T cells persist during fatal H7N9 disease. Nat Commun 2018;9:824.
52. Duraiswamy J, Ibegbu CC, Masopust D, Miller JD, Araki K, Doho GH, Tata P, Gupta S, Zilliox MJ, Nakaya HI, et al. Phenotype, function, and gene expression profiles of programmed death-1(hi) CD8 T cells in healthy human adults. J Immunol 2011;186:4200–4212.
53. Sun C, Mezzadra R, Schumacher TN. Regulation and function of the PD-L1 checkpoint. Immunity 2018;48:434–452.
54. Liu W, Putnam AL, Xu-Yu Z, Szot GL, Lee MR, Zhu S, Gottlieb PA, Kapranov P, Gingeras TR, Fazekas de St Groth B, et al. CD127 expression inversely correlates with FoxP3 and suppressive function of human CD4+ T reg cells. J Exp Med 2006; 203:1701–1711.
55. Mahnke YD, Beddall MH, Roederer M. OMIP-015: Human regulatory and activated T-cells without intracellular staining. Cytom Part A 2013;83A:179–181.
56. Deaglio S, Dwyer KM, Gao W, Friedman D, Usheva A, Erat A, Chen JF, Enjyoji K, Linden J, Oukka M, et al. Adenosine generation catalyzed by CD39 and CD73 expressed on regulatory T cells mediates immune suppression. J Exp Med 2007;204: 1257–1265.
57. Dwyer KM, Hanidziar D, Putheti P, Hill PA, Pommey S, McRae JL, Winterhalter A, Doherty G, Deaglio S, Koulmanda M, et al. Expression of CD39 by human peripheral blood CD4+ CD25+ T cells denotes a regulatory memory phenotype. Am J Transplant 2010;10:2410–2420.
58. Borsellino G, Kleinewietfeld M, Di Mitri D, Sternjak A, Diamantini A, Giometto R, Hopner S, Centonze D, Bernardi G, Dell'Acqua ML, et al. Expression of ectonucleotidase CD39 by Foxp3+ Treg cells: Hydrolysis of extracellular ATP and immune suppression. Blood 2007;110:1225–1232.
59. Klein U, Rajewsky K, Kuppers R. Human immunoglobulin (Ig)M+IgD+ peripheral blood B cells expressing the CD27 cell surface antigen carry somatically mutated variable region genes: CD27 as a general marker for somatically mutated (memory) B cells. J Exp Med 1998;188:1679–1689.
60. von Borstel A, Lintermans LL, Heeringa P, Rutgers A, Stegeman CA, Sanders JS, Abdulahad WH. Circulating CD24hiCD38hi regulatory B cells correlate inversely with the ThEM17 cell frequency in granulomatosis with polyangiitis patients. Rheumatology (Oxford) 2019;58(8):1361–1366.
61. Rosser EC, Mauri C. Regulatory B cells: Origin, phenotype, and function. Immunity 2015;42:607–612.

62. Avery DT, Ellyard JI, Mackay F, Corcoran LM, Hodgkin PD, Tangye SG. Increased expression of CD27 on activated human memory B cells correlates with their commitment to the plasma cell lineage. J Immunol 2005;174:4034–4042.
63. Allman D, Pillai S. Peripheral B cell subsets. Curr Opin Immunol 2008;20:149–157.
64. Griffith JW, Sokol CL, Luster AD. Chemokines and chemokine receptors: Positioning cells for host defense and immunity. Annu Rev Immunol 2014;32:659–702.
65. Wu L, Paxton WA, Kassam N, Ruffing N, Rottman JB, Sullivan N, Choe H, Sodroski J, Newman W, Koup RA, et al. CCR5 levels and expression pattern correlate with infectability by macrophage-tropic HIV-1, in vitro. J Exp Med 1997;185: 1681–1691.
66. Glatzel A, Wesch D, Schiemann F, Brandt E, Janssen O, Kabelitz D. Patterns of chemokine receptor expression on peripheral blood gamma delta T lymphocytes: Strong expression of CCR5 is a selective feature of V delta 2/V gamma 9 gamma delta T cells. J Immunol 2002;168:4920–4929.
67. Lim HW, Broxmeyer HE, Kim CH. Regulation of trafficking receptor expression in human forkhead box P3+ regulatory T cells. J Immunol 2006;177:840–851.
68. Geginat J, Paroni M, Facciotti F, Gruarin P, Kastirr I, Caprioli F, Pagani M, Abrignani S. The CD4-centered universe of human T cell subsets. Semin Immunol 2013;25:252–262.
69. Elgueta R, Marks E, Nowak E, Menezes S, Benson M, Raman VS, Ortiz C, O'Connell S, Hess H, Lord GM, et al. CCR6-dependent positioning of memory B cells is essential for their ability to mount a recall response to antigen. J Immunol 2015;194:505–513.
70. Maurice NJ, McElrath MJ, Andersen-Nissen E, Frahm N, Prlic M. CXCR3 enables recruitment and site-specific bystander activation of memory CD8(+) T cells. Nat Commun 2019;10:4987.
71. Chevalier N, Jarrossay D, Ho E, Avery DT, Ma CS, Yu D, Sallusto F, Tangye SG, Mackay CR. CXCR5 expressing human central memory CD4 T cells and their relevance for humoral immune responses. J Immunol 2011;186:5556–5568.
72. Henneken M, Dorner T, Burmester GR, Berek C. Differential expression of chemokine receptors on peripheral blood B cells from patients with rheumatoid arthritis and systemic lupus erythematosus. Arthritis Res Ther 2005;7: R1001–R1013.
73. Ziegler-Heitbrock L, Ancuta P, Crowe S, Dalod M, Grau V, Hart DN, Leenen PJ, Liu YJ, MacPherson G, Randolph GJ, et al. Nomenclature of monocytes and dendritic cells in blood. Blood 2010;116:e74–e80.
74. Strauss-Ayali D, Conrad SM, Mosser DM. Monocyte subpopulations and their differentiation patterns during infection. J Leukoc Biol 2007;82:244–252.
75. Han X, Jorgensen JL, Brahmandam A, Schlette E, Huh YO, Shi Y, Awagu S, Chen W. Immunophenotypic study of basophils by multiparameter flow cytometry. Arch Pathol Lab Med 2008;132:813–819.
76. Bianca Bennstein S, Riccarda Manser A, Weinhold S, Scherenschlich N, Uhrberg M. OMIP-055: Characterization of human innate lymphoid cells from neonatal and peripheral blood. Cytom Part A 2019;95A:427–430.
77. Roan F, Stoklasek TA, Whalen E, Molitor JA, Bluestone JA, Buckner JH, Ziegler SF. CD4+ group 1 innate lymphoid cells (ILC) form a functionally distinct ILC subset that is increased in systemic sclerosis. J Immunol 2016;196:2051–2062.
78. Jongbloed SL, Kassianos AJ, McDonald KJ, Clark GJ, Ju X, Angel CE, Chen CJ, Dunbar PR, Wadley RB, Jeet V, et al. Human CD141+ (BDCA-3)+ dendritic cells (DCs) represent a unique myeloid DC subset that cross-presents necrotic cell antigens. J Exp Med 2010;207:1247–1260.
79. Collin M, McGovern N, Haniffa M. Human dendritic cell subsets. Immunology 2013;140:22–30.
80. Meskas J, Wang S, Brinkman R. flowCut — An R package for precise and accurate automated removal of outlier events and flagging of files based on time versus fluorescence analysis. bioRxiv 2020.
81. McInnes L, Healy J, Melville J. UMAP: Uniform manifold approximation and projection for dimension rReduction. ArXiv e-prints 2018;1802.03426.
82. Van Gassen S, Callebaut B, Van Helden MJ, Lambrecht BN, Demeester P, Dhaene T, Saeys Y. FlowSOM: Using self-organizing maps for visualization and interpretation of cytometry data. Cytom Part A 2015;87A:636–645.
83. Wei C, Jung J, Sanz I. OMIP-003: Phenotypic analysis of human memory B cells. Cytom Part A 2011;79A:894–896.
84. Biancotto A, Dagur PK, Fuchs JC, Langweiler M, McCoy JP Jr. OMIP-004: In-depth characterization of human T regulatory cells. Cytom Part A 2012;81A:15–16.
85. Murdoch DM, Staats JS, Weinhold KJ. OMIP-006: Phenotypic subset analysis of human T regulatory cells via polychromatic flow cytometry. Cytom Part A 2012; 81A:281–283.
86. Mahnke YD, Beddall MH, Roederer M. OMIP-013: Differentiation of human T-cells. Cytom Part A 2012;81A:935–936.
87. Mahnke YD, Beddall MH, Roederer M. OMIP-017: Human CD4(+) helper T-cell subsets including follicular helper cells. Cytom Part A 2013;83A:439–440.
88. Brodie T, Brenna E, Sallusto F. OMIP-018: Chemokine receptor expression on human T helper cells. Cytom Part A 2013;83A:530–532.
89. Mahnke YD, Beddall MH, Roederer M. OMIP-019: Quantification of human gammadeltaT-cells, iNKT-cells, and hematopoietic precursors. Cytom Part A 2013; 83A:676–678.
90. Wistuba-Hamprecht K, Pawelec G, Derhovanessian E. OMIP-020: Phenotypic characterization of human gammadelta T-cells by multicolor flow cytometry. Cytom Part A 2014;85A:522–524.
91. Gherardin NA, Ritchie DS, Godfrey DI, Neeson PJ. OMIP-021: Simultaneous quantification of human conventional and innate-like T-cell subsets. Cytom Part A 2014; 85A:573–575.
92. Brodie T, Rothaeusler K, Sospedra M. OMIP-033: A comprehensive single step staining protocol for human T- and B-cell subsets. Cytom Part A 2016;89A: 629–632.
93. Hammer Q, Romagnani C. OMIP-039: Detection and analysis of human adaptive NKG2C(+) natural killer cells. Cytom Part A 2017;91A:997–1000.
94. Nowatzky J, Stagnar C, Manches O. OMIP-053: Identification, classification, and isolation of major FoxP3 expressing human CD4(+) Treg subsets. Cytom Part A 2019;95A:264–267.
95. Bocsi J, Melzer S, Dahnert I, Tarnok A. OMIP-023: 10-color, 13 antibody panel for in-depth phenotyping of human peripheral blood leukocytes. Cytom Part A 2014; 85A:781–784.
96. Moncunill G, Han H, Dobano C, McElrath MJ, De Rosa SC. OMIP-024: Panleukocyte immunophenotypic characterization of PBMC subsets in human samples. Cytom Part A 2014;85A:995–998.

Supplementary Material

OMIP-069: Forty-Color Full Spectrum Flow Cytometry Panel for Deep Immunophenotyping of Major Cell Subsets in Human Peripheral Blood

Lily M. Park[1], Joanne Lannigan[2], and Maria C. Jaimes[3]

[1]Research and Development, Cytek Biosciences, Inc., Fremont, California, 94538-6407
[2]Flow Cytometry Support Services, LLC, Alexandria, Virginia, 22314
[3]Research and Development, Cytek Biosciences, Inc., Fremont, California, 94538-6407

INSTRUMENT CONFIGURATION AND INSTRUMENT SETUP OPTIMIZATION

This panel was developed on a Cytek® Aurora (Cytek Biosciences, Fremont, California) equipped with 5 lasers (355, 405, 488, 561, 640 nm) and 64 detectors. In this instrument, the optical design is such that the lasers are spatially separated with independent optical paths. The detection modules consist of avalanche photodiodes (APDs) coupled with narrow bandpass filters ranging from just above the laser wavelength up to 830 nm (**Supplemental Figure 1**). The number of detectors per laser module and bandwidth of the filters is detailed in Supplemental Table 1.

To determine optimal instrument/APD setup, the following approach was taken:

- A comprehensive set of commercially available fluorochromes was identified, making sure to cover as many possible peak emission wavelengths as possible across all 5 lasers.
- Gains were set such that each fluorochrome's peak emission channel corresponds to their maximum emission wavelength, and the spectral patterns did not exhibit any steep changes from one channel to the next.
- PBMCs stained with anti-CD4 labeled with each fluorochrome were acquired at a gain of 50 for each detector across all lasers (range on the Cytek Aurora is from 1 to 3000) and then at 2-fold increments, until the stain index was stable. If, at gain 50, the stain index was already maximal, 2-fold decrease gains were tested. Stain index was calculated using peak channel statistics. The following formula was used:

$$\text{Stain Index} = \frac{MFI_{\text{positive population}} - MFI_{\text{negative population}}}{2 * rSD_{\text{negative population}}}$$

- Gains were then set for optimal stain index in the peak emission channel. If no fluorochrome peaked in a given channel, the gain was adjusted based on an adjacent emitting fluorochrome, so that the signal did not exceed the signal from the peak detector and a smooth transition to the peak channel was maintained.
- To accommodate brighter signals (due to antigens with higher expression level, differences in expression level across donors, or up-regulation of receptors), PBMCs stained with anti-CD8 labeled with each fluorochrome were acquired at the optimal gains established in the previous step and signals verified to be on scale (< $2x10^6$ on a full scale of $4x10^6$). If needed, gains were adjusted proportionately across the detectors to put the brightest signals on scale.
- To identify gains which had the least impact on spillover spread, we compared spread values based on the Spillover Spreading Matrix (SSM) at different gains; using the gains established in the previous step, and with a 2- and 4-fold increase, to ensure the lower gains minimized spread values.
- The final gain settings were saved in the SpectroFlo® software as CytekAssaySetting. These settings are automatically updated during daily QC based on calibrated bead MFI targets to ensure consistent setup across days.

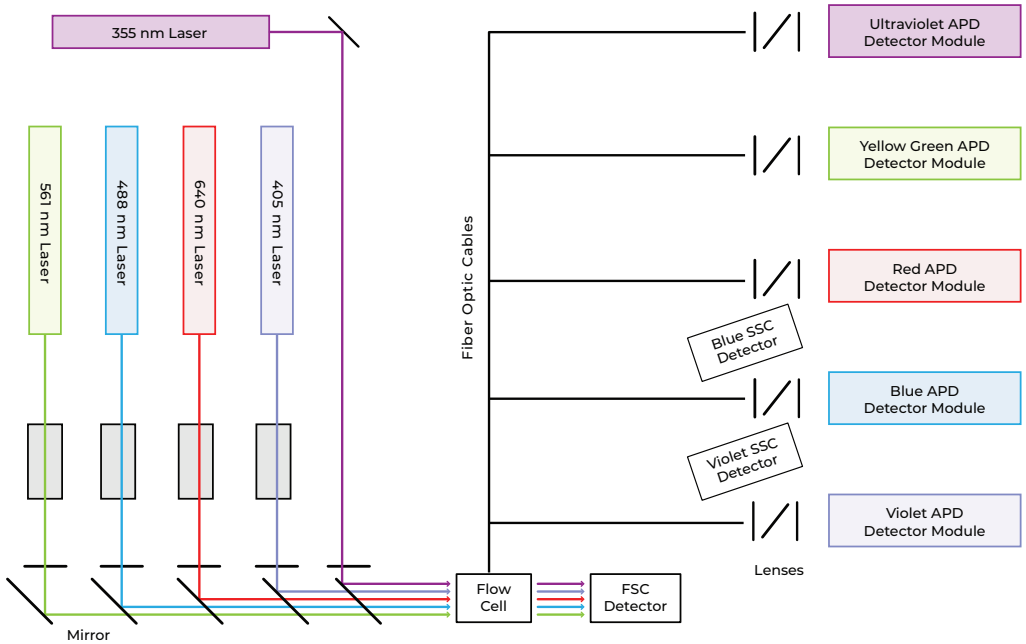

Supplemental Figure 1. Schematic of Optical Layout for 5 Laser Aurora
The Cytek Aurora used to develop the panel was equipped with 5 lasers. The optical paths for each of the 5 lasers (UV 355 nm, Violet 405 nm, Blue 488 nm, Yellow Green 561 nm, and Red 640 nm) are represented. The lasers are spatially separated, each has an independent optical path, and through optical fibers light is directed to individual detector modules using avalanche photodiodes (APD) as photodetectors.

UV (355 nm - 20 mW)			Violet (405 nm - 100 mW)			Blue (488 nm - 50 mW)			Yellow Green (561 nm - 50 mW)			Red (640 nm - 80 mW)		
Detector	Center Wavelength	Bandwidth	Detector	Center Wavelength	Bandwidth	Detector	Center Wavelength	Bandwidth	Detector	Center Wavelength	Bandwidth	Detector	Center Wavelength	Bandwidth
1	372.5	15	1	427.5	15	1	508	20	1	577	20	1	661	17
2	387.5	15	2	443	15	2	524.5	17	2	598	20	2	679	18
3	427.5	15	3	458	15	3	541.5	17	3	615	20	3	697	19
4	443	15	4	473	15	4	580.5	19	4	661	17	4	717	20
5	458	15	5	508	20	5	598	20	5	679	18	5	738	21
6	473	15	6	524.5	17	6	615	20	6	697	19	6	760	23
7	514	28	7	541.5	17	7	661	17	7	720	29	7	783	23
8	542	28	8	580.5	19	8	679	18	8	749.5	30	8	811.5	34
9	581.5	31	9	598	20	9	697	19	9	779.5	30			
10	612.5	31	10	615	20	10	717	20	10	811.5	34			
11	664	27	11	664	27	11	738	21						
12	691.5	28	12	691.5	28	12	760	23						
13	720	29	13	720	29	13	783	23						
14	749.5	30	14	749.5	30	14	811.5	34						
15	779.5	30	15	779.5	30									
16	811.5	34	16	811.5	34									

Supplemental Table 1. Detector Modules Configuration for 5 Laser Aurora
The detectors and wavelength information of the bandpass filters associated with each laser detector are listed. UV laser detector module: 16 detectors (UV1-UV16); violet laser detector module: 16 detectors (V1-V16); blue detector module: 14 detectors (B1-B14); yellow green laser detector module: 10 detectors (YG1-YG10); red laser detector module: 8 detectors (R1-R8). Wavelengths of the filters are continuous, except for wavelengths associated with the laser line emissions (UV2-UV3, UV6-UV7, UV8-UV9, UV10-UV11, V4-V5, V7-V8, V10-V11, B3-B4, B6-B7, YG3-YG4).

STRATEGY FOR FLUOROCHROME SELECTION AND FLUOROCHROME CHARACTERIZATION

The first step for the panel development consisted of identifying the best possible 40 fluorochrome combination. The following criteria were applied for this selection:

- **Unique spectra**: The spectra of over 65 commercially available fluorochromes were analyzed. Fluorochromes with peak emissions occurring in different channels were identified, as well as fluorochromes that, despite sharing the same peak emission, have a different spectrum. Next, the fluorochrome signature uniqueness, determined by comparing the full spectrum across all 64 detectors, was quantified using an index developed by Cytek Biosciences, and available through the SpectroFlo software, called Similarity Index. This index uses the cosine of the angle between the vectors defined for each fluorochrome in a 64-dimensional space to compare two signatures. This index ranges from 0 to 1; 0 indicating the 2 fluorochromes do not share any spectral characteristics, and 1 indicating that the spectra are identical. Based on testing of multiple fluorochrome combinations, it was determined that similarity indices of 0.98 or less indicated that fluorochromes were different enough to be used together.
- **Overall fluorochrome combination compatibility**: This assessment was guided by a Cytek developed metric, also available in the SpectroFlo software, called the Complexity Index. This index measures the interference among a specific combination of fluorochromes and predicts the impact on the autofluorescence distribution of the spectrally unmixed results while also considering spillover (1,2). The lower the complexity index, the higher the probability that the fluorochrome combination will work together and yield high resolution data through reduced spread. Similarity Index and Complexity Index together provide a measure of the degree of overall interferences due to spillover between and among fluorochromes. Note: Similarity and Complexity Indices are currently under patent application. Once issued, formulas will be made publicly available.

Based on the above criteria, 40 fluorochromes were selected (**Supplemental Figures 2A and 2B**), minimizing fluorochrome pairs with very high similarity indices and providing the lowest complexity index (complexity index=54). The distribution of the selected fluorochromes across lasers and emission wavelengths is presented in **Supplemental Table 2**. The pairs with the highest similarity indices, and hence higher predicted spread between them, were BB515 and FITC (0.98), BV421 and Super Bright 436 (0.97), Super Bright 436 and eFluor 450 (0.94), and Alexa Fluor 647 and Spark NIR 685 (0.92). Additionally, an effort was made to minimize the use of custom reagents. Out of the 40 fluorochromes used in this panel, only one is custom, and is commercially available through BioLegend® (San Diego, CA): PE-Fire 810. This fluorochrome was selected to take advantage of the high detection efficiency that APDs have in the far-red range of emission.

Next, the selected 40 fluorochromes were ranked for brightness using anti-CD4 single stained cells available for 38 of the fluorochromes, and using HLA-DR PE-Fire 810 and CD38 APC-Fire 810 (**Supplemental Figure 2C**). Finally, spread was assessed by calculating the SSM using FlowJo™ version 10.6.2 with the same data used to rank fluorochrome brightness (**Supplemental Figure 2D**). As expected, based on the spectrum and similarity indices, the pairs with the highest SSM values were BB515 into FITC (SSM=29) and FITC into BB515 (SSM=23). Other combinations showing high spread were APC into Alexa Fluor 647 (SSM=14.2), Spark Blue 550 into FITC (SSM=13.2), BUV661 into APC (SSM=11.7), and BV480 into BV510 (SSM=11.45). Of the 1,560 combinations of fluorochromes, only 13 had an SSM greater than 10, with the majority (91%) having SSM values of 4 or less. Differences of 10-fold in the SSM are equivalent to approximately a log greater spread in the data (3).

PANEL DESIGN STRATEGY

Basic principles for best practices for panel design based on previously published approaches used for conventional cytometry were followed (4). Antigens were classified as primary, secondary, and tertiary based on level of expression, and co-expression was assessed using a schematic gating tree and researching the expression for each marker on the subsets of interest. Next, fluorochrome assignment was made following these steps:

Step 1: Assignment of Fluorochromes with Limited Conjugate Availability

In order to minimize the use of custom reagents, there were limitations on the fluorochrome assignment for certain markers:

- HLA-DR PE-Fire 810, a custom reagent, was readily available through BioLegend® and fit into the panel.
- CD38 APC-Fire 810 was originally a custom conjugate but is now commercially available (**Supplemental Table 4**).

2A

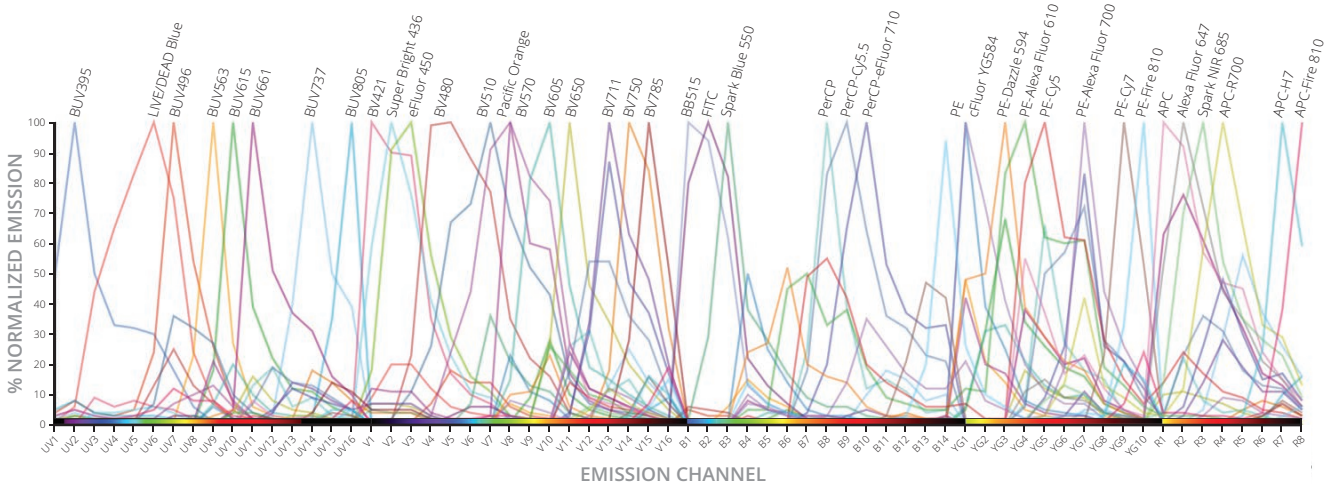

2B

Similarity Index Color Coding

0 — 0.5 — 1

	BUV395	LIVE/DEAD Blue	BUV496	BUV563	BUV615	BUV661	BUV737	BUV805	BV421	Super Bright 436	eFluor 450	BV480	BV510	Pacific Orange	BV570	BV605	BV650	BV711	BV750	BV785	BB515	FITC	Spark Blue 550	PerCP	PerCP-Cy5.5	PerCP-eFluor 710	PE	cFluor YG584	PE-Dazzle 594	PE-Alexa Fluor 610	PE-Cy5	PE-Alexa Fluor 700	PE-Cy7	PE-Fire 810	APC	Alexa Fluor 647	Spark NIR 685	APC-R700	APC-H7	APC-Fire 810
BUV395	1																																								
LIVE/DEAD Blue	0.51	1																																							
BUV496	0.25	0.58	1																																						
BUV563	0.05	0.09	0.29	1																																					
BUV615	0.03	0.03	0.08	0.4	1																																				
BUV661	0.04	0.03	0.02	0.06	0.35	1																																		
BUV737	0.03	0.02	0.01	0.01	0.1	0.37	1																																	
BUV805	0.11	0.06	0.03	0.01	0.04	0.1	0.39	1																																
BV421	0.05	0.26	0.09	0.01	0	0	0	0.01	1																															
Super Bright 436	0.03	0.25	0.1	0.01	0	0	0	0	0.97	1																														
eFluor 450	0	0.21	0.08	0	0	0	0	0	0.85	0.94	1																													
BV480	0.02	0.2	0.38	0.07	0.04	0.01	0	0	0.28	0.36	0.46	1																												
BV510	0.02	0.2	0.48	0.22	0.14	0.04	0.02	0	0.17	0.22	0.27	0.84	1																											
Pacific Orange	0.01	0.07	0.22	0.14	0.15	0.04	0.02	0	0.07	0.09	0.11	0.58	0.88	1																										
BV570	0.01	0.04	0.09	0.37	0.29	0.06	0.02	0	0.15	0.16	0.14	0.26	0.54	0.77	1																									
BV605	0.01	0.02	0.05	0.2	0.51	0.17	0.05	0.01	0.06	0.06	0.06	0.16	0.4	0.62	0.7	1																								
BV650	0	0.02	0.02	0.04	0.26	0.4	0.13	0.02	0.09	0.09	0.08	0.06	0.16	0.25	0.25	0.53	1																							
BV711	0	0.02	0	0.01	0.07	0.25	0.41	0.09	0.09	0.09	0.08	0.03	0.06	0.08	0.07	0.17	0.45	1																						
BV750	0	0.01	0	0	0.03	0.09	0.37	0.14	0.05	0.05	0.04	0.02	0.04	0.05	0.04	0.1	0.23	0.69	1																					
BV785	0	0.01	0	0	0.02	0.05	0.25	0.21	0.07	0.07	0.07	0.02	0.03	0.03	0.03	0.07	0.15	0.49	0.82	1																				
BB515	0.01	0.01	0.07	0.04	0	0	0	0	0	0	0	0.06	0.01	0	0.01	0	0	0	0	0	1																		
FITC	0.01	0.01	0.09	0.06	0.01	0	0	0	0.01	0.01	0.01	0.1	0.06	0.04	0.03	0.01	0	0	0	0	0.98	1																	
Spark Blue 550	0.02	0.01	0.09	0.15	0.05	0.01	0.01	0	0.02	0.03	0.03	0.22	0.3	0.33	0.24	0.16	0.06	0.02	0.01	0.01	0.53	0.67	1																
PerCP	0	0.01	0.01	0.04	0.22	0.38	0.15	0.03	0.01	0.01	0.01	0.01	0.01	0.03	0.06	0.18	0.38	0.23	0.13	0.07	0.01	0.01	0.06	1															
PerCP-Cy5.5	0	0	0.01	0.03	0.19	0.39	0.31	0.06	0	0.01	0.01	0.01	0.02	0.04	0.06	0.17	0.38	0.5	0.28	0.19	0.01	0	0.06	0.81	1														
PerCP-eFluor 710	0	0	0	0.02	0.12	0.29	0.39	0.07	0	0	0	0	0.02	0.04	0.05	0.14	0.31	0.65	0.38	0.26	0	0	0.05	0.46	0.86	1														
PE	0.01	0	0.03	0.51	0.25	0.03	0	0	0	0.01	0.01	0.05	0.12	0.16	0.52	0.28	0.05	0.01	0	0	0.05	0.09	0.24	0.06	0.05	0.03	1													
cFluor YG584	0	0	0.01	0.46	0.36	0.06	0	0	0	0	0	0.02	0.04	0.07	0.42	0.3	0.06	0.01	0	0	0.01	0.01	0.05	0.07	0.06	0.04	0.88	1												
PE-Dazzle 594	0.01	0	0.02	0.36	0.58	0.13	0.02	0	0	0	0	0.04	0.09	0.14	0.41	0.47	0.16	0.04	0.01	0.01	0.03	0.06	0.19	0.27	0.25	0.16	0.67	0.72	1										
PE-Alexa Fluor 610	0	0	0	0.16	0.54	0.29	0.06	0	0	0	0	0.01	0.04	0.08	0.22	0.4	0.31	0.11	0.04	0.03	0.01	0.02	0.1	0.54	0.55	0.38	0.28	0.37	0.78	1									
PE-Cy5	0	0	0	0.07	0.32	0.42	0.1	0.01	0	0	0	0	0.01	0.02	0.09	0.21	0.29	0.14	0.05	0.03	0.01	0.01	0.06	0.77	0.72	0.47	0.14	0.19	0.43	0.82	1								
PE-Alexa Fluor 700	0	0	0	0.12	0.18	0.19	0.2	0.02	0	0	0	0.01	0.02	0.03	0.12	0.14	0.14	0.25	0.12	0.07	0.01	0.02	0.06	0.3	0.63	0.73	0.23	0.24	0.3	0.47	0.51	1							
PE-Cy7	0	0	0	0.01	0.04	0.05	0.14	0.08	0	0	0	0	0	0	0.01	0.03	0.04	0.11	0.15	0.17	0	0	0.01	0.09	0.23	0.29	0.02	0.03	0.05	0.11	0.14	0.35	1						
PE-Fire 810	0	0	0	0.11	0.07	0.03	0.09	0.08	0	0	0	0.01	0.01	0.02	0.1	0.06	0.03	0.06	0.07	0.11	0.01	0.02	0.06	0.07	0.17	0.23	0.23	0.2	0.18	0.14	0.12	0.28	0.7	1					
APC	0	0.01	0	0.03	0.17	0.78	0.24	0.02	0	0	0	0	0.02	0.03	0.05	0.14	0.37	0.23	0.07	0.04	0	0	0.01	0.34	0.37	0.29	0.04	0.08	0.16	0.35	0.52	0.21	0.05	0.04	1				
Alexa Fluor 647	0	0.01	0	0.01	0.05	0.71	0.22	0.02	0	0	0	0	0	0	0.01	0.03	0.18	0.18	0.02	0.01	0	0	0	0.23	0.29	0.23	0.01	0.03	0.06	0.14	0.32	0.12	0.03	0.02	0.9	1			
Spark NIR 685	0	0.01	0	0.01	0.05	0.65	0.28	0.03	0	0	0	0	0	0.01	0.01	0.03	0.19	0.27	0.06	0.04	0	0	0	0.21	0.35	0.31	0.01	0.02	0.04	0.11	0.28	0.15	0.04	0.02	0.75	0.92	1		
APC-R700	0	0.01	0	0.01	0.06	0.5	0.45	0.04	0	0	0	0.01	0.01	0.02	0.05	0.18	0.39	0.11	0.07	0	0	0	0	0.17	0.41	0.49	0.01	0.02	0.06	0.17	0.28	0.39	0.1	0.05	0.57	0.63	0.78	1	
APC-H7	0	0	0	0	0.01	0.12	0.3	0.21	0	0	0	0.01	0.01	0.01	0	0.01	0.05	0.18	0.18	0.23	0	0	0	0.03	0.12	0.17	0	0	0.01	0.02	0.06	0.1	0.27	0.18	0.14	0.15	0.22	0.28	1	
APC-Fire 810	0.04	0.11	0.15	0.09	0.06	0.13	0.22	0.26	0.03	0.03	0.03	0.07	0.1	0.06	0.06	0.05	0.07	0.14	0.13	0.19	0.02	0.02	0.04	0.04	0.1	0.14	0.02	0.01	0.03	0.04	0.07	0.09	0.21	0.24	0.15	0.14	0.17	0.21	0.76	1
	BUV395	LIVE/DEAD Blue	BUV496	BUV563	BUV615	BUV661	BUV737	BUV805	BV421	Super Bright 436	eFluor 450	BV480	BV510	Pacific Orange	BV570	BV605	BV650	BV711	BV750	BV785	BB515	FITC	Spark Blue 550	PerCP	PerCP-Cy5.5	PerCP-eFluor 710	PE	cFluor YG584	PE-Dazzle 594	PE-Alexa Fluor 610	PE-Cy5	PE-Alexa Fluor 700	PE-Cy7	PE-Fire 810	APC	Alexa Fluor 647	Spark NIR 685	APC-R700	APC-H7	APC-Fire 810
→ **Complexity Index:**	**53.72**																																							

2C

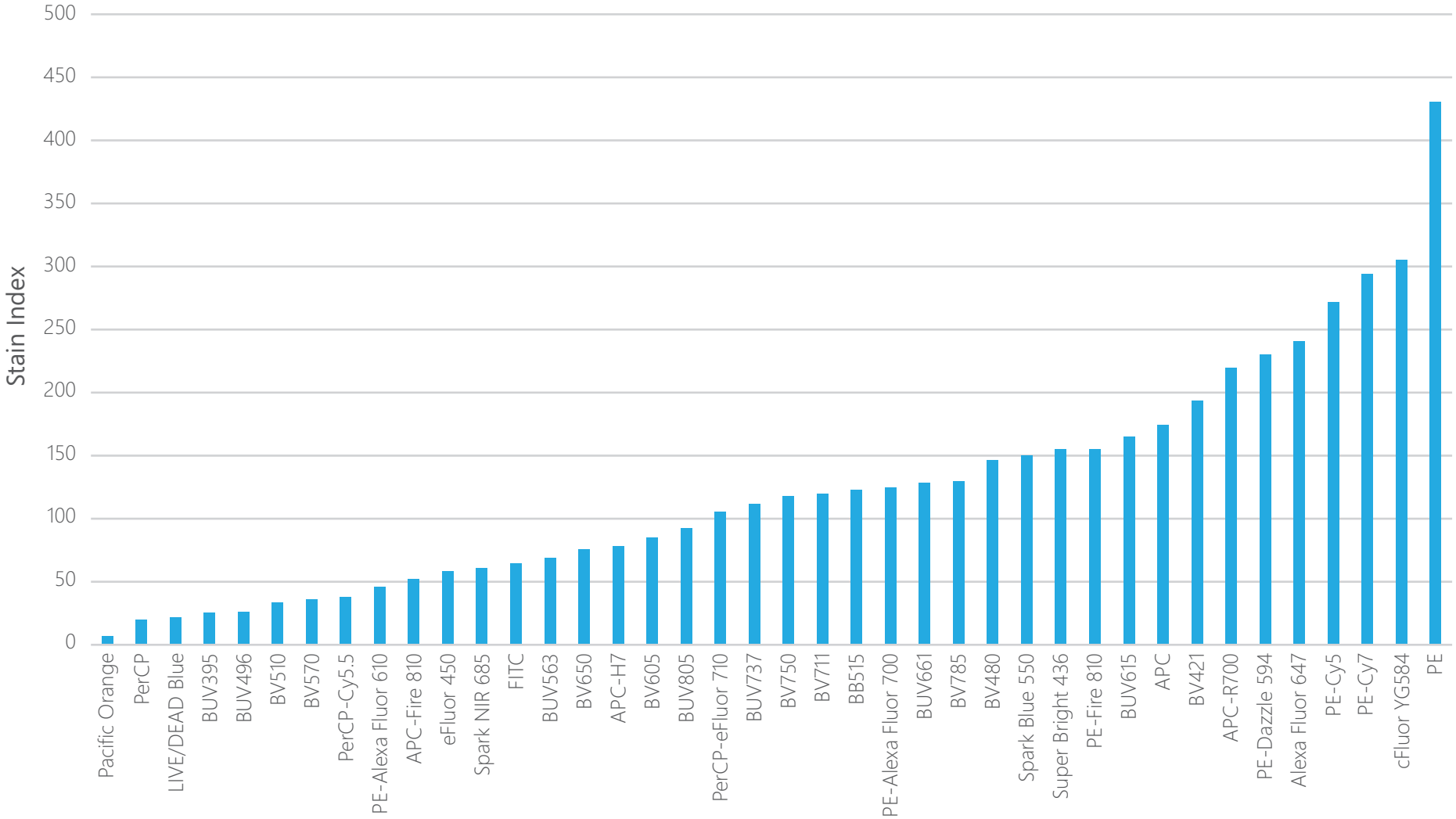
Stain Index
500
450
400
350
300
250
200
150
100
50
0
Pacific Orange
PerCP
LIVE/DEAD Blue
BUV395
BUV496
BV510
BV570
PerCP-Cy5.5
PE-Alexa Fluor 610
APC-Fire 810
eFluor 450
Spark NIR 685
FITC
BUV563
BV650
APC-H7
BV605
BUV805
PerCP-eFluor 710
BUV737
BV750
BV711
BB515
PE-Alexa Fluor 700
BUV661
BV785
BV480
Spark Blue 550
Super Bright 436
PE-Fire 810
BUV615
APC
BV421
APC-R700
PE-Dazzle 594
Alexa Fluor 647
PE-Cy5
PE-Cy7
cFluor YG584
PE

2D

	BUV395	LIVE/DEAD Blue	BUV496	BUV563	BUV615	BUV661	BUV737	BUV805	BV421	Super Bright 436	eFluor 450	BV480	BV510	Pacific Orange	BV570	BV605	BV650	BV711	BV750	BV785	BB515	FITC	Spark Blue 550	PerCP	PerCP-Cy5.5	PerCP-eFluor 710	PE	cFluor YG584	PE-Dazzle 594	PE-Alexa Fluor 610	PE-Cy5	PE-Alexa Fluor 700	PE-Cy7	PE-Fire 810	APC	Alexa Fluor 647	Spark NIR 685	APC-R700	APC-H7	APC-Fire 810	Sum
BUV395		2.19	0.00	0.00	0.04	0.00	0.00	0.55	0.00	0.00	1.14	0.00	3.27	0.00	0.87	0.74	1.43	1.12	0.65	0.65	0.00	0.00	0.00	0.00	0.00	0.00	0.00	0.00	0.00	0.00	0.09	1.48	0.00	0.78	0.74	0.00	1.95	0.00	0.00	0.58	0.00	18.27
LIVE/DEAD Blue	4.55		7.51	1.32	0.50	0.81	0.34	0.00	3.21	4.32	5.76	2.45	9.64	5.51	1.75	1.05	1.39	0.00	0.00	0.26	2.66	1.11	2.48	0.00	0.73	0.00	1.79	1.96	2.99	0.91	1.69	0.26	0.00	0.00	1.07	0.00	0.00	0.26	0.33	0.00	68.61
BUV496	0.81	1.09		1.77	0.81	0.44	0.25	0.39	0.58	1.55	0.98	1.53	5.91	5.30	1.96	1.02	0.61	0.32	0.03	0.33	6.31	6.00	1.38	0.00	0.55	0.50	0.04	0.67	0.00	0.00	0.00	0.43	0.00	0.00	0.00	0.00	0.00	0.00	0.00	0.00	0.00	41.56
BUV563	0.46	0.62	0.00		1.50	0.81	0.41	0.71	0.00	0.54	0.00	0.68	2.24	1.55	1.25	0.75	0.61	0.00	0.00	0.00	0.00	1.94	0.98	2.02	1.08	0.45	4.15	7.32	4.38	4.12	2.90	0.65	0.01	0.00	1.17	2.22	1.12	0.39	0.00	0.33	47.37
BUV615	0.67	0.67	0.00	2.25		2.84	2.60	3.02	0.28	1.04	0.04	0.28	0.00	0.00	0.00	1.88	1.31	1.00	1.07	0.79	1.17	2.18	0.44	2.68	2.15	1.97	5.68	2.81	6.14	4.62	3.81	1.75	1.01	0.52	2.58	3.75	2.15	1.28	0.55	0.46	67.41
BUV661	0.58	0.58	0.00	0.00	0.69		3.35	3.08	0.80	1.05	0.69	0.00	0.00	0.98	0.00	0.82	2.59	1.80	1.35	1.17	1.97	0.00	0.68	3.16	2.33	2.42	1.16	0.49	3.69	3.79	5.54	2.57	1.13	0.67	5.40	11.70	6.74	2.90	1.70	1.33	78.88
BUV737	0.80	0.98	0.00	0.00	0.00	0.74		6.22	0.79	0.00	0.00	0.00	0.00	0.00	0.09	0.00	0.00	1.92	3.20	2.23	0.00	0.00	0.00	1.97	2.73	4.00	0.68	0.00	0.00	0.88	0.00	2.72	1.16	1.08	1.72	2.96	3.91	4.06	2.44	1.98	49.26
BUV805	1.15	1.08	0.00	0.00	0.40	0.00	1.33		0.74	0.81	0.59	0.80	1.14	0.00	0.00	0.00	0.04	0.59	0.49	1.57	0.00	0.00	0.00	0.00	0.00	0.54	0.00	0.58	0.05	0.00	0.00	0.02	0.72	0.69	0.77	0.57	0.70	0.47	1.60	2.10	19.54
BV421	0.27	0.93	1.52	0.39	0.24	0.00	0.00	0.00		9.84	5.25	2.42	6.09	4.76	1.44	0.78	0.00	0.00	0.00	0.42	1.69	0.00	0.70	0.00	0.00	0.01	0.58	0.51	0.00	0.59	0.00	0.20	0.00	0.28	0.00	0.00	0.03	0.00	0.00	0.29	39.25
Super Bright 436	0.20	0.83	0.00	0.00	0.00	0.00	0.18	0.00	5.16		4.73	2.52	6.54	5.59	1.51	0.77	0.44	0.41	0.00	0.00	0.98	2.73	0.06	0.00	0.03	0.00	0.30	0.71	0.00	0.76	0.00	0.00	0.00	0.19	0.00	1.08	0.00	0.40	0.00	0.00	36.12
eFluor 450	0.00	1.11	0.00	0.00	0.00	0.00	0.00	0.00	5.45	10.36		2.78	6.25	5.21	1.85	0.67	0.94	0.61	0.59	0.95	0.00	0.00	0.00	0.55	0.00	0.00	0.53	0.00	0.00	0.00	0.00	0.00	0.36	0.34	0.56	0.00	0.87	0.41	0.38	0.42	41.16
BV480	0.30	0.76	3.40	1.90	0.61	0.26	0.18	0.28	1.98	3.74	2.50		11.46	10.45	4.14	2.15	0.71	0.62	0.58	0.58	7.26	7.27	1.95	0.52	0.51	0.00	1.05	1.22	1.30	0.73	0.54	0.00	0.00	0.01	0.00	0.00	0.87	0.23	0.01	0.33	70.36
BV510	0.26	1.14	1.36	2.35	1.13	0.67	0.29	0.78	1.36	2.81	1.66	2.41		8.76	4.45	2.55	1.36	0.92	0.65	0.83	3.29	0.00	0.71	0.00	1.22	0.00	1.41	1.02	1.10	1.39	0.00	0.00	0.31	0.30	0.00	2.40	0.00	0.82	0.00	0.53	50.23
Pacific Orange	0.00	0.16	0.00	1.11	0.00	0.00	1.10	0.00	2.18	0.00	0.00	1.72	0.00		5.15	3.03	2.11	1.48	1.22	0.86	0.00	0.00	0.00	0.00	0.00	0.00	1.05	0.00	0.00	1.70	0.00	0.00	0.00	0.00	1.14	1.46	0.00	0.00	0.00	0.00	25.48
BV570	0.00	0.97	0.00	0.50	0.78	0.42	0.39	0.31	1.95	2.91	1.70	1.05	0.00	2.61		2.64	1.71	0.64	0.96	0.88	0.00	0.00	0.00	2.05	1.24	0.03	2.66	3.35	3.63	3.48	2.43	0.88	0.00	0.29	1.62	2.07	0.91	0.50	0.00	0.00	45.56
BV605	0.17	0.94	0.00	0.00	1.64	0.95	0.87	1.01	1.08	1.60	0.89	0.28	0.00	0.00	1.49		2.14	1.40	1.43	1.42	0.00	0.00	0.00	2.55	1.90	1.42	6.12	3.92	5.72	4.73	3.64	1.50	0.78	0.55	2.06	3.62	1.84	0.84	0.21	0.23	58.92
BV650	0.00	1.14	0.00	0.00	0.43	1.30	0.93	1.21	1.02	2.50	1.32	0.60	2.03	1.30	0.00	1.17		1.80	2.06	1.80	0.00	0.00	0.00	1.57	1.53	1.42	1.06	0.00	2.60	2.57	2.65	1.40	0.62	0.53	2.85	4.73	3.20	1.14	0.77	0.52	49.76
BV711	0.26	0.86	0.00	0.00	0.00	0.57	1.77	2.29	1.40	2.37	1.20	0.70	0.58	1.30	0.32	0.00	0.82		3.96	3.64	0.98	0.00	0.46	1.27	1.97	1.99	0.80	0.00	0.00	0.79	0.66	3.00	0.86	0.66	1.68	3.28	3.47	2.91	1.42	1.15	49.39
BV750	0.15	0.98	0.00	0.00	0.00	0.20	2.49	2.84	1.14	2.01	0.73	0.84	1.49	0.00	0.47	0.48	0.39	1.51		5.43	0.00	0.85	0.34	0.00	0.95	1.11	0.00	0.53	0.88	0.62	0.66	0.72	0.75	0.60	0.34	1.14	1.28	1.28	1.29	1.19	35.66
BV785	0.34	0.75	0.00	0.00	0.00	0.17	1.20	3.03	1.54	2.14	1.21	0.46	0.87	0.38	0.00	0.34	0.54	0.65	3.01		0.90	0.00	0.00	0.82	0.39	0.56	0.38	0.37	0.00	0.54	0.41	0.43	0.73	0.62	0.60	0.67	0.92	0.44	1.48	1.30	28.20
BB515	0.00	0.58	0.00	0.23	0.00	0.13	0.00	0.00	0.00	0.78	0.57	0.90	5.13	5.58	1.89	0.79	0.38	0.00	0.00	0.30		28.98	7.65	0.96	0.57	0.33	1.85	1.83	1.65	1.07	1.08	0.17	0.20	0.14	0.23	0.30	0.49	0.00	0.00	0.00	64.74
FITC	0.00	0.00	0.00	0.00	0.44	0.29	0.00	0.00	0.00	1.26	0.00	1.07	3.94	5.56	1.85	0.71	0.81	0.64	0.00	0.37	23.33		6.60	0.00	0.00	0.71	2.02	2.31	1.45	1.69	1.32	0.62	0.00	0.00	1.50	0.00	1.52	0.36	0.00	0.60	60.96
Spark Blue 550	0.12	1.13	1.31	0.10	0.51	0.00	0.26	0.30	0.45	0.00	0.00	0.74	2.90	6.50	3.66	1.56	1.02	0.68	0.61	0.49	10.25	13.17		3.10	2.15	1.42	4.08	3.58	3.68	2.68	2.56	0.77	0.58	0.56	0.94	2.30	1.52	0.48	0.00	0.00	76.13
PerCP	0.00	0.00	0.00	0.00	0.00	0.90	1.04	1.12	1.71	0.00	0.00	0.91	0.00	3.11	0.00	0.13	3.37	1.12	1.13	1.34	0.00	1.78	0.00		5.24	3.28	1.70	0.00	5.61	6.20	7.28	1.96	1.16	0.00	4.72	5.61	4.16	1.68	0.00	0.92	67.17
PerCP-Cy5.5	0.00	1.83	0.00	0.00	0.00	1.19	1.77	2.34	0.94	0.00	0.00	0.00	0.00	0.00	0.00	0.00	3.02	2.84	2.68	2.48	0.00	4.39	1.28	9.48		5.63	1.84	0.00	4.93	5.86	6.79	4.91	2.28	1.91	4.69	8.19	6.32	2.90	1.67	1.75	93.92
PerCP-eFluor 710	0.00	1.18	0.00	0.00	0.00	0.69	1.66	2.14	0.69	0.00	0.39	0.00	0.00	0.00	0.92	0.36	1.60	4.63	3.23	2.87	1.96	0.00	0.62	6.01	6.89		2.17	0.00	2.55	2.96	3.37	8.12	2.57	2.31	2.78	5.66	5.14	3.68	2.03	1.60	80.80
PE	0.00	0.40	0.00	1.22	0.45	0.35	0.14	0.16	0.29	0.45	0.36	0.22	0.29	0.96	2.42	1.34	0.79	0.42	0.28	0.13	1.22	2.02	0.73	2.66	1.54	0.93		9.88	6.10	5.37	3.89	0.91	0.40	0.29	1.39	2.50	1.29	0.46	0.00	0.19	52.42
cFluor YG584	0.00	0.00	0.00	0.57	0.41	0.30	0.01	0.28	0.00	0.96	0.00	0.00	1.29	0.39	1.54	1.08	0.85	0.36	0.36	0.26	0.00	1.51	0.36	2.34	1.62	1.05	4.05		5.64	5.36	3.92	1.43	0.76	0.39	1.62	2.38	1.68	0.58	0.00	0.16	43.53
PE-Dazzle 594	0.27	0.75	0.00	0.00	0.99	0.62	0.38	0.41	0.00	0.46	0.00	0.00	1.56	1.23	1.25	1.71	1.57	0.96	0.64	0.53	3.53	3.46	1.65	4.12	2.96	1.94	7.96	6.71		5.85	4.78	2.03	1.03	0.64	2.59	3.59	2.61	0.88	0.00	0.20	69.84
PE-Alexa Fluor 610	0.00	0.70	2.63	0.00	0.88	1.00	0.50	0.66	0.00	0.00	0.00	0.00	2.91	2.68	1.20	1.36	1.67	1.83	0.68	0.66	2.37	4.15	1.56	6.28	4.96	3.47	3.19	3.54	6.24		6.40	4.41	1.96	1.33	5.35	6.97	5.25	1.63	0.74	0.00	89.13
PE-Cy5	0.00	0.57	0.00	0.00	0.77	0.94	0.71	0.61	0.28	0.27	0.28	0.26	1.73	2.08	0.00	0.98	2.97	3.12	1.13	1.05	4.86	5.31	2.46	10.65	5.41	4.86	4.82	1.74	9.18	10.68		5.92	1.94	1.33	5.39	10.59	6.28	2.11	0.92	0.63	112.84
PE-Alexa Fluor 700	0.00	0.37	0.00	0.00	0.20	0.38	0.81	0.82	0.00	0.91	0.00	0.39	0.00	1.43	0.85	0.53	0.81	2.97	1.33	1.18	1.52	0.00	0.57	2.70	3.72	5.67	3.41	2.21	2.69	2.51	1.86		2.61	1.87	1.75	2.76	2.99	1.57	0.76	0.29	54.42
PE-Cy7	0.00	0.53	0.00	0.00	0.00	0.23	0.89	1.66	0.00	0.41	0.18	0.00	0.00	0.00	0.43	0.00	0.39	3.42	0.96	1.92	1.22	0.86	0.39	0.90	2.47	4.84	1.85	0.53	1.14	1.10	0.55	3.67		3.81	0.82	1.75	1.56	1.17	1.53	1.49	42.65
PE-Fire 810	0.15	1.41	3.29	1.37	0.30	0.27	0.69	3.55	0.00	1.09	0.44	0.00	1.90	0.83	1.11	0.52	0.03	1.82	1.04	2.66	2.81	2.23	0.90	2.31	2.75	4.26	5.09	2.36	2.70	2.69	1.83	2.30	4.31		1.36	2.19	1.94	0.92	0.94	1.61	67.99
APC	0.00	1.07	0.00	0.00	0.31	0.95	1.09	0.93	0.00	0.07	0.00	0.00	0.00	0.00	0.68	0.64	3.30	1.29	1.20	1.08	0.00	1.39	0.61	2.37	3.49	1.63	1.43	1.08	4.03	4.62	7.60	2.38	1.09	0.63		14.17	8.37	2.82	1.97	1.31	73.59
Alexa Fluor 647	0.00	0.85	0.00	0.00	0.00	0.40	0.60	0.41	0.38	0.00	0.27	0.00	0.00	0.00	0.00	0.53	1.64	0.68	0.49	0.37	0.00	0.00	0.30	1.83	1.41	1.13	1.05	0.38	2.67	3.41	4.77	1.58	0.75	0.40	5.42		7.24	3.03	1.94	1.17	45.11
Spark NIR 685	0.00	0.00	0.00	0.00	0.00	0.45	0.72	0.81	0.00	0.94	0.00	0.74	1.82	1.67	1.16	0.00	1.71	0.87	0.87	0.74	3.07	0.00	1.64	1.67	1.45	1.07	0.39	0.00	2.12	1.60	1.92	1.69	1.07	0.51	4.82	10.61		3.25	2.22	1.44	53.05
APC-R700	0.14	0.40	0.90	0.00	0.18	0.56	0.94	0.85	0.53	0.51	0.00	0.00	0.00	0.00	0.50	0.23	1.18	3.71	1.22	1.13	0.68	0.77	0.00	2.16	3.36	4.24	1.70	0.00	1.10	1.32	1.63	9.39	1.67	0.98	3.33	6.88	6.81		3.59	0.00	62.58
APC-H7	0.00	1.39	0.23	0.00	0.30	0.00	0.55	1.87	0.05	0.00	0.00	0.00	0.00	0.00	0.00	0.39	0.68	0.82	0.75	1.93	0.00	0.00	0.00	0.00	0.62	0.69	0.00	0.00	1.38	0.00	0.66	0.62	2.48	1.46	0.69	1.09	0.05	0.50		0.00	19.21
APC-Fire 810	0.69	1.25	5.16	2.00	0.00	0.26	0.67	4.72	0.85	0.00	0.85	0.39	0.00	0.61	0.00	0.07	0.00	0.54	0.98	1.52	2.42	4.03	0.00	0.00	0.00	1.14	1.15	0.53	0.45	1.54	0.03	0.77	1.52	1.99	1.44	3.14	1.69	0.70	3.13		46.24
Sum	12.32	32.17	27.32	17.09	14.51	20.12	31.09	49.33	36.84	57.71	33.71	27.13	80.97	86.34	46.20	33.77	46.92	49.50	40.82	46.81	86.45	96.10	37.51	78.69	69.90	64.73	79.17	62.13	97.78	98.80	88.66	70.18	37.59	28.58	74.38	134.30	94.93	47.05	34.20	25.53	4394.65

Spillover Spreading Matrix Color Coding: 0 3 9

Supplemental Figure 2. Fluorochrome Selection Evaluations

A series of evaluations were conducted to identify the best combination of 40 fluorochromes that would provide unique spectral signatures, adequate signal intensities, and minimal spread into neighboring channels. **(A)** Spectral signatures of 40 fluorochromes visualized using the Cytek Spectrum Viewer. All signatures were normalized to peak channels for direct comparison. **(B)** Results of the Similarity Index Matrix (SIM) which measures how similar two spectra are to each other. A value of "1" indicates there is virtually no difference between 2 fluorochromes, while a value of "0" indicates two fluorochromes are completely unique. The chart displays the numerical value for each pair of fluorochromes identified for use in the OMIP-069 panel. Based on the testing of multiple fluorochrome combinations (data not shown), it was determined that any fluorochrome pair having a similarity index of 0.98 or lower could be accurately unmixed with appropriate single stained controls. At the bottom of the matrix, the complexity index (blue arrow), a metric to evaluate the complexity of the entire combination of fluorochromes, is displayed. **(C)** Display of stain indices calculated for each of the fluorochromes in the panel, ranked from low to high. Stain indices were calculated using CD4 stained cells labeled with the indicated fluorochromes, except for PE-Fire 810 (HLA-DR) and APC-Fire 810 (CD38). **(D)** SSM calculated for all fluorochromes in the panel. Spillover values are color-coded as follows: white: <3, shades of orange: 3-9, and red: >9.

Approx. Emission Wavelength (nm)	UV	Violet	Blue	Yellow Green	Red
395	BUV395				
420		BV421			
440		Super Bright 436			
450	Viability UV (L/D Blue)	eFluor 450			
480		BV480			
500	BUV496		BB515		
520		BV510	FITC		
550		Pacific Orange	Spark Blue 550		
570	BUV563	BV570/Pacific Orange			
580				cFluor YG584/PE	
600	BUV615	BV605		PE-Dazzle 594	
660	BUV661	BV650		PE-Alexa Fluor 610	APC
680			PerCP	PE-Cy5	Alexa Fluor 647
690			PerCP-Cy5.5		Spark NIR 685
700		BV711	PerCP-eFluor 710	PE-Alexa Fluor 700	APC-R700
730	BUV737				
750		BV750			
780		BV785		PE-Cy7	APC-H7
800	BUV805			PE-Fire 810	APC-Fire 810

Supplemental Table 2. Fluorochrome Optical Layout
Fluorochromes intended for use in the OMIP-069 panel are presented by primary laser excitation (columns) and approximate emission wavelengths of the peak detector (rows). Fluorochromes which peaked in the same detector (cFluor YG584 and PE; BV570 and Pacific Orange) are shown as sharing the same emission block. This table layout provided the information regarding potential sources of spread and helped to inform the assignment of markers to fluorochromes to minimize any loss of population resolution.

- CD4 was the only reagent commercially available in cFluor YG584.
- There were limited choices for PE-Alexa Fluor 700, of which CD25 was the only option based on the markers in the panel.
- There were limited choices for PE-Alexa Fluor 610, of which CD24 was the only option based on the markers in the panel.

Step 2: Selection of Viability Dye
LIVE/DEAD™ Fixable Blue (Thermo Fisher, Waltham, MA) was selected for assessing viability as it has a unique signature that does not interfere with the use of other UV excitable fluorochromes.

Step 3: Assignment of Fluorochromes Based on Primary Antigen Classification and Co-Expression
Dimmest fluorochromes were assigned to antigens expressed at high levels and with high level of co-expression with other markers in the panel, while also minimizing spread:
- CD45 in PerCP, co-expressed with all markers in the panel
- CD20 in Pacific Orange, co-expressed with all B cell makers
- CD45RA in BUV395, co-expressed with a high number of markers
- CD3 in BV510, co-expressed with all T cell markers
- CD16 in BUV496, co-expressed with all NK and monocyte markers
- CD2 in PerCP-Cy5.5, co-expressed with T cells and NK cell markers
- CD8 in BUV805, high antigen density

Step 4: Assignment of Fluorochromes Based on Tertiary Antigen Classification
Next, to maximize resolution, tertiary markers were assigned to bright fluorochromes, trying when possible to use fluorochromes whose signals were not severely impacted by spread from multiple fluorochromes. Moreover, information about clones/performance from previous panels developed and tested in the lab was used to make these selections:
- CD123 in Super Bright 436, used successfully in previous panels
- CD1c in Alexa Fluor 647, per OMIP-044 (5)
- CD141 in BB515
- TCRγδ in PerCP-eFluor 710, used successfully in previous panels
- CD159a in APC, desired clone from OMIP-039 (6) with limited availability, no co-expression or loss of resolution with CD1c Alexa Fluor 647
- CD159c in PE, desired clone from OMIP-039 (6) with limited availability, no co-expression or loss of resolution with CD4 cFluor YG584
- PD-1, originally tested in BV650, in BV785 with improved resolution (data not shown)
- CXCR3 and CXCR5 in PE-Cy7 and BV750, respectively, both used successfully in previous panels

Step 5: Assignment of Fluorochromes for Remaining Markers
Finally, for the remaining markers (mainly secondary antigen markers), it was important to take into consideration possible sources of spread that could impact resolution utilizing **Supplemental Table 2** and assign markers so that the following two conditions were met:
- Regarding fluorochromes in columns (indicating primary excitation laser): avoid highly expressed antigens being placed in cells adjacent to co-expressed antigens with lower expression.
- Regarding fluorochromes in rows (indicating similar emission wavelength): avoid highly expressed antigens being placed in cells on the same row as co-expressed markers with lower expression.

Beginning with assignments within the same column/primary laser excitation:
- CD56 in BUV737, previous experience indicated no impact on CD8 BUV805 resolution
- CCR7 in BV421, no co-expression or loss of resolution with CD123 Super Bright 436
- IgD in BV480, no co-expression or loss of resolution with CD3 BV510
- CD11c in eFluor 450, high level of expression, no co-expression or loss of resolution with CD123 Super Bright 436 or IgD BV480
- IgM in BV570 and IgG to BV605, mutually exclusive expression and resolution not impacted by CD20 Pacific Orange
- CD57 in FITC, used in previous panels, no co-expression or loss of resolution with CD141 BB515
- CD14 in Spark Blue 550, no co-expression with CD57 FITC and testing showed no loss of resolution
- CD337 in PE-Dazzle 594, no co-expression or loss of resolution with CD4 cFluor YG584 or CD24 PE-Alexa

Fluor 610
- CD19 in Spark NIR 685, limited reagent availability, no co-expression or loss of resolution with CD1c Alexa Fluor 647
- CD127 in APC-R700, used in previous panels, no co-expression or loss of resolution with CD19 Spark NIR 685. Of note, CD127 clone A019D5 was originally tested in APC-Fire 750, but severe loss of signal was observed in the multicolor tube. We then switched to clone HIL-7R-M21 and tested in parallel BUV737 and APC-R700, and consistent results were only achieved with the APC-R700 conjugate and hence this reagent was selected.

Next steps focused on the remaining assignments per row/emission wavelength:
- CD16 in BUV496, used in previous panels with good resolution and no co-expression or loss of resolution with CD141 BB515
- CCR5 in BUV563, low level of expression mitigated spread into CD4 cFluor YG584
- CD314 in BUV615, low level of expression mitigated spread into CD337 PE-Dazzle 594
- CD39 in BUV661, low level of expression, and no co-expression with CD1c, mitigated spread into Alexa Fluor 647
- CD28 in BV650, no co-expression or loss of resolution with CD159a APC
- CD95 in PE-Cy5, used in previous panels with good resolution and no co-expression or loss of resolution with CD1c Alexa Fluor 647 or CD159a APC
- CCR6 in BV711, low level of expression mitigated spread into other ~700 nm emitting fluorochromes
- CD27 in APC-H7, used in previous panels with good resolution and no spread into other fluorochromes

The distribution of the final panel of reagents across lasers and emission wavelengths is presented in **Supplemental Table 3**.

PANEL TESTING

Once the theoretical panel design was finalized, testing of the panel included the following steps:

Step 1: Antibody Titration

All reagents were titered using frozen PBMCs, at an average of 100,000 cells per test. The cells were resuspended in a final volume of 200 µl of staining buffer (BD Stain Buffer) to mimic the final staining volume of the multicolor (MC) tube. The antibodies that came bottled for use at 5 µl/test were tested in 2-fold serial dilutions ranging from 10 µl to 0.15 µl per test, and the antibodies that came bottled at a concentration in µg/ml were tested from 1 µg (1000 ng) to 15 ng per test. In both cases, titers were reported in nanograms (ng) per test (**Supplemental Figure 3**). Note that the selected titer was not necessarily the optimal titer (higher stain index) in the single stained titration. This was a result of performance comparison of the single stain (SS) to the MC samples, see step 4 below (**Supplemental Figure 6B**).

Step 2: Reference Control Optimization (Supplemental Figure 4)

As for compensation, the unmixing accuracy is highly dependent on the quality of the reference controls and their ability to accurately represent the spectra of fluorochromes present in the MC staining. Using a full spectrum flow cytometer allows detection of even the smallest differences in fluorochrome emission. It is a well known phenomena that fluorochrome antibodies bound to beads vs. cells can produce slight differences in the spectra that are emitted (7). To determine which reference control materials could be used to produce identical spectra for the fully stained sample, both beads and cells were tested. For this purpose, beads and cells stained with exactly the same reagents included in the panel were tested in parallel. Unmixing accuracy using beads as controls was tested by evaluating the umixing results of the SS cells. For some of the markers/fluorochromes, the use of a bead reference control led to unmixing inaccuracies. Errors were identified with the following fluorochromes: BUV496, BUV563, BUV661, BUV805, BV480, BV570, Spark Blue 550, PE-Cy5, APC, and APC-Fire 750. See **Supplemental Figure 4** for two examples where such an error occurred. In order to fully document why errors were observed, the normalized full spectrum of each of these dyes when the antibody was bound to the beads was compared to the normalized full spectrum of the same fluorochrome when the antibody was bound to cells. As expected, differences in the spectrum in specific wavelength regions fully correlated with the unmixing errors observed (**Supplemental Figure 4**). Beads could potentially be used for controls for all other fluorochromes. In the experiments run for this publication, cells were always used as controls and used to evaluate panel performance, see step 4 below.

Approx. Emission Wavelength (nm)	UV	Violet	Blue	Yellow Green	Red
395	CD45RA BUV395				
420		CCR7 BV421			
440		CD123 Super Bright 436			
450	Viability UV (L/D Blue)	CD11c eFluor 450			
480		IgD BV480			
500	CD16 BUV496		CD141 BB515		
520		CD3 BV510	CD57 FITC		
550			CD14 Spark Blue 550		
570	CCR5 BUV563	IgM BV570/ CD20 Pacific Orange			
580				CD4 cFluor YG584/ CD159c PE	
600	CD314 BUV615	IgG BV605		CD337 PE-Dazzle 594	
660	CD39 BUV661	CD28 BV650		CD24 PE-Alexa Fluor 610	NKG2A APC
680			CD45 PerCP	CD95 PE-Cy5	CD1c Alexa Fluor 647
690			CD2 PerCP-Cy5.5		CD19 Spark NIR 685
700		CCR6 BV711	TCR$\gamma\delta$ PerCP-eFluor 710	CD25 PE-Alexa Fluor 700	CD127 APC-R700
730	CD56 BUV737				
750		CXCR5 BV750			
780		PD-1 BV785		CXCR3 PE-Cy7	CD27 APC-H7
800	CD8 BUV805			HLA-DR PE-Fire 810	CD38 APC-Fire 810

Supplemental Table 3. Fluorochrome and Reagent Optical Layout
Using the information from Supplemental Table 2, assignment of fluorochromes to antigens were based on 1) reagent fluorochrome availability, 2) whether an antigen was classified as primary, secondary, and tertiary based on level of expression, and 3) co-expression assessed based on a schematic gating tree. Assignments were also made based on the following goals: 1) avoid highly expressed antigens being placed in adjacent cells in the same column (indicating primary excitation laser) as co-expressed antigens with lower expression; and 2) avoid highly expressed antigens being placed in cells on the same row (indicating similar emission wavelength) as co-expressed markers with lower expression.

3A

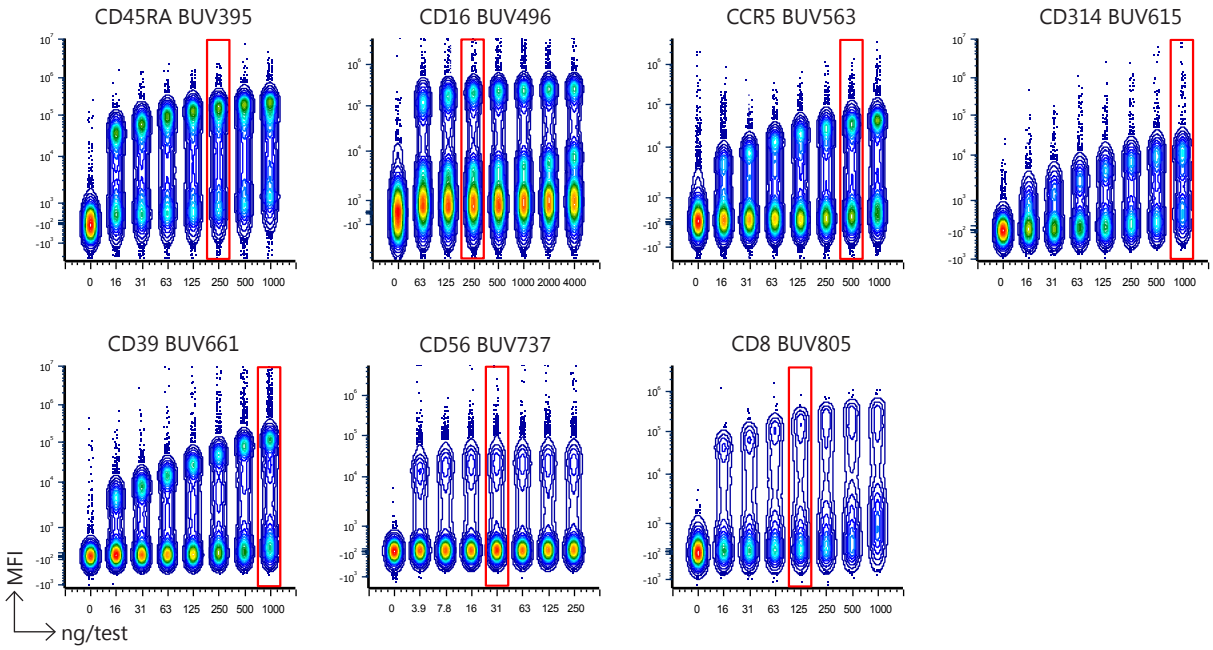
CD45RA BUV395
CD16 BUV496
CCR5 BUV563
CD314 BUV615
CD39 BUV661
CD56 BUV737
CD8 BUV805
MFI
ng/test

3B

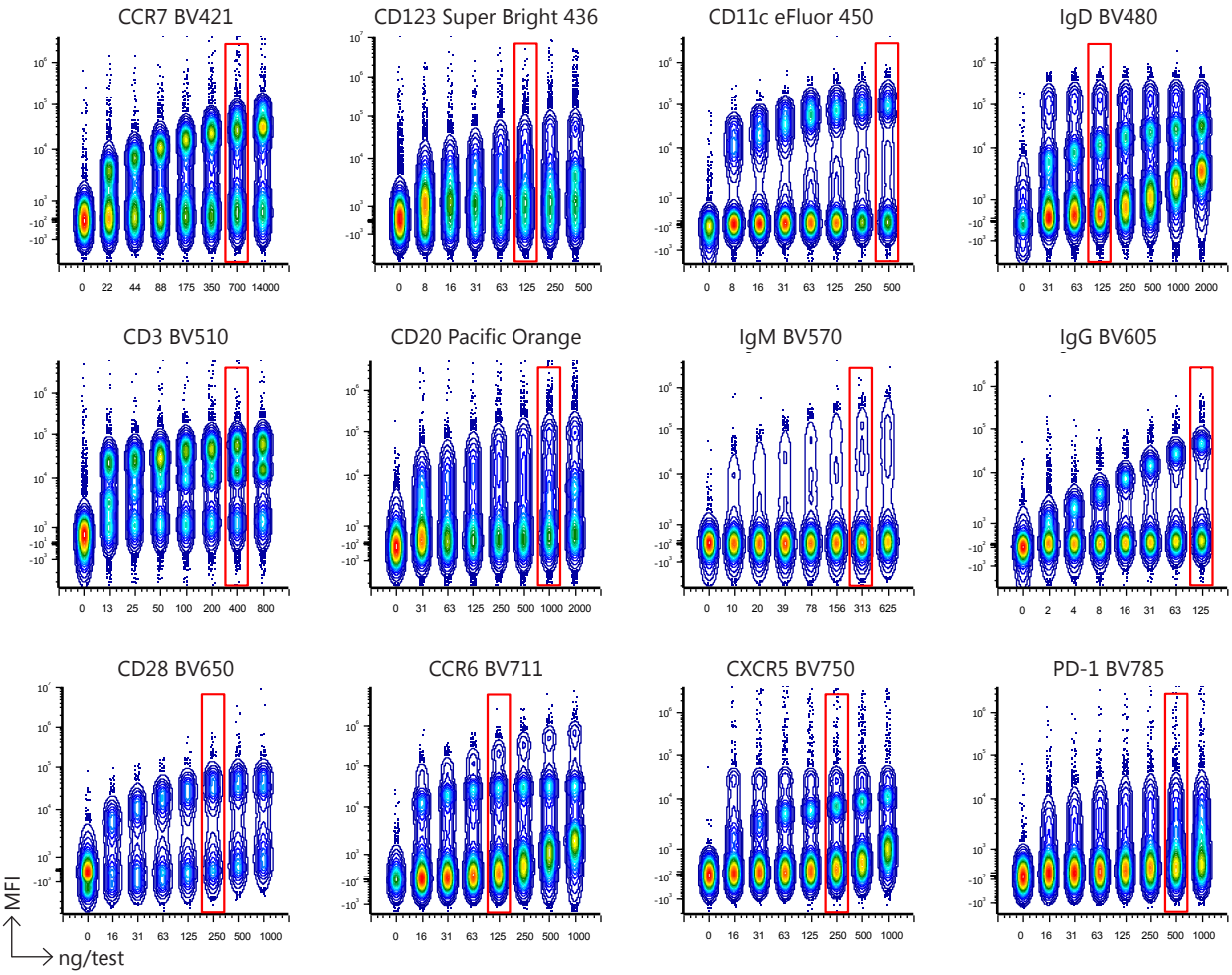
CCR7 BV421
CD123 Super Bright 436
CD11c eFluor 450
IgD BV480
CD3 BV510
CD20 Pacific Orange
IgM BV570
IgG BV605
CD28 BV650
CCR6 BV711
CXCR5 BV750
PD-1 BV785
MFI
ng/test

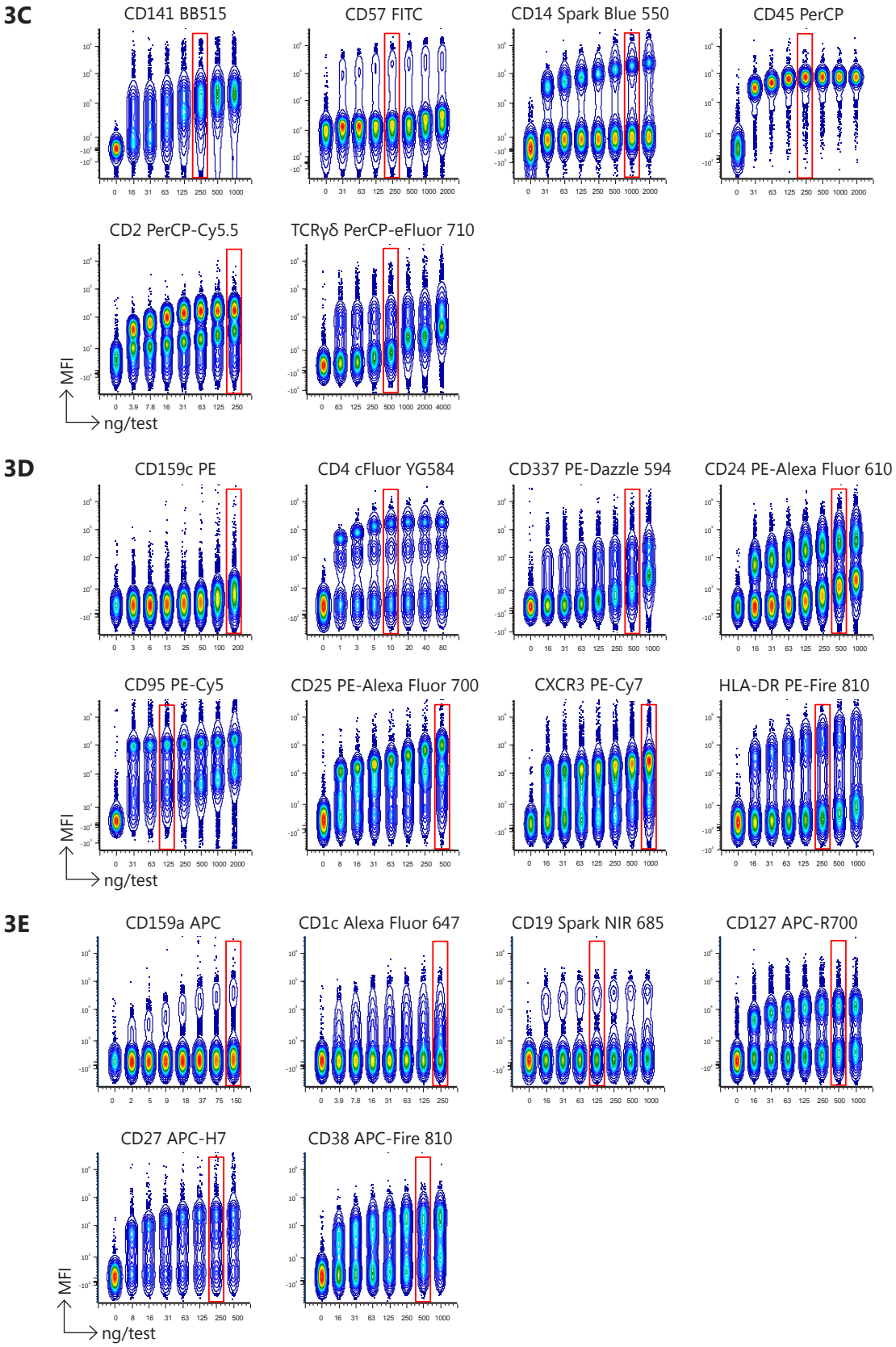

Supplemental Figure 3. Antibody Reagent Titrations

Optimal concentrations of all antibodies were determined through titration experiments. Two-fold dilutions of antibodies were tested. For antibodies that came bottled for use at 5 µl/test, a range from 10 µl to 0.15 µl/test was tested, while concentrations from 1 µg to 15 ng/test was tested for antibodies that came bottled at a concentration in µg/ml. Files were concatenated for analysis using FCS Express version 7 (De Novo Software). Titrations for reagents primarily excited by the UV laser (355 nm) **(A)**, violet laser (405 nm) **(B)**, blue laser (488 nm) **(C)**, yellow-green laser (561 nm) **(D)**, and red laser (640 nm) **(E)** are shown. Final titration results are expressed as ng/test (see Supplemental Table 4).

4A

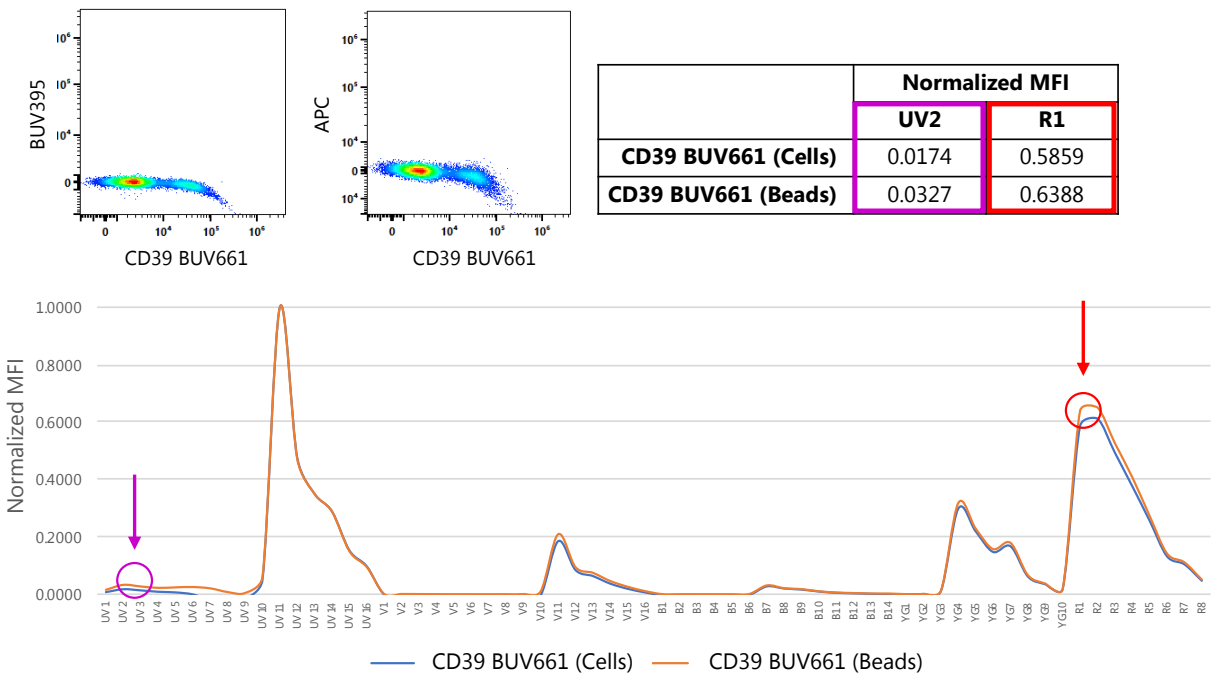

	Normalized MFI	
	UV2	R1
CD39 BUV661 (Cells)	0.0174	0.5859
CD39 BUV661 (Beads)	0.0327	0.6388

4B

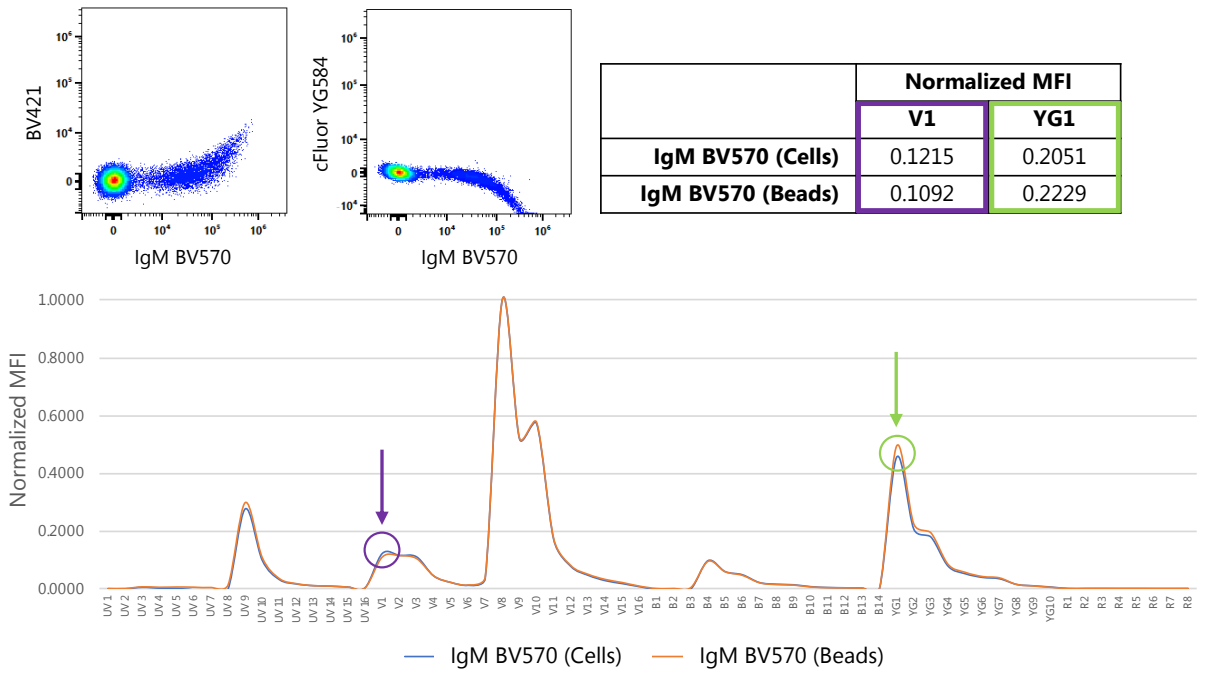

	Normalized MFI	
	V1	YG1
IgM BV570 (Cells)	0.1215	0.2051
IgM BV570 (Beads)	0.1092	0.2229

Supplemental Figure 4. Examples of Unmixing Errors Using Beads vs. Cells as Reference Controls
In evaluating the unmixing outcome when using beads vs. cells as reference controls, several fluorochromes were identified for which the use of beads led to unmixing inaccuracies. These unmixing inaccuracies were the result of minor differences in the spectra of fluorochromes when the same antibody was bound to beads vs. cells. **(A)** When CD39 BUV661 bound beads were used to unmix CD39 BUV661 single stained cells, unmixing inaccuracies were observed in BUV395 (peak channel UV2) and APC (peak channel R1). The normalized overlay demonstrates where differences in the spectra were observed between the two reference control materials (beads vs. cells). The box in the upper right shows the normalized MFIs for the two channels where the differences are highlighted (colored circles and arrows). **(B)** IgM BV570 bound beads, used to unmix IgM BV570 SS cells, resulted in inaccurate unmixing in BV421 (peak channel V1) and cFluor YG584 (peak channel YG1). The normalized overlay demonstrates where differences in the spectra were observed between the two reference control materials (beads vs. cells). The box in the upper right shows the normalized MFIs of the two channels where the differences are highlighted (colored circles and arrows).

Step 3: Unmixing Accuracy of the MC Tube
Data was unmixed using the SpectroFlo software v2.2 using an ordinary least squares algorithm. To check that the unmixing of the MC tube was accurate, data was cleaned up (singlets, live, scatter gate, aggregate exclusion if needed) and NxN plot permutations were screened (**Supplemental Figure 5**). For most of the markers, unmixing was very accurate (**Supplemental Figure 5A**). Errors were only visually identified in 16 of the 1560 combinations. An example of the errors that were encountered is presented in **Supplemental Figure 5B**. Corrections were applied only when the errors were observed between fluorochromes that had spillover between them and when the authors had solid knowledge of the expected expression pattern. The correction was estimated visually to align the median of the negative and positive populations in the y-dimension. The maximum correction that had to be applied was 2.8%, corresponding to BUV737 into BV750. Of note, these corrections did not have an impact on the outcome of the analysis, either manual or unsupervised.

Step 4: SS Control vs. MC Resolution for Each Marker (Supplemental Figure 6A-B)
After unmixing accuracy was checked, the resolution of every marker in the panel was checked by comparing the SS control tube to the same marker in the MC sample. Three different scenarios were observed:

1. Resolution was identical, and no action was needed.
2. The positive population in the MC tube was dimmer. In this case the titer was adjusted **(Supplemental Figure 6B)**, and the staining protocol was evaluated for any possible staining optimization (see step 6 below and **Supplemental Figure 9B**).
3. The negative population in the MC tube was significantly wider, resulting in lower population resolution (lower stain index). In this case, data was gated according to the population gating hierarchy and evaluated for any compromise in resolving the population of interest. In all cases it was determined that the introduction of spread for a given marker did not negatively impact the overall performance of the panel.

Step 5: Assessment of Spread Impact on Resolution (Supplemental Figures 7 and 8)
One of the great advantages of full spectrum flow cytometry is the ability to utilize highly overlapping fluorochromes that traditionally could not be used together in conventional flow cytometers. This capability was critical for the development of a 40-color panel. However, highly overlapping fluorochromes are known to exhibit increased spread into other fluorochromes, which could impact resolution quality. For highly overlapping fluorochromes where significant spread was anticipated, visual inspection of those combinations and impact of the spread were evaluated **(Supplemental Figure 7)**. In general, based on good panel design practices, these occurred in combinations of markers that are not co-expressed and therefore did not have a substantive negative impact.

FMO controls were used to guide and/or assess positive and negative delineations (**Supplemental Figure 8A**). FMOs were run for the following markers with low level of expression: CD25, CXCR5, CCR5, CCR6, and PD-1. For each of the main cellular subsets (monocytes, TCRγδ$^+$, CD3$^+$, CD4$^+$, CD8$^+$, CD3$^+$CD56$^+$, CD19$^+$CD20$^+$, and CD3$^-$CD56$^+$), gates to identify positive events for these markers were set based on the FMO control (lower row for each marker) and applied to the MC samples (upper row for each marker). For all the markers evaluated, identification of positive events was straightforward.

In addition, the impact of spread on population resolution was evaluated by comparing the MC samples with FMOs of the highly overlapping dye (**Supplemental Figure 8B**). FMOs for BB515, FITC, PE-Alexa Fluor 610, and Spark NIR 685 were run to assess the impact of spread introduced by these fluorochromes into fluorochromes with a high similarity. BB515 and FITC were chosen because these dyes had the highest values in the SSM matrix. PE-Alexa Fluor 610 and Spark NIR 685 were chosen because, prior to this panel, there was no experience using them in combination with PE-Dazzle 594 and Alexa Fluor 647, respectively. Plots on the left show the population resolution in the MC sample while plots on the right show the resolution of the same population in the indicated FMO control. When differences in spread of the negative population were observed, a bar measuring the spread was added to each plot to facilitate visual comparison. To assess the impact of spread from FITC into BB515, lineage negative (Lin$^-$) cells were plotted by HLA-DR vs. CD141 to visualize the resolution of CD141$^+$ dendritic cells (first row). For BB515 spread into FITC, cells were gated to evaluate CD57 resolution on NK cells (second row). The spread from PE-Alexa Fluor 610 into PE-Dazzle 594 was evaluated by observing the resolution of CD337 on NK cells (third row). Finally, to assess the spread introduced by Spark NIR 685 into Alexa Fluor 647, cells were gated on Lin$^-$ and HLA-DR vs CD1c plotted to represent the impact on resolution of CD1c$^+$ dendritic cells (last row). This analysis demonstrated minimal

5A

CD39 BUV661

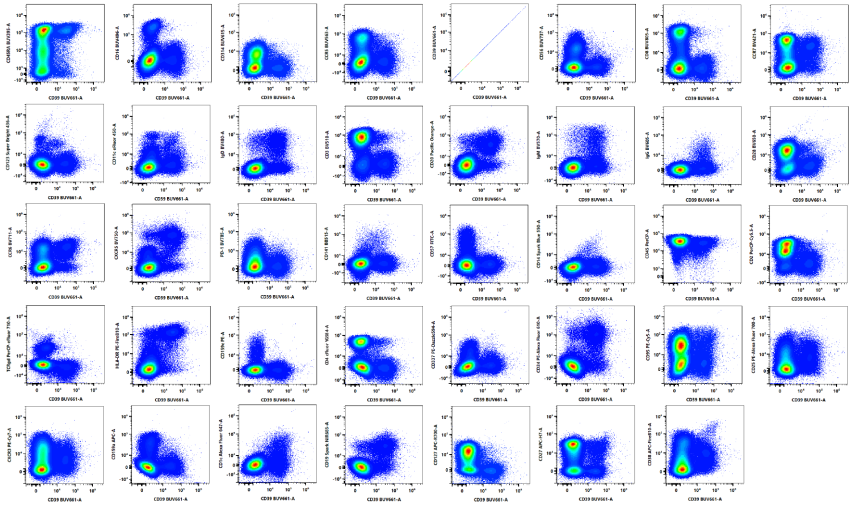

IgM BV570

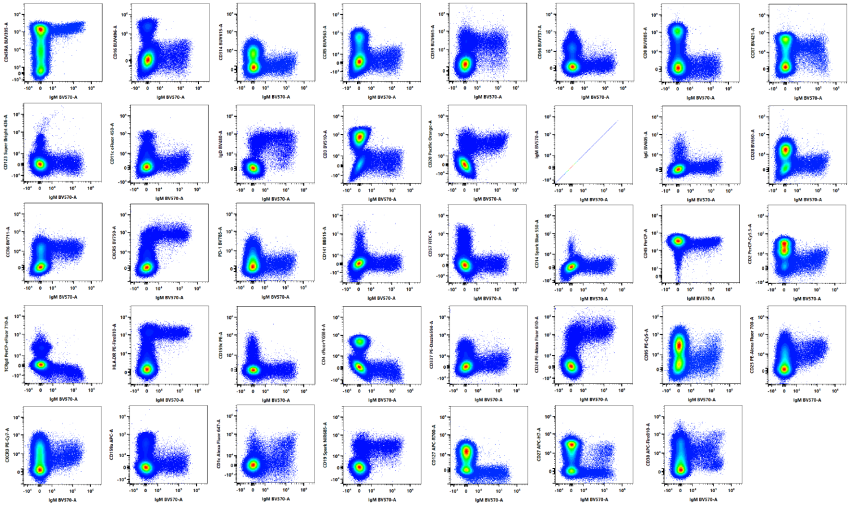

5B

CD56 BUV737

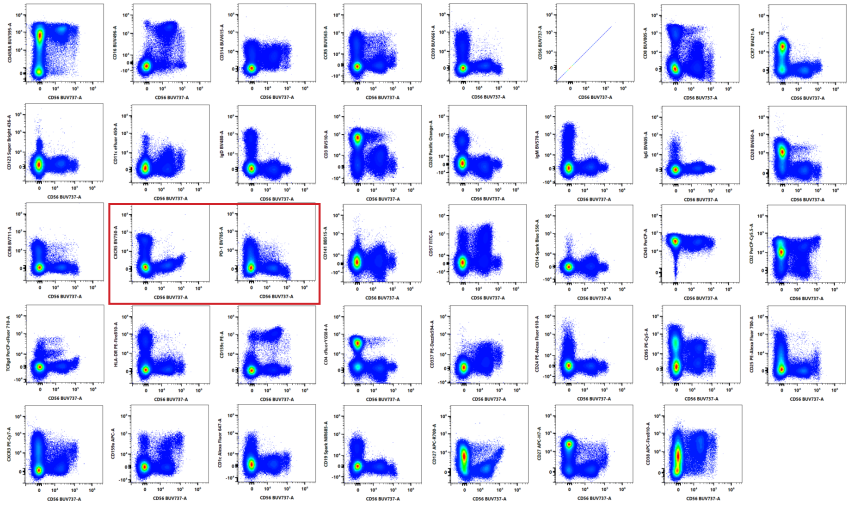

CD56 BUV737, Errors Corrected

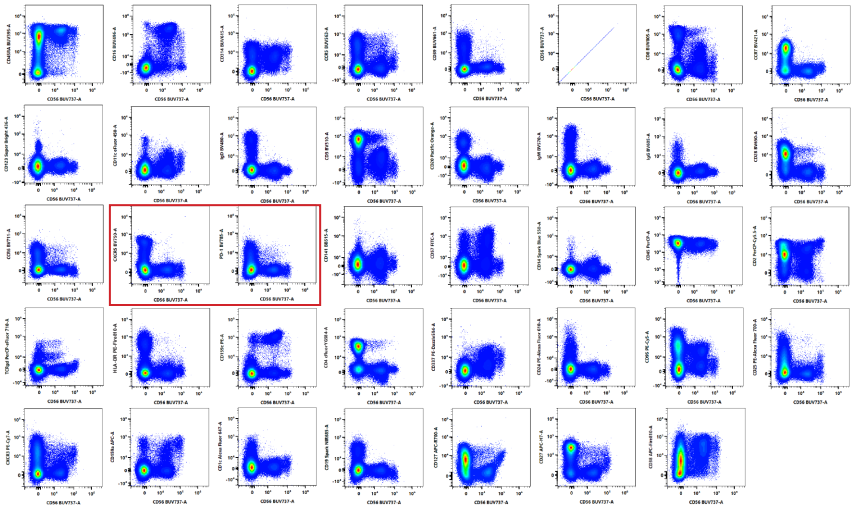

Supplemental Figure 5. QC of Unmixing Accuracy of MC Stained Sample

For the MC samples, NxN plots were generated to visually assess the unmixing accuracy. Data plotted for evaluation was gated on singlets, scatter, live, and non-aggregates. **(A)** Two representative examples where unmixing was accurate are presented; CD39 BUV661 and IgM BV570. The plots presented are based on the data from Supplemental Figure 4. In each of the presented NxN plots, the same marker is plotted on the x-axis (CD39 BUV661 on the left and IgM BV570 on the right) and the y-axes represent every other fluorochrome in the panel. When unmixing was performed using SS cells as reference controls, no significant unmixing inaccuracies were observed. **(B)** Unmixing errors were observed in a minority of combinations (16 in the 40x40 matrix). A representative example of an error observed in the unmixing accuracy of CD56 BUV737 is presented (left panel, red box), namely into BV750 and BV785. Minimal corrections were required to align the negative and positive populations (right panel, red box): 2.8% into BV750 and -1% into BV785.

6A

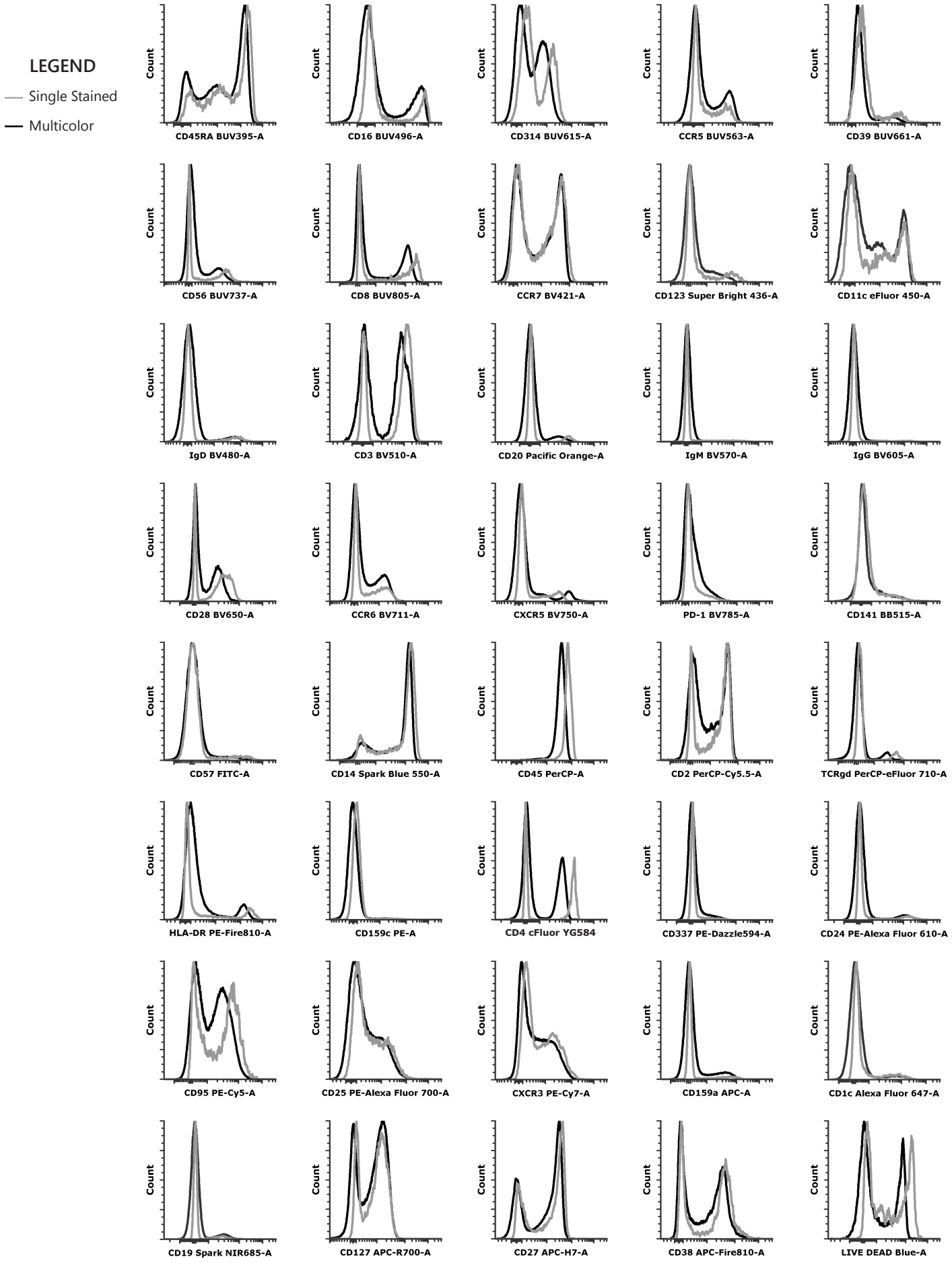
LEGEND
Single Stained
Multicolor
Count
CD45RA BUV395-A
CD16 BUV496-A
CD314 BUV615-A
CCR5 BUV563-A
CD39 BUV661-A
CD56 BUV737-A
CD8 BUV805-A
CCR7 BV421-A
CD123 Super Bright 436-A
CD11c eFluor 450-A
IgD BV480-A
CD3 BV510-A
CD20 Pacific Orange-A
IgM BV570-A
IgG BV605-A
CD28 BV650-A
CCR6 BV711-A
CXCR5 BV750-A
PD-1 BV785-A
CD141 BB515-A
CD57 FITC-A
CD14 Spark Blue 550-A
CD45 PerCP-A
CD2 PerCP-Cy5.5-A
TCRgd PerCP-eFluor 710-A
HLA-DR PE-Fire810-A
CD159c PE-A
CD4 cFluor YG584
CD337 PE-Dazzle594-A
CD24 PE-Alexa Fluor 610-A
CD95 PE-Cy5-A
CD25 PE-Alexa Fluor 700-A
CXCR3 PE-Cy7-A
CD159a APC-A
CD1c Alexa Fluor 647-A
CD19 Spark NIR685-A
CD127 APC-R700-A
CD27 APC-H7-A
CD38 APC-Fire810-A
LIVE DEAD Blue-A

6B

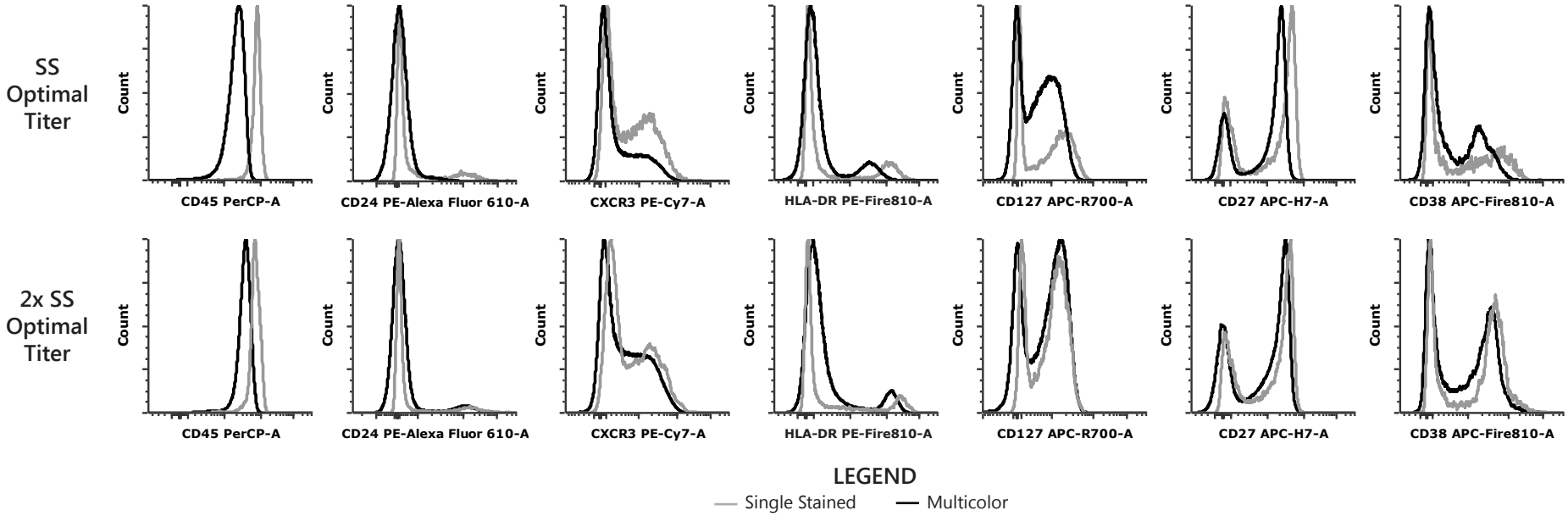

Supplemental Figure 6. Staining Resolution: SS vs. MC Samples
As part of the panel optimization, each marker in the MC stained samples was evaluated to determine whether an optimal resolution was maintained. To assess this, staining patterns were compared between the SS controls and the MC sample using PBMCs from the same donor. **(A)** For both SS (gray line) and MC (black line) samples, the data in the overlays were gated on singlets and, depending on the marker, lymphocyte or monocyte scatter gates. **(B)** In cases where this assessment identified reduced resolution in the MC samples for a given marker due to lower intensity of the positive signal (top row), antibody concentrations were increased by one titer point to get as close as possible to the resolution obtained in the SS tube (bottom row). Note that in those cases, doubling the titer in the MC tube increased the brightness of the positive population and had no impact on the negative population (no shifts were observed), resulting in increased resolution.

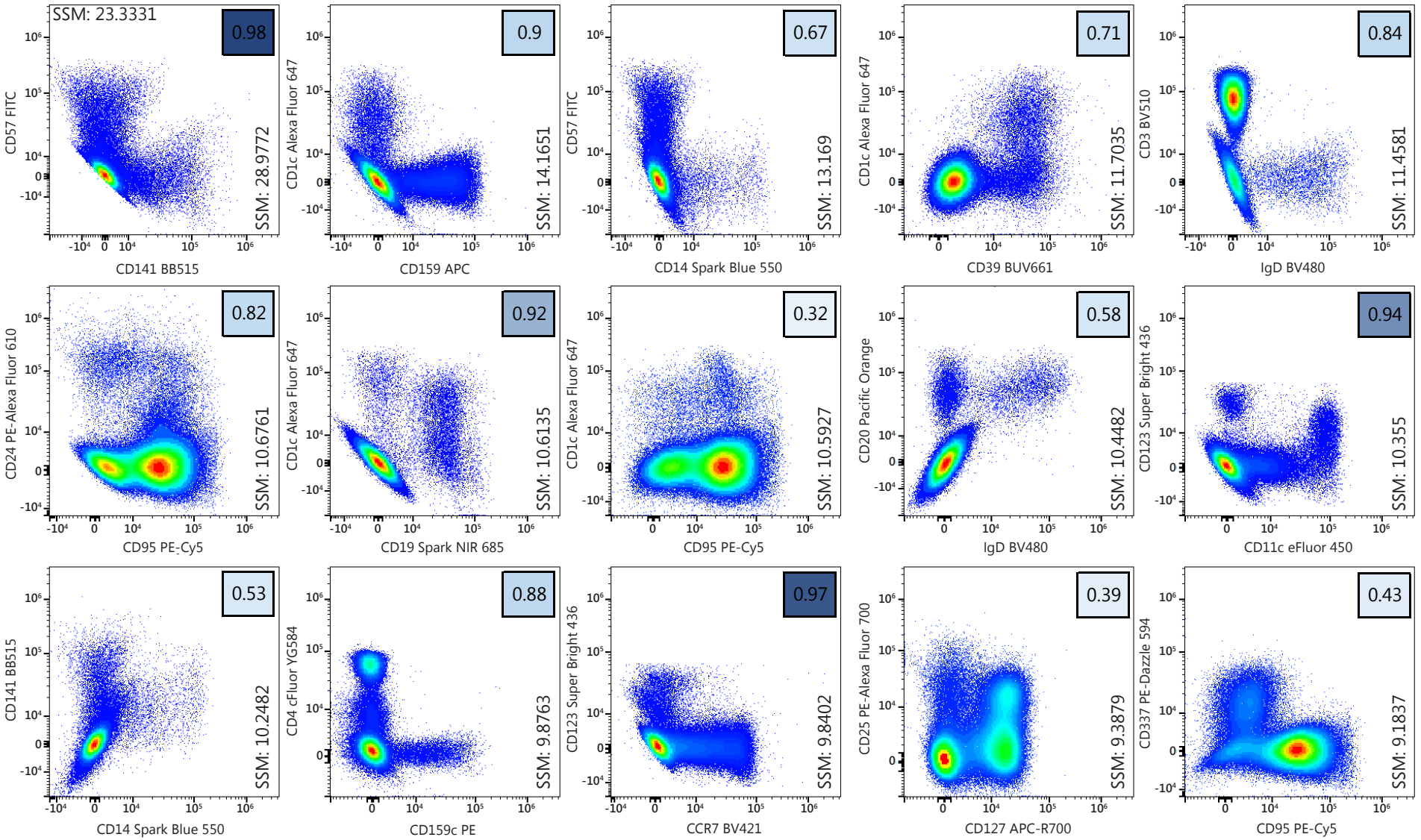

Supplemental Figure 7. Assessment of Highly Overlapping Fluorochromes

The impact of spread introduced by using highly overlapping fluorochromes was assessed using the MC sample. Fluorochrome combinations having the 16 highest values in the spillover spread matrix (SSM) (Supplemental Figure 2D) are presented. Plots are gated on singlets, live, non-aggregates, FSC/ SSC low/ intermediate, and CD45^{+}. The fluorochrome on the x-axis introduces spread to the fluorochrome on the y-axis, except for the first plot (BB515 and FITC), as in this case both fluorochromes have a significant spread into each other. SSM values are presented in each plot. Note that the antigens assigned to the pairs with the highest SSM values (FITC and BB515, APC and Alexa Fluor 647, Spark Blue 550 and FITC) have no co-expression. The Similarity Index for each fluorochrome pair is indicated in the box in the upper right hand corner. The highly correlated distributions (diagonals) of the autofluorescent populations in the combinations that have high Similarity Indices is expected behavior for such highly overlapping dyes (2).

8A

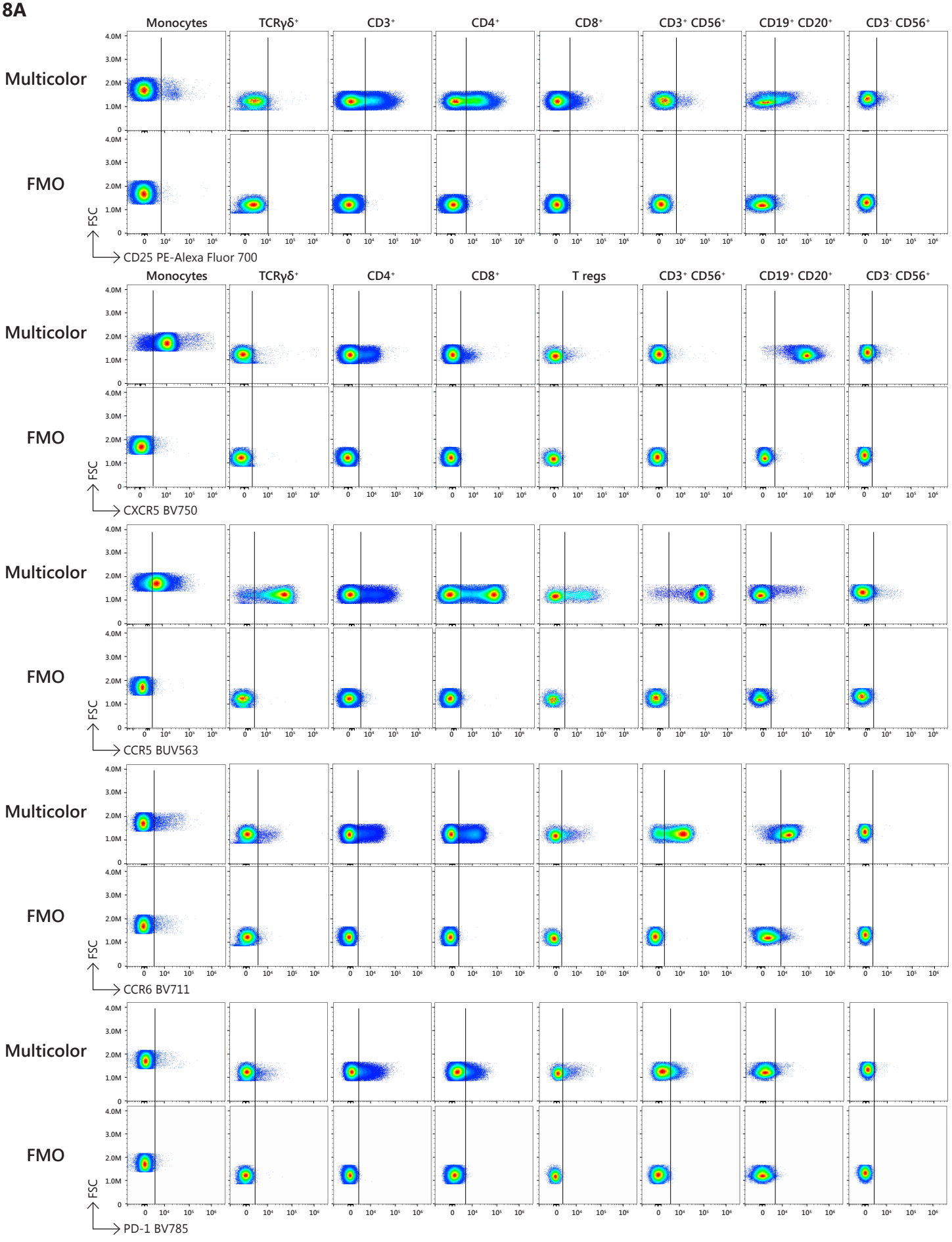
Monocytes
TCRγδ+
CD3+
CD4+
CD8+
CD3+ CD56+
CD19+ CD20+
CD3- CD56+
Multicolor
FMO
FSC
CD25 PE-Alexa Fluor 700
Monocytes
TCRγδ+
CD4+
CD8+
T regs
CD3+ CD56+
CD19+ CD20+
CD3- CD56+
Multicolor
FMO
FSC
CXCR5 BV750
Multicolor
FMO
FSC
CCR5 BUV563
Multicolor
FMO
FSC
CCR6 BV711
Multicolor
FMO
FSC
PD-1 BV785

8B

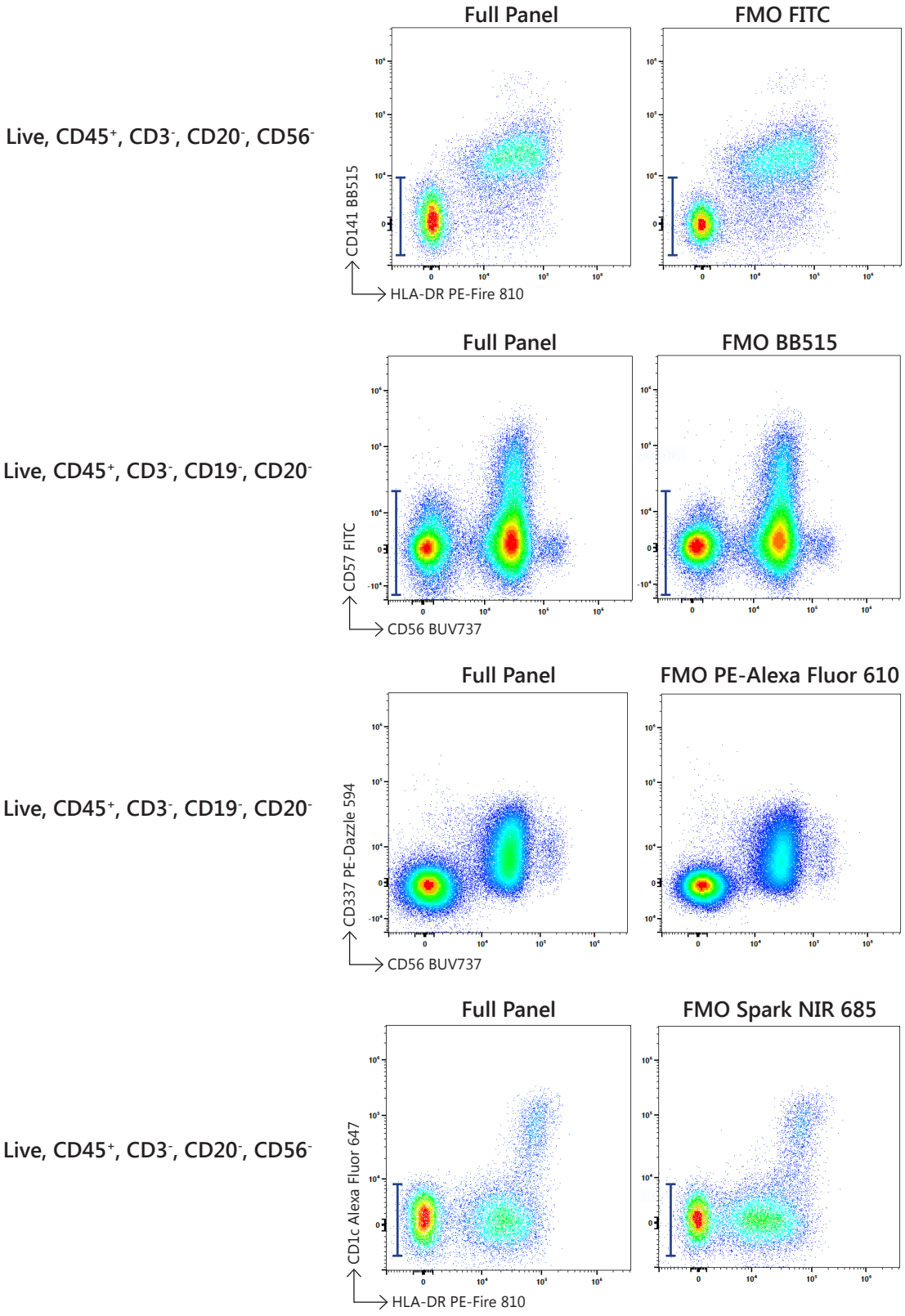

Supplemental Figure 8. Fluorescence Minus One (FMO) Controls
FMOs were used as a quality control for two different purposes: to assess the accuracy in the gating/identification of populations where there was low level expression **(A)** or to assess the impact of spread in the resolution of a given marker/population **(B)**. All the markers evaluated with FMOs show clear identification of positive events **(A)**, while minimal spread of the negative populations were observed (black lines). Nearly identical population resolution was achieved with and without the highly overlapping fluorochrome present in the panel (blue bars) (**B**).

impact on the spread of the negative population and hence no loss of resolution resulting from the use of these highly overlapping dyes.

Step 6: Fine Tuning of Staining Protocol (Supplemental Figure 9)
Based on the results of the above assessments of the panel's performance and other independent observations, several adjustments to the staining protocol were made to further optimize its performance. These adjustments were as follows:

- Titers were adjusted, where deemed necessary, based on SS vs. MC assessment (see step 4 above and **Supplemental Figure 6B**).
- Based on previous reports (8) of interference when multiple chemokine receptors are stained in the same panel, the staining of the chemokine receptors in the panel was optimized. Sequential vs. simultaneous staining was assessed to determine whether any improvements in resolution could be achieved. For some chemokine receptors (CCR5 and CXCR5 on B cells) an improvement was seen, while no differences were noted for CCR6 (**Supplemental Figure 9A**).
- Initial staining for TCRγδ yielded poor resolution of this population. Optimization of TCRγδ staining was achieved by the addition of the reagent at a different step in the staining process, subsequently improving the identification of this subpopulation of T cells (**Supplemental Figure 9B**).
- A significant amount of antibody aggregates were observed during the panel development with CD24 PE-Alexa Fluor 610 and CXCR5 BV750. Centrifugation of these reagents at 10,000 x g for 5 minutes decreased the presence of aggregates.

A summary of the reagents used in the panel, including their final titer, is provided in **Supplemental Table 4**.

DATA ANALYSIS

Manual gating of the main populations is displayed in Figure 1A. Detailed immunophenotyping of each cellular subset is presented in **Supplemental Figure 10**. While this display is commonly used to demonstrate the ability to resolve populations based on traditional gating strategies, manual data analysis of a 40-color panel is generally not practical as it is very time consuming, suffers from individual user bias, and compromises the ability to characterize subsets in multiple dimensions (9-11). Dimensionality reduction techniques for exploratory data analysis, such as Uniform Manifold Approximation and Projection (UMAP), have been used for mass cytometry data and single cell RNA-seq (12). These techniques can also be applied to fluorescent high-dimensional datasets, given that appropriate QC is performed prior to performing this kind of analysis.

Data from OMIP-069 were analyzed with the OMIQ platform (https://www.omiq.ai/, Figures 1B, and **Supplemental Figure 11**) utilizing the following pipeline. First, the scaling was adjusted to ensure greater than 99% of events were on scale for each channel and the negative population was unimodal around 0. The data were manually gated to remove aggregates, dead cells, debris, and CD45 negative events, and then the data were sub-sampled to include 400,000 CD45+ live singlets from each sample. Next, flowCut (13) was run to check for any aberrant regions of the file. FlowCut settings were as follows: all files used, all fluorescent channels and time selected, Segment = 500, Max Contin = 0.15, Mean of Means = 0.13, Max of Means = 0.15, Max of Valley Height = 0.15, Max Percent to Cut = 0.3, Low Density Removal = 0.1, no Gate Line set, Max Channel for Mean Range = 1, Max Channel for Mean SD = 2, no Flagged Rerun, Uniform of Time Check = 0.22, Remove Multi SD = 7. Results were as follows: largest continuous jump = 0.095, largest mean of % of range of means divided by range of data = 0.084, Max of % of range of means divided by range of data = 0.118, no events removed). Subsequently, a UMAP (14) analysis was performed to visualize the different sub-populations in groups. UMAP settings were as follows: all files used, all fluorescent parameters were used besides CD45 and Live/Dead, Neighbors = 80, Minimum Distance = 0.7, Components = 2, Metric = Euclidean, Learning Rate = 1, Epochs = 250, Random Seed = 9346, Embedding Initialization = spectral. Following the UMAP analysis, FlowSOM (15) was run to cluster the data. FlowSOM settings were as follows: all files used, clustering features CD4, CD8, CD45RA, CCR7, CD25, CD127, CD27, CD28, TCRγδ, CD16, CD1c, CD11c, IgD, IgM, and IgG, umap_1, umap_2, 625 clusters with xdim = 25 and ydim = 25, rlen = 10, Distance Metric = euclidian, consensus metaclustering with k = 100, Random Seed = 1337. After the FlowSOM analysis, the metaclusters were grouped into commonly recognized biological populations if possible. A heatmap was generated with the resulting populations and clustered hierarchically on all surface markers with a euclidean distance metric to indicate the similarity of the populations. This pipeline allows the FlowSOM clusters to be verified and translated into well-recognized populations via the heatmap, then those populations can be visualized on the UMAP parameters for ease of comparison between samples.

9A

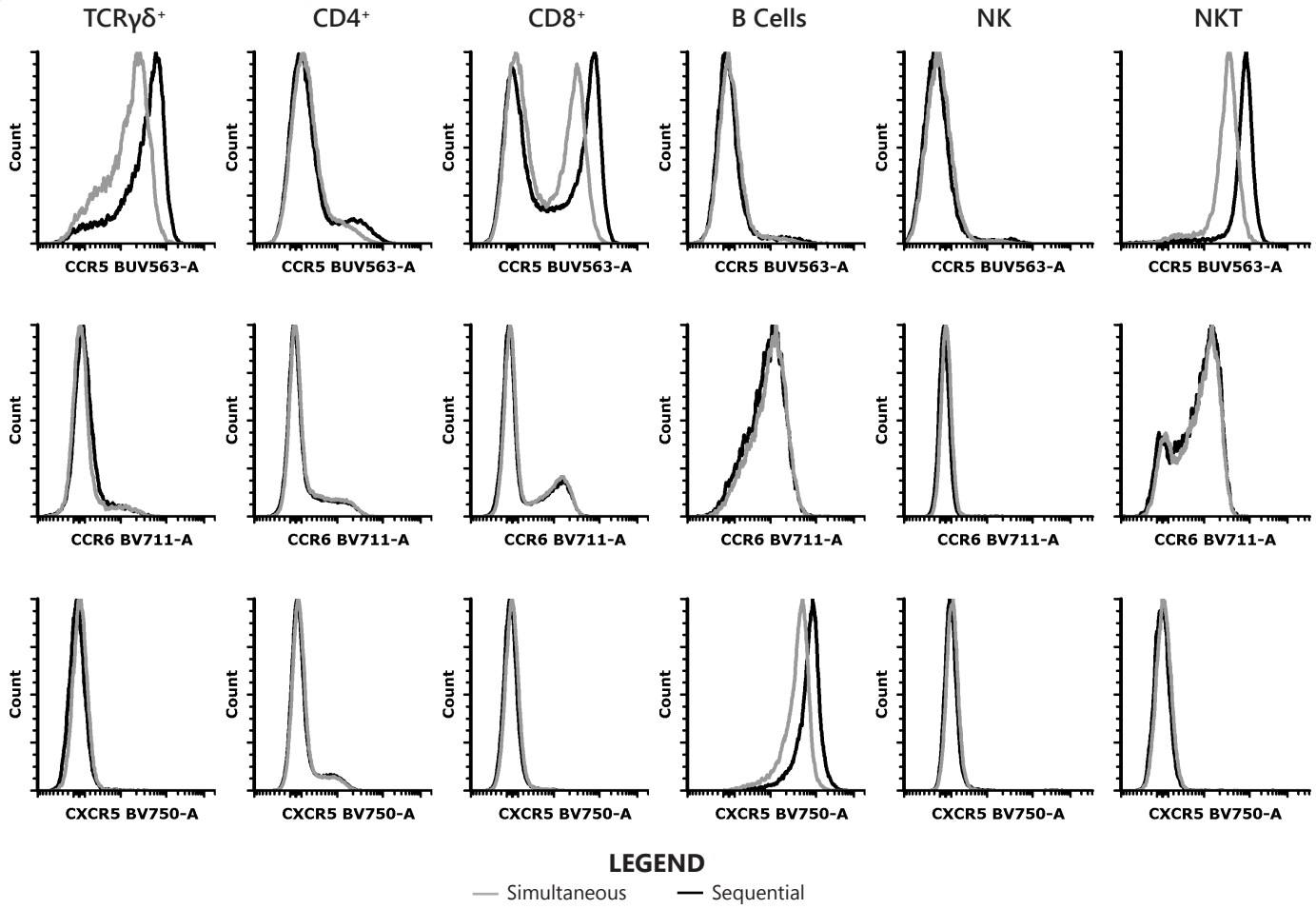

9B

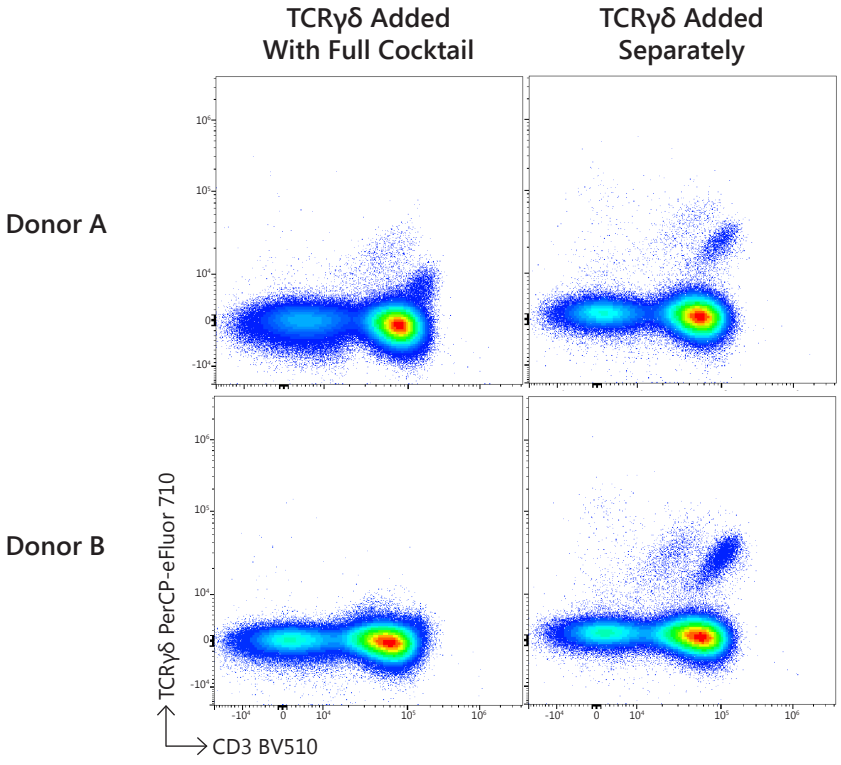

Supplemental Figure 9. Effects of Staining Conditions on Staining Quality

Optimization of the staining protocol was performed to improve the resolution of populations of interest. **(A)** Staining protocols were compared by overlaying MC cells stained simultaneously (gray line) or sequentially (black line) with chemokine receptor antibodies to determine differences in staining quality for these reagents. Indicated subpopulations were used to verify performance across multiple cell types. **(B)** Improvements in staining quality of TCRγδ+ cells: comparison of resolution when antibody was added as part of the full cocktail (left) or added separately (right). Data from two different donors is presented.

SPECIFICITY	FLUOROCHROME	CLONE	CATALOG #	VENDOR	Titer (ng/test)
Viability	LIVE/DEAD Blue	-	L34962	Thermo Fisher	5 µL of 1:40 dilution of stock
CD45	PerCP	2D1	368506	BioLegend	250
CD3	BV510	SK7	344828	BioLegend	400
CD4	cFluor YG584	SK3	R7-20041-100T	CYTEK	10
CD8	BUV805	SK1	612889	BD Biosciences	125
CD25	PE-Alexa Fluor 700	CD25-3G10	MHCD2524	Thermo Fisher	500
PD-1	BV785	EH12.2H7	329930	BioLegend	500
TCRγδ	PerCP-eFluor 710	B1.1	46-9959-42	Thermo Fisher	500
CD14	Spark Blue 550	63D3	367148	BioLegend	1000
CD16	BUV496	3G8	612944	BD Biosciences	250
CD11c	eFluor 450	3.9	48-0116-42	Thermo Fisher	500
CD19	Spark NIR 685	HIB19	302270	BioLegend	125
CD20	Pacific Orange	HI47	MHCD2030	Thermo Fisher	1000
CD24	PE-Alexa Fluor 610	SN3	MHCD2422	Thermo Fisher	500
CD39	BUV661	TU66	749967	BD Biosciences	1000
IgD	BV480	IA6-2	566138	BD Biosciences	125
IgG	BV605	G18-145	563246	BD Biosciences	125
IgM	BV570	MHM-88	314517	BioLegend	312.5
CD141	BB515	1A4	566017	BD Biosciences	250
CD1c	Alexa Fluor 647	L161	331510	BioLegend	250
CD123	Super Bright 436	6H6	62-1239-42	Thermo Fisher	125
CD2	PerCP-Cy5.5	TS1/8	309226	BioLegend	250
CD56	BUV737	NCAM16.2	564447	BD Biosciences	31.25
CCR7	BV421	G043H7	353208	BioLegend	700
CD27	APC-H7	M-T271	560222	BD Biosciences	250
CD45RA	BUV395	5H9	740315	BD Biosciences	250
CD95	PE-Cy5	DX2	305610	BioLegend	125
CD127	APC-R700	HIL-7R-M21	565185	BD Biosciences	500
CD337	PE-Dazzle 594	P30-15	325231	BioLegend	500
CCR6	BV711	G034E3	353436	BioLegend	125
CCR5	BUV563	2D7/CCR5	741401	BD Biosciences	500
CXCR5	BV750	RF8B2	747111	BD Biosciences	250
CXCR3	PE-Cy7	G025H7	353720	BioLegend	1000
HLA-DR	PE-Fire 810	L243	custom*	BioLegend	250
CD38	APC-Fire 810	HIT2	356643	BioLegend	500
CD57	FITC	HNK-1	359604	BioLegend	250
CD28	BV650	CD28.2	302946	BioLegend	250
CD159a	APC	REA110	130-113-563	Miltenyi	150
CD159c	PE	REA205	130-119-776	Miltenyi	200
CD314	BUV615	1D11	751232	BD Biosciences	1000

* Custom conjugation is available through BioLegend

Supplemental Table 4. Final Selection of Reagents Used in OMIP-069
Staining reagents used in the final panel with antibody clone, manufacturer information, and final concentrations used in the staining protocol provided.

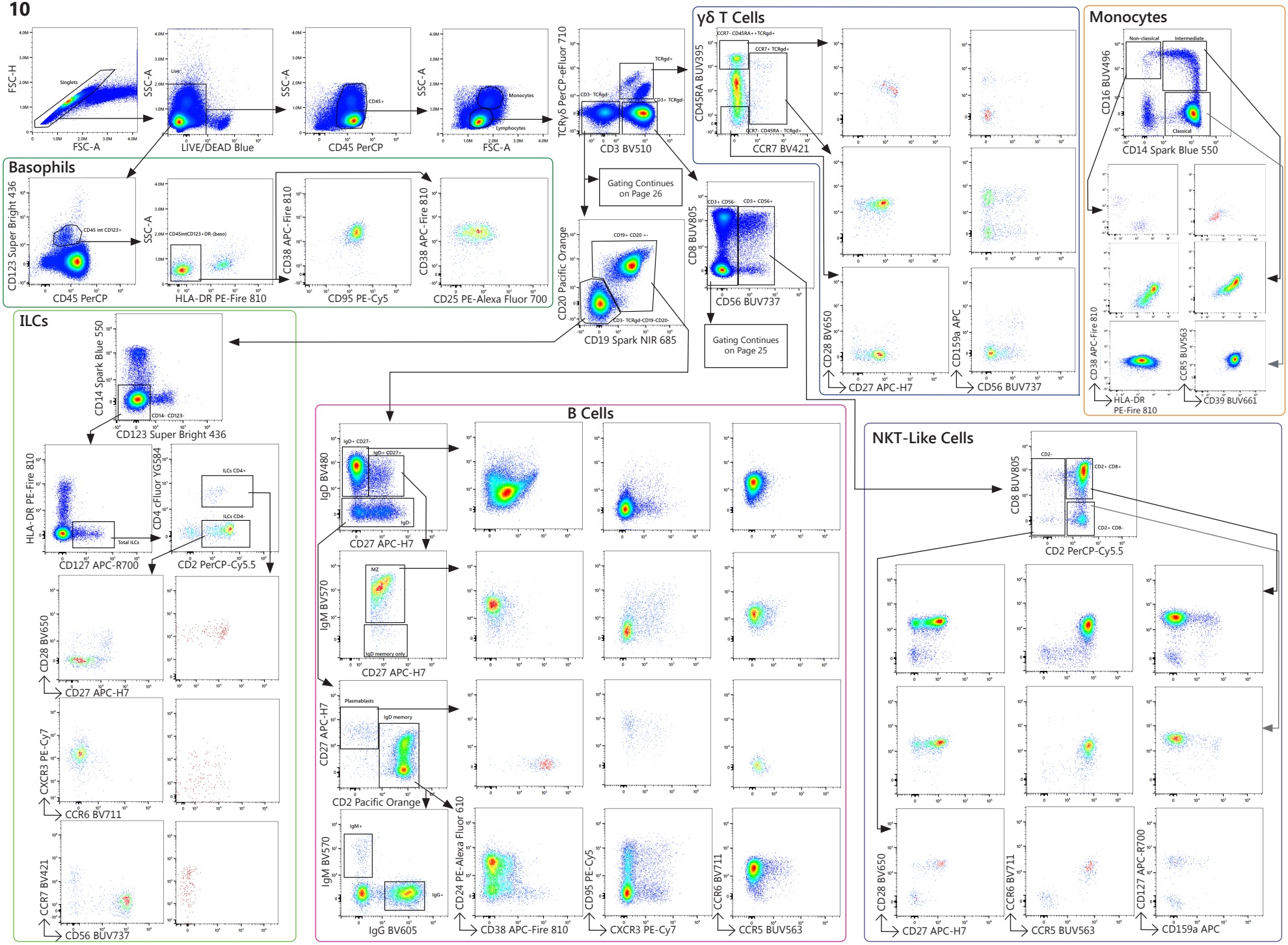
FSC-H
FSC-A
Singlets
SSC-A
LIVE/DEAD Blue
Live
CD45 PerCP
CD45+
FSC-A
Monocytes
Lymphocytes
TCRγδ PerCP-eFluor 710
CD3 BV510
CD3- TCRgd-
CD3+ TCRgd-
TCRgd+
Gating Continues on Page 26
γδ T Cells
CD45RA BUV395
CCR7 BV421
CCR7- CD45RA++TCRgd+
CCR7+ TCRgd+
CCR7- CD45RA - TCRgd+
CD28 BV650
CD27 APC-H7
CD159a APC
CD56 BUV737
Monocytes
CD16 BUV496
CD14 Spark Blue 550
Non-classical
Intermediate
Classical
CD38 APC-Fire 810
HLA-DR PE-Fire 810
CCR5 BUV563
CD39 BUV661
Basophils
CD123 Super Bright 436
CD45 int CD123+
CD45 PerCP
SSC-A
CD45intCD123+DR-(baso)
HLA-DR PE-Fire 810
CD38 APC-Fire 810
CD95 PE-Cy5
CD38 APC-Fire 810
CD25 PE-Alexa Fluor 700
CD20 Pacific Orange
CD19+ CD20 +-
CD3- TCRgd-CD19-CD20-
CD19 Spark NIR 685
CD8 BUV805
CD3+ CD56-
CD3+ CD56+
CD56 BUV737
Gating Continues on Page 25
ILCs
CD14 Spark Blue 550
CD14- CD123-
CD123 Super Bright 436
HLA-DR PE-Fire 810
Total ILCs
CD127 APC-R700
CD4 cFluor YG584
ILCs CD4+
ILCs CD4-
CD2 PerCP-Cy5.5
CD28 BV650
CD27 APC-H7
CXCR3 PE-Cy7
CCR6 BV711
CCR7 BV421
CD56 BUV737
B Cells
IgD BV480
IgD+ CD27-
IgD+ CD27+
IgD-
CD27 APC-H7
IgM BV570
MZ
IgD memory only
CD27 APC-H7
CD27 APC-H7
Plasmablasts
IgD memory
CD2 Pacific Orange
IgM BV570
IgM+
IgG+
IgG BV605
CD24 PE-Alexa Fluor 610
CD38 APC-Fire 810
CD95 PE-Cy5
CXCR3 PE-Cy7
CCR6 BV711
CCR5 BV563
NKT-Like Cells
CD8 BUV805
CD2-
CD2+ CD8+
CD2+ CD8-
CD2 PerCP-Cy5.5
CD28 BV650
CD27 APC-H7
CCR6 BV711
CCR5 BV563
CD127 APC-R700
CD159a APC

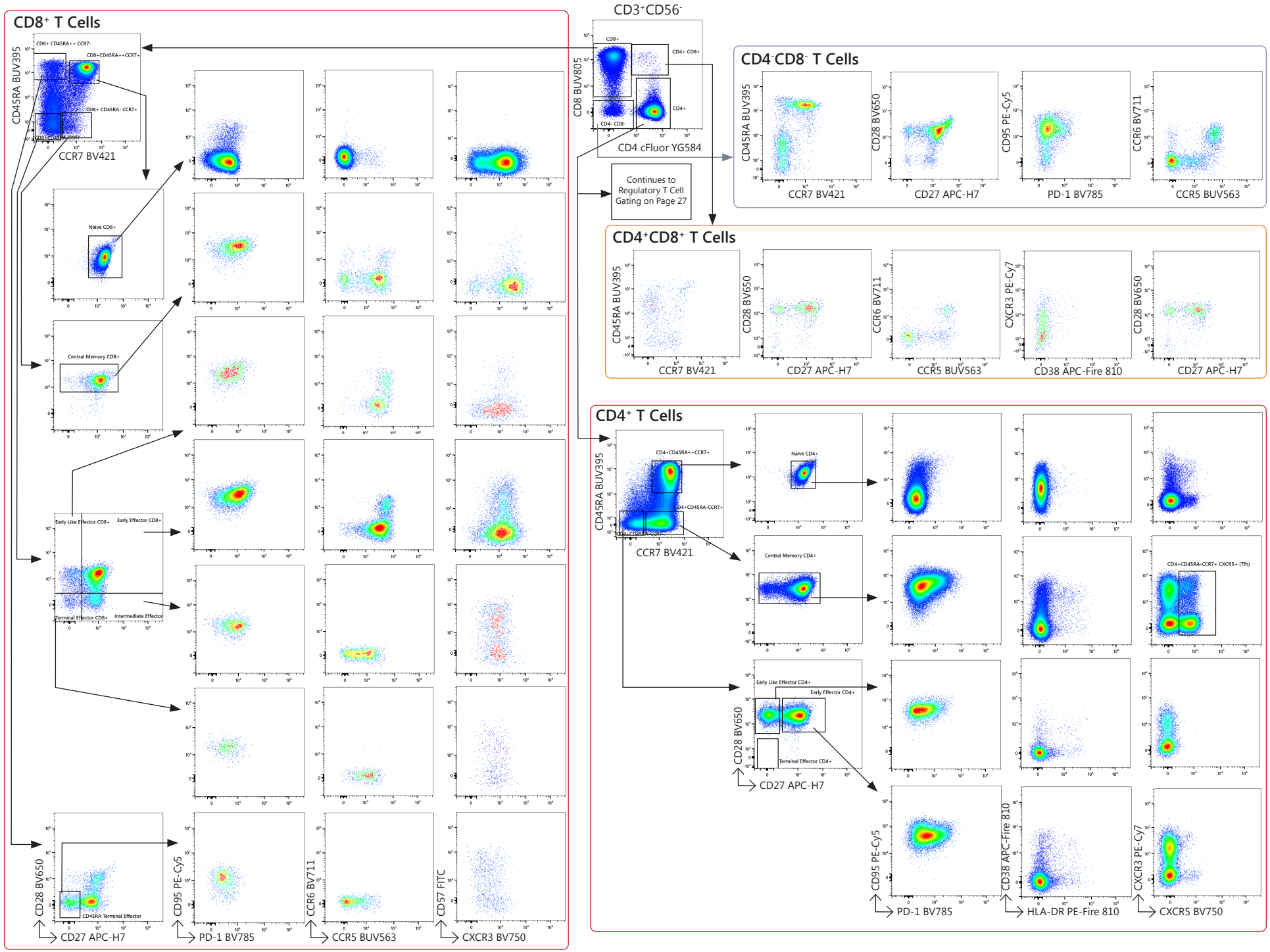
CD8⁺ T Cells
CD3⁺CD56⁻
CD4⁻CD8⁻ T Cells
CD4⁺CD8⁺ T Cells
CD4⁺ T Cells
Continues to Regulatory T Cell Gating on Page 27
CD8+ CD45RA++ CCR7-
CD8+CD45RA++CCR7+
CD8+ CD45RA- CCR7+
CD45RA BUV395
CCR7 BV421
Naive CD8+
Central Memory CD8+
Early Like Effector CD8+
Early Effector CD8+
Terminal Effector CD8+
Intermediate Effector
CD45RA Terminal Effector
CD28 BV650
CD27 APC-H7
CD95 PE-Cy5
PD-1 BV785
CCR6 BV711
CCR5 BUV563
CD57 FITC
CXCR3 BV750
CD8+
CD4+ CD8+
CD4+
CD4- CD8-
CD8 BUV805
CD4 cFluor YG584
CD28 BV650
CD27 APC-H7
CD95 PE-Cy5
PD-1 BV785
CCR6 BV711
CCR5 BUV563
CD45RA BUV395
CCR7 BV421
CD27 APC-H7
CCR5 BUV563
CXCR3 PE-Cy7
CD38 APC-Fire 810
CD28 BV650
CD27 APC-H7
CD4+CD45RA++CCR7+
CD4+CD45RA-CCR7+
Naive CD4+
Central Memory CD4+
Early Like Effector CD4+
Early Effector CD4+
Terminal Effector CD4+
CD4+CD45RA-CCR7+ CXCR5+ (Tfh)
CD95 PE-Cy5
PD-1 BV785
CD38 APC-Fire 810
HLA-DR PE-Fire 810
CXCR3 PE-Cy7
CXCR5 BV750

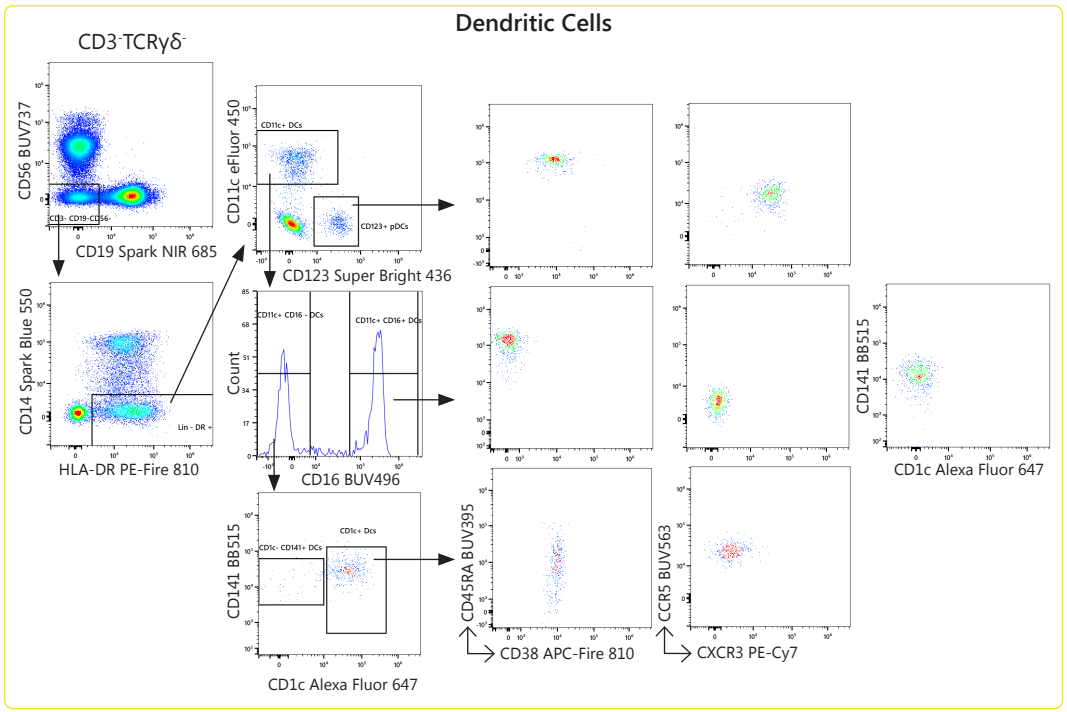
Dendritic Cells
CD3-TCRγδ-
CD56 BUV737
CD19 Spark NIR 685
CD14 Spark Blue 550
HLA-DR PE-Fire 810
CD11c eFluor 450
CD123 Super Bright 436
Count
CD16 BUV496
CD141 BB515
CD1c Alexa Fluor 647
CD45RA BUV395
CD38 APC-Fire 810
CCR5 BUV563
CXCR3 PE-Cy7

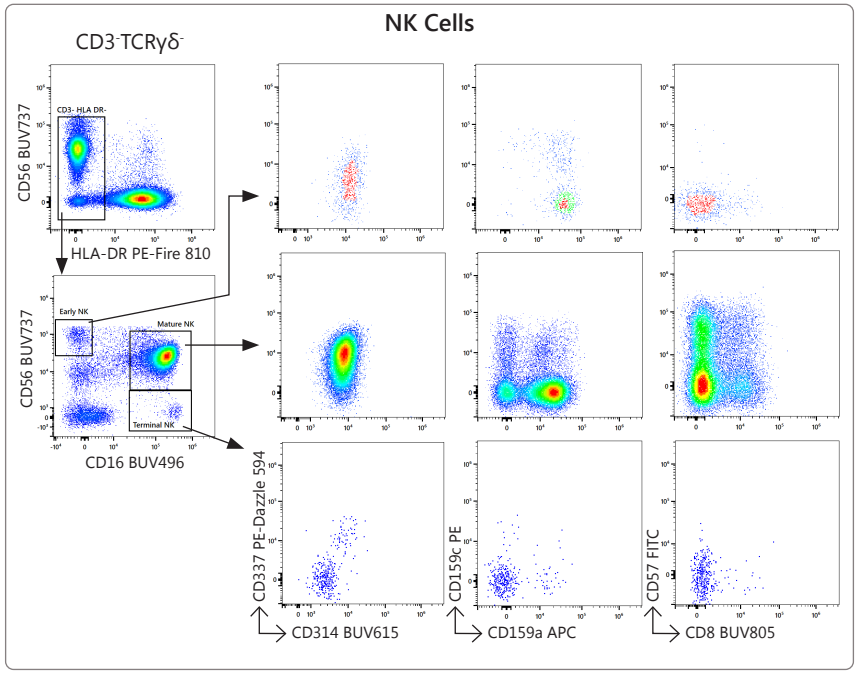
NK Cells
CD3-TCRγδ-
CD56 BUV737
HLA-DR PE-Fire 810
CD16 BUV496
CD337 PE-Dazzle 594
CD314 BUV615
CD159c PE
CD159a APC
CD57 FITC
CD8 BUV805

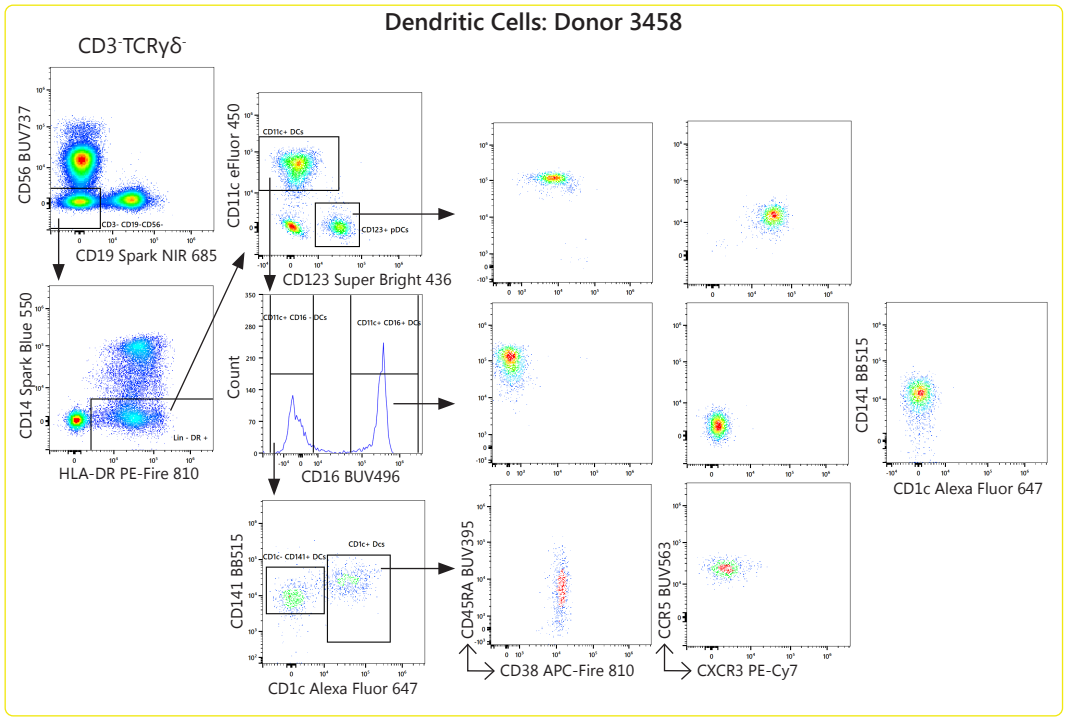
Dendritic Cells: Donor 3458
CD3-TCRγδ-
CD56 BUV737
CD19 Spark NIR 685
CD14 Spark Blue 550
HLA-DR PE-Fire 810
CD11c eFluor 450
CD123 Super Bright 436
Count
CD16 BUV496
CD141 BB515
CD1c Alexa Fluor 647
CD45RA BUV395
CD38 APC-Fire 810
CCR5 BUV563
CXCR3 PE-Cy7

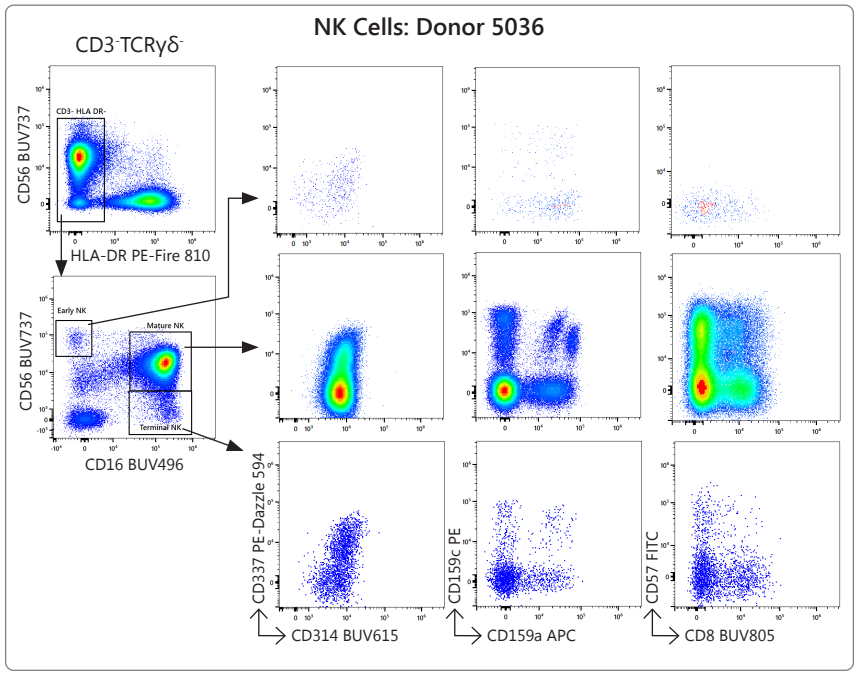
NK Cells: Donor 5036
CD3-TCRγδ-
CD56 BUV737
HLA-DR PE-Fire 810
CD16 BUV496
CD337 PE-Dazzle 594
CD314 BUV615
CD159c PE
CD159a APC
CD57 FITC
CD8 BUV805

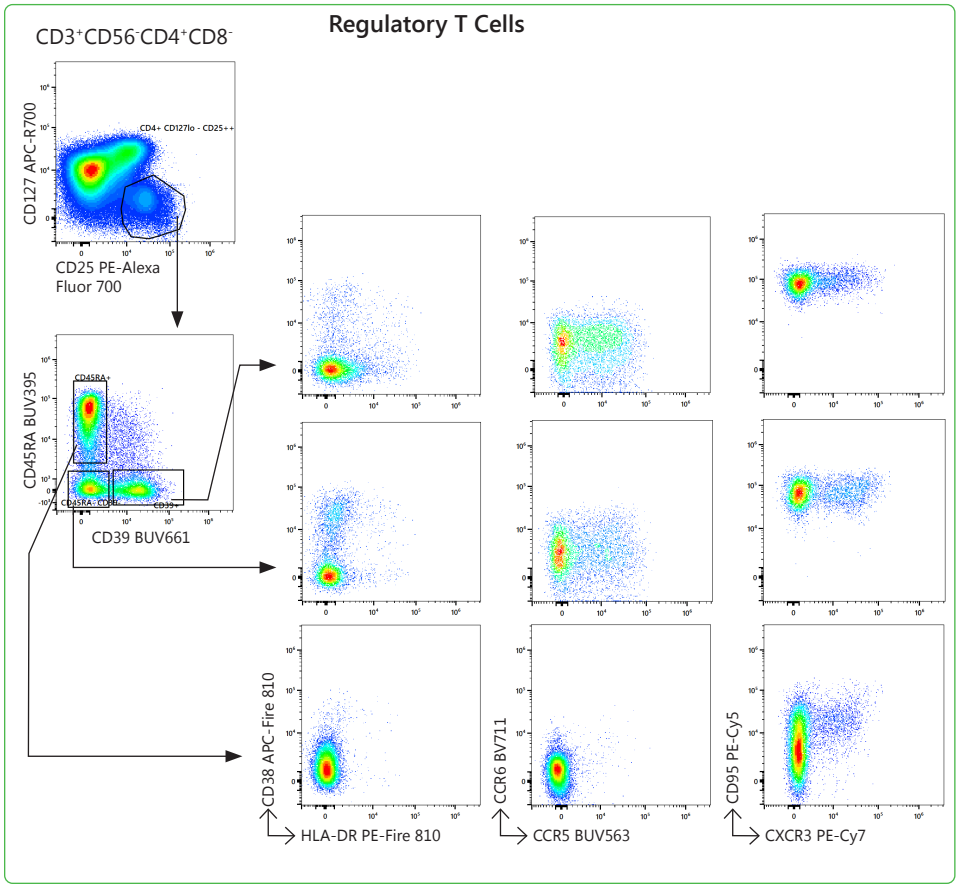

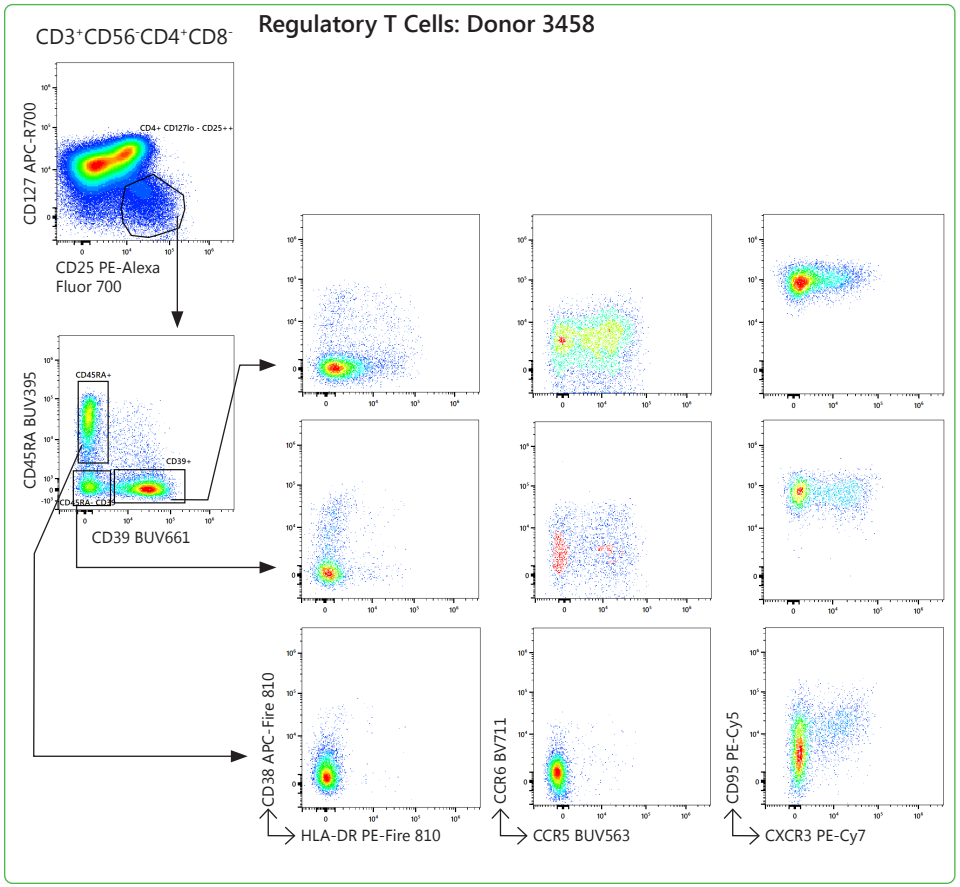

Supplemental Figure 10. Deep Immunophenotyping of All Cellular Subsets
Following the gating scheme presented in Figure 1A, the different cellular subsets were further characterized by manual gating. For each main population, the main markers that showed different levels of expression across the various subsets of that specific population are presented. Data presented corresponds to Donor 4559, as in Figure 1A. For the Tregs, DCs and NK populations, data from an additional donor is presented to illustrate observed difference in level of expression of certain markers.

11A

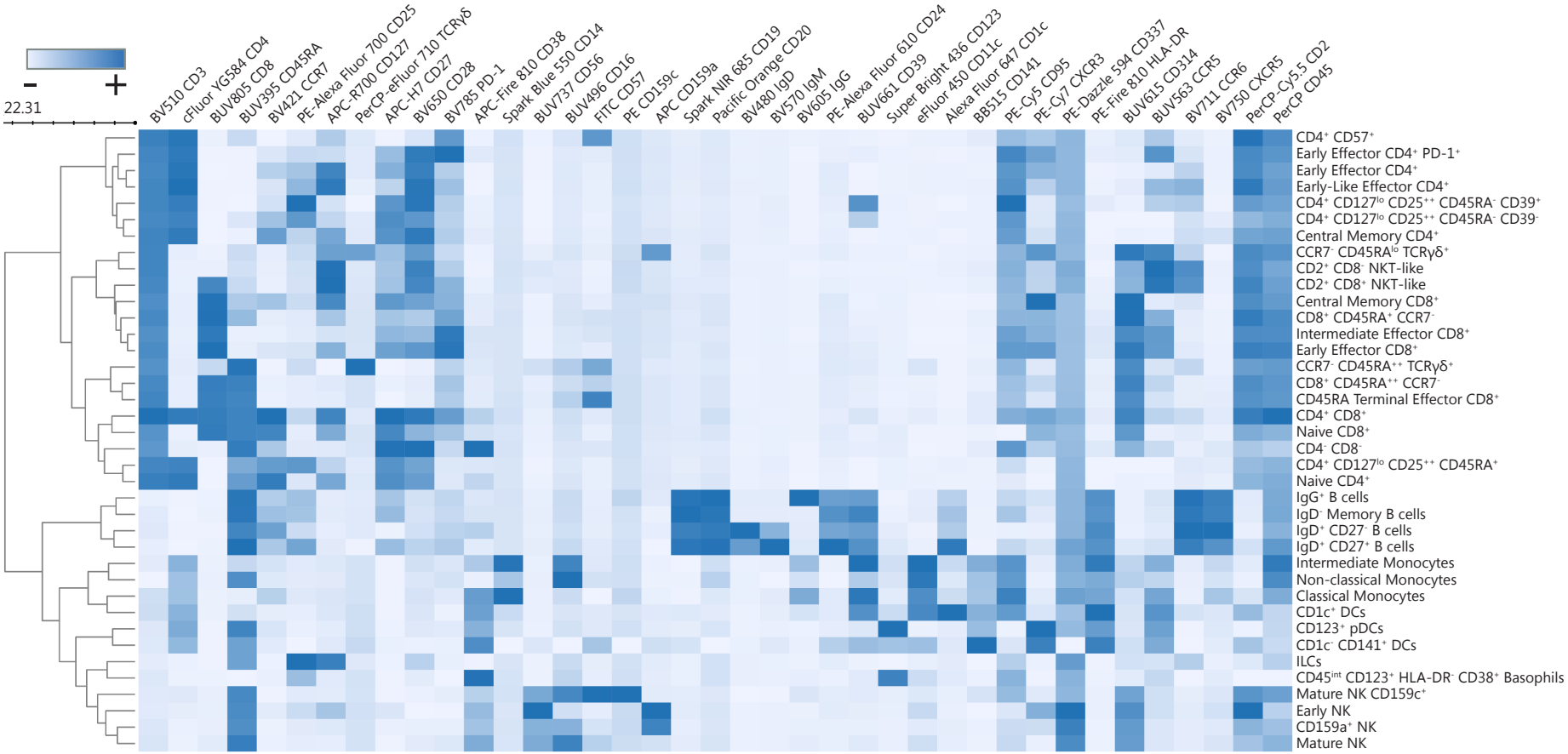
22.31
BV510 CD3
cFluor YG584 CD4
BUV805 CD8
BUV395 CD45RA
BV421 CCR7
PE-Alexa Fluor 700 CD25
APC-R700 CD127
PerCP-eFluor 710 TCRγδ
APC-H7 CD27
BV650 CD28
BV785 PD-1
APC-Fire 810 CD38
Spark Blue 550 CD14
BUV737 CD56
BUV496 CD16
FITC CD57
PE CD159c
APC CD159a
Spark NIR 685 CD19
Pacific Orange CD20
BV480 IgD
BV570 IgM
BV605 IgG
PE-Alexa Fluor 610 CD24
BUV661 CD39
Super Bright 436 CD123
eFluor 450 CD11c
Alexa Fluor 647 CD1c
BB515 CD141
PE-Cy5 CD95
PE-Cy7 CXCR3
PE-Dazzle 594 CD337
PE-Fire 810 HLA-DR
BUV615 CD314
BUV563 CCR5
BV711 CCR6
BV750 CXCR5
PerCP-Cy5.5 CD2
PerCP CD45
CD4+ CD57+
Early Effector CD4+ PD-1+
Early Effector CD4+
Early-Like Effector CD4+
CD4+ CD127lo CD25++ CD45RA- CD39+
CD4+ CD127lo CD25++ CD45RA- CD39-
Central Memory CD4+
CCR7- CD45RAlo TCRγδ+
CD2+ CD8- NKT-like
CD2+ CD8+ NKT-like
Central Memory CD8+
CD8+ CD45RA+ CCR7-
Intermediate Effector CD8+
Early Effector CD8+
CCR7- CD45RA++ TCRγδ+
CD8+ CD45RA++ CCR7-
CD45RA Terminal Effector CD8+
CD4+ CD8+
Naive CD8+
CD4- CD8-
CD4+ CD127lo CD25++ CD45RA+
Naive CD4+
IgG+ B cells
IgD- Memory B cells
IgD+ CD27- B cells
IgD+ CD27+ B cells
Intermediate Monocytes
Non-classical Monocytes
Classical Monocytes
CD1c+ DCs
CD123+ pDCs
CD1c- CD141+ DCs
ILCs
CD45int CD123+ HLA-DR- CD38+ Basophils
Mature NK CD159c+
Early NK
CD159a+ NK
Mature NK

11B

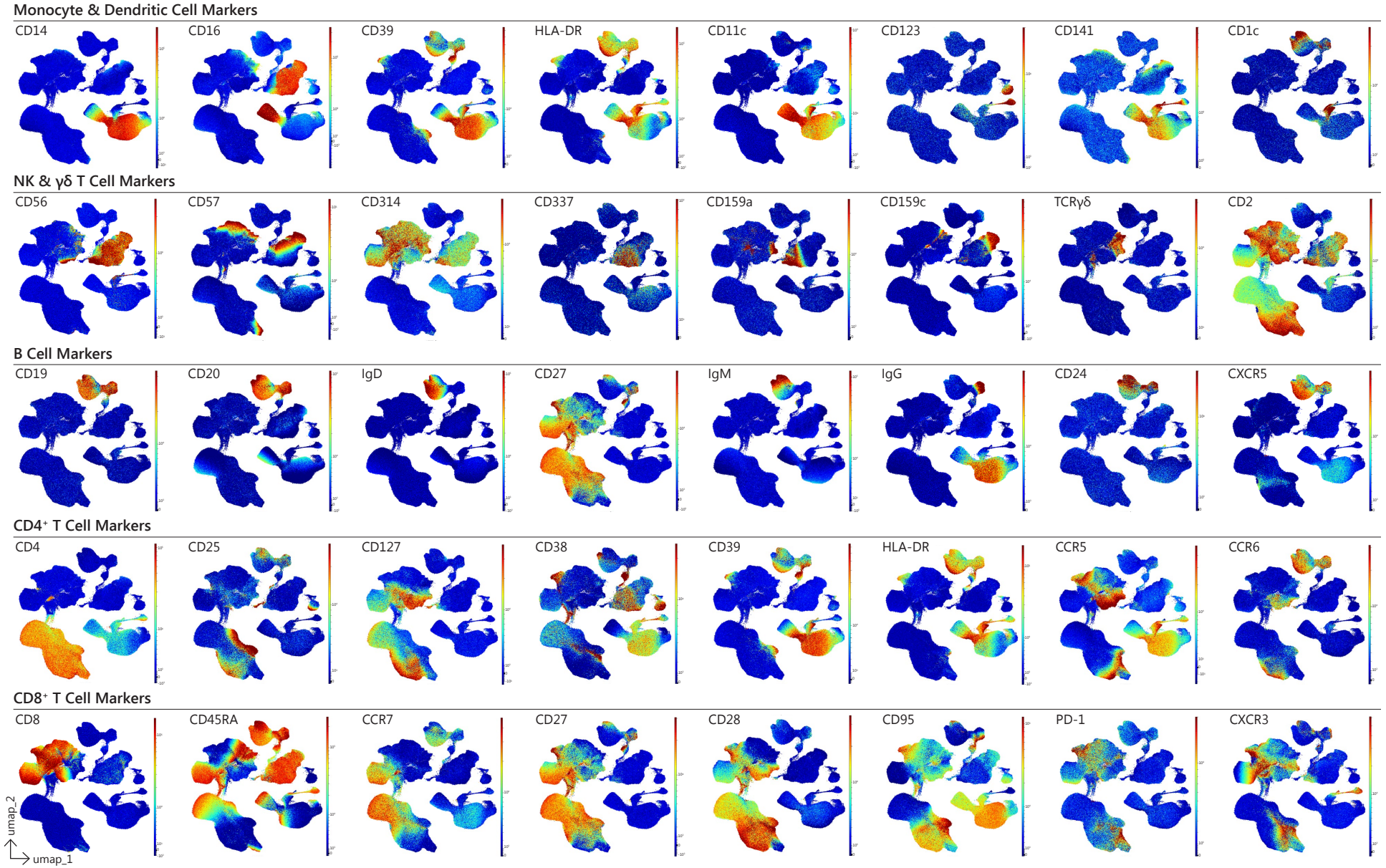

Supplemental Figure 11. High Dimensional Data Reduction of 40-Color Panel

Overview showing the expression of phenotypic markers on PBMCs in several unsupervised analyses. **(A)** Hierarchically clustered heatmap displaying the marker expressions of manually labeled FlowSOM clusters from four concatenated samples. The marker expression intensity is displayed on a scale from white (negative) to blue (positive). Each column's max and min are mapped to this scale so the values change between markers, consequently the scale is labeled with – and + to indicate relative magnitude. **(B)** Visualization of the phenotypic variation across all PBMC subsets using UMAP. Marker expression intensity is indicated by the scale bar to the right of each plot, where red is high and blue is low.

STAINING PROTOCOL

Materials and Reagents

12x75 mm (5 ml) Falcon® FACS tubes: Corning catalog #352063
RPMI: Sigma catalog # R8758
Fetal Bovine Serum (FBS): Gibco catalog #16000-036
Penicillin-Streptomycin: Gibco catalog #15640-055
PBS: Gibco catalog #20012-027
Brilliant Staining buffer: BD Biosciences, catalog #563794
True-Stain Monocyte Blocker™: BioLegend catalog #426101
UltraComp eBeads™ Compensation Beads: Thermo Fisher, catalog #01-2222-41
Wash/Stain Buffer: BD Stain Buffer (BSA) catalog #554657
Antibodies specified in **Supplemental Table 4**

Cryopreserved PBMCs were purchased from AllCells (www.allcells.com, California USA). Different donors were used throughout the panel development process.

Prepared buffers: complete RPMI: add 50 ml of FBS, 5 ml of Penicillin-Streptomycin into 500 ml of RPMI 1640 (with L-glutamine and sodium bicarbonate)

Thawing PBMCs

Note: Handling of human blood components should be done in accordance with regional and institutional Biosafety policies and/or requirements.

1. Pre-warm complete RPMI at 37°C for at least 30 minutes.
2. Thaw cells as quickly as possible.
    a. Thaw cryo-vial ($25x10^6$ cells) in 37°C water bath, until only small piece of ice remains.
    b. Transfer contents of cryo-vial to 50 mL conical tube.
    c. Add 1 ml of warm complete RPMI to cryo-vial. Leave aside until step f.
    d. Drop-by-drop add 5 ml of warm complete RPMI to the cells in the 50 mL tube. While adding, gently mix the 50 mL tube (with a pipette in one hand and in the other the 50 mL tube, add the complete RPMI while you gently swirl the tube).
    e. After first 5 ml of complete RPMI have been added, add the next 5 ml a little bit faster (a few drops at a time).
    f. After 10 ml have been added, pour the contents of the cryo-vial into the 50 mL tube.
    g. Add additional volume of complete RPMI to complete to 20 ml.
3. Spin at 400 x g for 8 minutes.
4. Decant supernatant carefully without disturbing the pellet.
5. Gently resuspend pellet in 2 ml of warm complete RPMI.
6. Complete to 20 ml.
7. Repeat steps 3 and 4.
8. Resuspend in 7.5 ml of complete RPMI or to an approximate concentration of $3.5x10^6$/ml.
9. Leave in incubator until ready to proceed (rest is not necessary, but once staining has begun, samples will need to be processed without delay).

Viability Dye and Antibody Preparation

1. Thaw aliquot of Live/Dead Blue (dried preparation is resuspended in DMSO following the manufacturer recommendation and 7 µl aliquots are stored at -20°C).
2. Transfer 5 µl of viability dye to a larger Eppendorf and add 195 µl 1X PBS (1:40 dilution).
3. Keep in dark until ready to use.
4. Prepare antibody dilutions as needed.
5. Prepare a master mix of all antibodies in brilliant stain buffer EXCEPT CCR5, CXCR5, and TCRγδ (see **Supplemental Figure 9**).

Staining

1. Label 12x75 mm (5 ml) FACS tubes: unstained, SS controls, and MC tubes.
2. Add 700 µL of cell suspension to each MC tube (approximately $2x10^6$ cells, to be able to collect enough events for very rare populations).

3. Add 100 µL of cells (approximately $3x10^5$ cells) to each of the SS and unstained controls.
   Note: Ideally, all controls should be cells, however, some antibody reagents showed no difference between cells and beads as reference controls, and in those cases, beads can be used. In this protocol, we used UltraComp eBeads™ Compensation Beads from ThermoFisher, however, beads from other manufacturers may perform differently. See step 2 under Panel Testing above.
4. MC and SS viability tubes need to be washed with PBS only.
   Note: Viability dye is an amine reactive dye and will be bound by any proteins in the buffer, so it is important to make sure the wash buffer is free of protein.
5. All other SS controls and MC tubes are washed with wash buffer, 3 ml per tube.
6. Spin at 500 x g for 5 minutes.
7. Carefully decant supernatant.
8. Add 5 µl of viability dye dilution to MC AND Viability SS control; vortex and incubate for 15 minutes at room temperature in the dark.
9. In the meantime, start staining SS controls with the pre-determined optimal amount of antibody.
10. After 15 minute incubation, wash MC and SS viability tubes with wash buffer.
11. Repeat steps 6 and 7.
12. Add 300 µl of wash buffer to SS viability tube, vortex, store at 4°C.
13. Add 10 µl of Brilliant Stain Buffer Plus to all MC tubes. Vortex well.
14. Add 5 µl of True-Stain Monocyte Blocker; vortex.
15. Add anti-TCRγδ; vortex.
16. Incubate for 10 minutes at room temperature in the dark.
17. Add anti-CXCR5 and anti-CCR5; vortex.
18. Incubate for 10 minutes at room temperature in the dark.
19. Add the remainder of antibodies from the MC mix cocktail; vortex.
20. Incubate at room temperature in the dark for 30 minutes.
21. Finish staining/washing SS controls.
22. Wash all tubes with 3 ml of wash buffer.
23. Decant supernatant carefully, then resuspend the pellet.
24. Add 300 µl of 1% paraformaldehyde (PFA) in PBS to all tubes, including SS control tubes; vortex.
    Note: It is very important to treat the SS controls in the same manner as the MC samples, including the fixation step. This is true whether beads or cells are used as SS controls. Fluorochrome emission properties can be slightly altered depending on their microenvironment. For accurate unmixing/ compensation, SS controls need to be treated exactly the same as the MC stained sample.
    If necessary due to biosafety issues, 4% PFA can be used. Some reduction in intensity for some markers may occur after fixation with this high concentration of PFA as described in the literature (16). CD45RA for example is one of the markers that is impacted, but the resolution with the conjugate in this panel should still be optimal.
25. Incubate for 20 minutes at room temperature.
26. Repeat steps 6 and 7.
27. Resuspend pellet in 400 µl of wash buffer.
28. Store at 4°C protected from light until ready to acquire on the instrument.

REFERENCES

1. Roederer M. Spectral compensation for flow cytometry: visualization artifacts, limitations, and caveats. Cytometry 2001;45:194-205.
2. Roederer M. Distributions of autofluorescence after compensation: Be panglossian, fret not. Cytometry A 2016;89:398-402.
3. Nguyen R, Perfetto S, Mahnke YD, Chattopadhyay P, Roederer M. Quantifying spillover spreading for comparing instrument performance and aiding in multicolor panel design. Cytometry A 2013;83:306-15.
4. Mahnke YD, Roederer M. Optimizing a multicolor immunophenotyping assay. Clin Lab Med 2007;27:469-85, v.
5. Mair F, Prlic M. OMIP-044: 28-color immunophenotyping of the human dendritic cell compartment. Cytometry A 2018;93:402-405.
6. Hammer Q, Romagnani C. OMIP-039: Detection and analysis of human adaptive NKG2C(+) natural killer cells. Cytometry A 2017;91:997-1000.

7. Biosciences B. Anti-Mouse Ig, κ/Negative Control Compensation Particles Set:BD™ CompBeads. In: Biosciences B, editor. Technical Data Sheet. 552843 Rev. 5 ed. BD Biosciences.com; 2017. p 1-2.
8. Jalbert E, Shikuma CM, Ndhlovu LC, Barbour JD. Sequential staining improves detection of CCR2 and CX-3CR1 on monocytes when simultaneously evaluating CCR5 by multicolor flow cytometry. Cytometry Part A 2013;83A:280-286.
9. Chester C, Maecker HT. Algorithmic Tools for Mining High-Dimensional Cytometry Data. J Immunol 2015;195:773-9.
10. Mair F, Hartmann FJ, Mrdjen D, Tosevski V, Krieg C, Becher B. The end of gating? An introduction to automated analysis of high dimensional cytometry data. Eur J Immunol 2016;46:34-43.
11. Palit S, Heuser C, de Almeida GP, Theis FJ, Zielinski CE. Meeting the Challenges of High-Dimensional Single-Cell Data Analysis in Immunology. Front Immunol 2019;10:1515.
12. Becht E, McInnes L, Healy J, Dutertre CA, Kwok IWH, Ng LG, Ginhoux F, Newell EW. Dimensionality reduction for visualizing single-cell data using UMAP. Nat Biotechnol 2018.
13. Meskas J, Wang S, Brinkman R. flowCut — An R package for precise and accurate automated removal of outlier events and flagging of files based on time versus fluorescence analysis. bioRxiv 2020.
14. McInnes L, Healy J, Melville J. UMAP: Uniform Manifold Approximation and Projection for Dimension Reduction; ArXiv e-prints 2018.
15. Van Gassen S, Callebaut B, Van Helden MJ, Lambrecht BN, Demeester P, Dhaene T, Saeys Y. FlowSOM: Using self-organizing maps for visualization and interpretation of cytometry data. Cytometry A 2015;87:636-45.
16. Stewart JC, Villasmil ML, Frampton MW. Changes in fluorescence intensity of selected leukocyte surface markers following fixation. Cytometry A 2007;71:379-85.